INVESTIGATION INTO THE PLUNGER COOLING TUBE SYSTEM DESIGN FOR THE NARROW NECK PRESS AND BLOW PROCESS

NOEL PERERA BEng (Hons)

A thesis submitted in partial fulfilment of the requirements of the University of Northumbria at Newcastle for the degree of Doctor of Philosophy

in collaboration with Rexam Glass Ltd

December 2001

Declaration

The candidate has not been registered for another award of a University during the research programme.

Work on the Investigation into the Plunger Cooling Tube System Design for the Narrow Neck Press and Blow Process has been undertaken at the University of Northumbria at Newcastle since April 1998. The candidate was employed full-time as a research student under the direction of Professor M.Sarwar and supervision of Dr. P.S Leung and Mr. A.W. Armitage. This programme of work has been financially supported by Rexam Glass Ltd.

Work carried out during the research programme has been reported in the following scientific papers:

1. Sarwar, M; Leung, P.S; Perera, N; Armitage, A.W;
   Mathematical Modelling of the Fluid Flow in the NNPB Plunger Cooling System
   International Glass Journal No.107 May-June 2000 pp 26-29
2. Sarwar, M; Leung, P.S; Perera, N; Armitage, A.W;
   CFD Modelling and Heat Transfer in a NNPB Process
   International Glass Journal No.112 March-April 2001 pp 33-38

Abstract

Although glass as a packaging material is well received by consumers, its manufacturing process is not fully understood. The two processes associated with glass container manufacture are the blow and blow and the press and blow processes. The narrow neck press and blow (NNPB) process was conceived to maintain the glass containers' competitive edge as a packaging material as it produces a lighter container at a lower cost.

The principal element of the NNPB process is the plunger. It shapes the cavity and disperses the glass within the container. The plunger operates both as a heat exchanger and a shaping tool. The plunger due to its harsh operating environment, experiences extreme wear. It is liable for product defect, uneven thermal distribution and machine downtime. Plunger wear is partly related to the ineffective extraction of thermal energy by the plunger cooling tube system. Areas of poor plunger cooling correspond to the poor circulation of coolant air hence leading to plungers exhibiting premature wear and failure.

The work presented here is a scientific study of the current NNPB plunger cooling tube system. This has been carried out systematically by designing a laboratory experiment to simulate the manufacturing process of glass containers and thus assess the boundary conditions (inlet airflow velocity and outlet pressure) for the cooling tube plunger system. In addition temperature

boundary conditions were established using the thermal imaging technique. The CFD models developed were in 2D, axisymmetric and 3D using the established boundary conditions (i.e. inlet airflow velocity, outlet pressure and parison temperature) to assess the performance of the plunger cooling tube system.

CFD modelling has enabled the modification of the cooling tube system design (i.e. 1.2mm hole diameter and hole positioning) to reduce the power/energy consumption by up to 80% during the heat extraction process. Furthermore the CFD modelling has allowed a better understanding of the airflow behaviour (i.e. recirculation, stagnation) and performance of the plunger cooling tube system. This information is useful knowledge to the designer and manufacturing engineer and should result in finding the design solutions for the cooling tube system more readily.

Acknowledgement

The candidate wishes to acknowledge the financial assistance of the University of Northumbria as well as the financial and technical assistance of Rexam Glass Ltd (formerly known as PLM Redfearn Ltd). In particular the assistance of Mr. A. Armitage and Mr. Tony White.

The candidate also wishes to express his thanks to his Director of Studies Professor M. Sarwar and supervisor Dr. Ken P.S. Leung for their guidance and valued advice. The candidate also wishes to thank the Technical Staff at the University of Northumbria for their valued advice and assistance during the research programme.

Nomenclature

V_{in}	Inlet velocity (m/s)
V_X	Velocity in the x direction
$\|V\|$	Magnitude of velocity
V_x, V_y, V_z	Components of the velocity vector in the x, y and z directions respectively
x, y, z	Global Cartesian coordinates
t	Time
τ_{ij}	Stress tensor
u_i	Orthogonal velocities (u1 =V_x , u2 = V_y, u3 = V_z)
μ	Dynamic viscosity
λ	Second coefficient of viscosity
K	Thermal conductivity
W^v	Viscous work term
Q_v	Volumetric heat source
ϕ	Viscous heat generation term
E^K	Kinetic energy
P	Pressure
P_{in}	Inlet pressure (bar)
$P_{in\ CFD'}$	Inlet CFD pressure (bar)
$P_{in\ exp}$	Inlet laboratory experimental study pressure
P_{out}	Outlet pressure (bar)
T_o	Total temperature (K)
T_{inlet}	Inlet temperature (K)
T_{outlet}	Outlet temperature (K)

k	Distributed resistance
C_p	Specific heat of air at constant pressure (J/kgK)
ρ, ρ	Density (kg/m^3)
$\dot{m}$	Mass flow rate (kg/s)
$\dot{Q}$	Heat absorbed (W)
Q	Volumetric airflow (m^3/s)
P	Power (W)

TABLE OF CONTENTS

ABSTRACT

ACKNOWLEDGEMENTS

NOMENCLATURE

CHAPTER 1 INTRODUCTION 1

1.1 BLOW AND BLOW PROCESS 4

1.2 NARROW NECK PRESS AND BLOW (NNPB) PROCESS 5

1.3 AIMS AND OBJECTIVES OF THE INVESTIGATION 17

CHAPTER 2 LITERATURE SURVEY 25

CHAPTER 3 DESIGN AND DEVELOPMENT OF THE PLUNGER AND COOLING TUBE TEST RIG AND EXPERIMENTAL WORK.....29

3.1 INTRODUCTION.....29

3.2 TEST RIG.....29

3.3 EXPERIMENTAL METHOD 31

3.4 RESULTS.....32

3.5 OBSERVATION 40

CHAPTER 4 THERMAL IMAGING STUDY FOR THE TEMPERATURE DISTRIBUTION IN THE PLUNGER AND PARISON.....41

4.1 INTRODUCTION.....41

4.2 THERMAL IMAGING EQUIPMENT [65] 42

4.3 WINDOW AND OFFSET CONTROLS OF THE THERMAL IMAGER 44

4.4 EXPERIMENTAL STUDY 45

4.5 RESULTS 45

4.5.1 Plunger Temperature *45*

4.5.2 Parison Temperature *46*

4.6 OBSERVATION 47

CHAPTER 5 ASSESSING THE AIRFLOW DISTRIBUTION IN THE 2D AND AXISYMMETRIC MODEL OF THE NNPB PLUNGER COOLING TUBE SYSTEM USING THE CFD ANALYSIS TECHNIQUE 48

5.1 INTRODUCTION 48

5.2 DETERMINING THE POROSITY OF THE COOLING TUBE HOLES FOR THE PRESSURE DIFFERENCE RANGE OF 0.5 BAR TO 3 BAR 60

5.3 ASSESSING THE AXISYMMETRIC MODEL WITH UNIFORM PARISON SKIN TEMPERATURE 66

5.3.1 Introduction *66*

5.3.2 Results *67*

5.3.3 Discussion *68*

5.3.4 Conclusion *70*

5.4 ASSESSING THE AXISYMMETRIC MODEL WITH DIFFERENT SCHEMES OF COOLING TUBE HOLE DISTRIBUTION 71

5.4.1 Introduction *71*

5.4.2 Results *74*

5.4.3 Discussion *77*

5.4.4 Conclusion *81*

5.5 ASSESSING THE AXISYMMETRIC MODEL WITH THE INCORPORATED PLUNGER MATERIAL PROPERTIES **84**

5.5.1 Introduction *84*

5.5.2 Results *84*

5.5.3 Discussion *86*

5.5.4 Conclusion *90*

CHAPTER 6 CFD INVESTIGATION OF THE AIRFLOW DISTRIBUTION INTO THE NNPB PLUNGER COOLING TUBE SYSTEM WITH THE 3D MODEL **94**

6.1 INTRODUCTION **94**

6.2 ASSESSING THE CURRENT COOLING TUBE MODEL WITH UNIFORM PARISON SKIN TEMPERATURE **94**

6.2.1 Introduction *94*

6.2.2 Results *96*

6.2.3 Discussion *99*

6.2.4 Conclusion *100*

6.3 ASSESSING THE 3D MODEL WITH DIFFERENT SCHEMES OF COOLING TUBE HOLE DISTRIBUTION AND UNIFORM PARISON SKIN TEMPERATURE **101**

6.3.1 Introduction *101*

6.3.2 Results *102*

6.3.3 Discussion *108*

6.3.4 Conclusion *114*

6.4 ASSESSING THE 3D MODEL WITH DIFFERENT SCHEMES OF COOLING TUBE HOLE SIZES **115**

6.4.1 Introduction *115*

6.4.2 Results *115*

6.4.3 Discussion *122*

6.4.4 Conclusion *129*

CHAPTER 7 DISCUSSION OF RESULTS **130**

CHAPTER 8 CONCLUSIONS **143**

CHAPTER 9 PROPOSED FUTURE WORK **145**

REFERENCES **146**

APPENDIX 1

APPENDIX 2

APPENDIX 3

LIST OF FIGURES

Figure 1.1. IS Machine 19
Figure 1.2. Blow and Blow Process 19
Figure 1.3. Narrow Neck Press and Blow (NNPB) Process 20
Figure 1.4. Blank/parison forming stage; loading position 20
Figure 1.5. Blank/parison forming stage; start of press 21
Figure 1.6. Blank/parison forming stage; end of press 21
Figure 1.7. Narrow neck glass containers 22
Figure 1.8. The Narrow Neck Press and Blow (NNPB) plunger 22
Figure 1.9. Cross section of a typical NNPB plunger and cooling tube 23
Figure 1.10. Enlarged view of the tip of the cooling tube 23
Figure 1.11. Stages of the container forming process 24
Figure 3.1. Experimental set-up of the plunger cooling tube system 30
Figure 3.2. Enlarged view of the plunger cooling tube enclosed in the casing 31
Figure 3.3. Schematic diagram of the plunger cooling tube experimental set-up 31
Figure 3.4. Graph of Airflow Vs Pressure Difference along the plunger and cooling tube for Experiment 1 33
Figure 3.5. Graph of Airflow Vs Pressure Difference along the plunger and cooling tube for Experiment 2 34
Figure 3.6. Graph of Airflow Vs Pressure Difference along the plunger and cooling tube for Experiment 3 35
Figure 3.7. Graph of Airflow Vs Pressure Difference along the plunger and cooling tube for Experiment 4 36
Figure 3.8. Graph of Airflow Vs Pressure Difference along the plunger and cooling tube for Experiment 5 37
Figure 3.9. Graph of Airflow Vs Pressure Difference along the plunger and cooling tube for Experiment 6 38

Figure 3.10. Graph of Airflow Vs Pressure Difference along the plunger and cooling tube for Experiment 7.....39
Figure 4.1 Carrying out the thermal imaging analysis on the shop floor.....41
Figure 4.2. Schematic diagram of the thermal imager Land TI 35 sm [66].....44
Figure 4.3. The location of the temperature points chosen to investigate the temperature distribution in the plunger.....45
Figure 4.4. The location of the temperature points chosen to investigate the temperature distribution in the parison.....46
Figure 5.1. Diagram of airflow through the 2 dimensional model of the cooling tube. Inlet pressure: 1.5 bar, outlet pressure: 0.4 bar, iteration: 1200 and is compressible.....52
Figure 5.2. An enlarged sectional view of the airflow patterns after the first hole along the cooling tube. The tube is long and has a closed end.....52
Figure 5.3. An enlarged view of the airflow patterns at the inlet of the cooling tube. The tube is long and has a closed end at the tip.....53
Figure 5.4. Diagram of the airflow through the axisymmetric model of the cooling tube. Inlet pressure: 1.5 bar, outlet pressure: 0.4 bar, iteration: 1200 and is compressible.....53
Figure 5.5. An enlarged sectional view of the airflow patterns after the first hole along the cooling tube in the axisymmetrical model. The tube is long and has a closed end.....54
Figure 5.6. Diagram showing the plunger tip and cooling tube with the area of the applied distributed resistance.....55
Figure 5.7. Graph of Pressure Vs Vertical distance along the inlet of the cooling tube. Inlet velocity: 105.97 m/s, outlet pressure: 0.4 bar, iteration: 5000 and is compressible.....57

Figure 5.8. Diagram of the airflow through the rectified axisymmetric model of the cooling tube. Inlet velocity: 105.97 m/s, outlet pressure: 0.4 bar, iteration: 5000 and is compressible. 58
Figure 5.9. An enlarged sectional view of the airflow patterns at the center of the cooling tube. The tube is long and has a closed end. 59
Figure 5.10. An enlarged sectional view of the airflow patterns at the tip of the cooling tube. The tube was long and had a closed end. 59
Figure 5.11. Diagram of the pressure through the rectified axisymmetric model of the cooling tube. Inlet velocity: 105.97 m/s, outlet pressure: 0.4 bar, iteration: 5000 and is compressible. 60
Figure 5.12. Graph of Inlet Pressure Vs Distributed resistance for an inlet pressure of 1.5 bar. (Boundary conditions used were exit pressure P_{out} =0.4 bar and inlet velocity V_{in} =105.97 m/s) 62
Figure 5.13. Graph of Inlet Pressure (0.5 bar to 3 bar) Vs Distributed Resistance of the plunger cooling tube system 63
Figure 5.14. Graph of the Distributed Resistance Vs Inlet Pressure along the plunger cooling tube system 64
Figure 5.15. Graph of Distributed Resistance Vs Outlet Pressure along the plunger cooling tube system 65
Figure 5.16. Graph of Distributed Resistance Vs Inlet Velocity along the plunger cooling tube system 65
Figure 5.17. Graph of Heat Absorbed Vs Inlet Airflow Velocity along the plunger cooling tube system 69
Figure 5.18. Graph of Heat Absorbed Vs Inlet Pressure along the plunger cooling tube system 70

Figure 5.19. Diagram of the plunger cooling tube system showing the distance of 0.0133 m (1 spacing ratio) between the cooling tube holes 72
Figure 5.20. Diagram of the plunger cooling tube system showing the distance of 0.013 m (0.75 spacing ratio) between the cooling tube holes 72
Figure 5.21. Diagram of the plunger cooling tube system showing the distance of 0.01 m (0.5 spacing ratio) between the cooling tube holes 73
Figure 5.22. Diagram of the plunger cooling tube system showing the distance of 0.0068 m (0.25 spacing ratio) between the cooling tube holes 73
Figure 5.23. Graph of Heat Absorbed Vs Inlet Airflow Velocity of the plunger cooling tube system 78
Figure 5.24. Graph of Heat Absorbed Vs Pressure Difference of the plunger cooling tube system 79
Figure 5.25. Diagram airflow velocity distribution in the axisymmetrical model of the cooling tube. Inlet velocity: 131 m/s, outlet pressure: 0.83 bar. 81
Figure 5.26. Diagram airflow velocity distribution at the plunger tip of the cooling tube. Inlet velocity: 131 m/s, outlet pressure: 0.83 bar. 82
Figure 5.27. Diagram airflow velocity distribution at the first hole from the plunger tip of the cooling tube. Inlet velocity: 131 m/s, outlet pressure: 0.83 bar. 82
Figure 5.28. Diagram pressure distribution at the plunger tip of the cooling tube. Inlet velocity: 131 m/s, outlet pressure: 0.83 bar. 83
Figure 5.29. Diagram temperature distribution at the plunger tip of the cooling tube. Inlet velocity: 131 m/s, outlet pressure: 0.83 bar. 83

Figure 5.30. Graph of Heat Absorbed Vs Inlet Airflow Velocity of the plunger cooling tube system 87
Figure 5.31. Graph of Heat Absorbed Vs Inlet Pressure Difference of the plunger cooling tube system..... 88
Figure 5.32. Diagram of airflow velocity distribution in the axisymmetrical model of the cooling tube. Inlet velocity: 135.5 m/s, outlet pressure: 1 bar..... 91
Figure 5.33. Diagram of airflow velocity distribution at the plunger tip of the cooling tube. Inlet velocity: 135.5 m/s, outlet pressure: 1 bar. 91
Figure 5.34. Diagram of airflow velocity distribution at the first hole from the plunger tip of the cooling tube. Inlet velocity: 135.5 m/s, outlet pressure: 1 bar..... 92
Figure 5.35. Diagram of pressure distribution at the plunger tip of the cooling tube. Inlet velocity: 135.5 m/s, outlet pressure: 1 bar. 92
Figure 5.36. Diagram of temperature distribution at the plunger tip of the cooling tube. Inlet velocity: 135.5 m/s, outlet pressure: 1 bar. 93
Figure 5.37. Graph of Heat Absorbed Vs Inlet Airflow Velocity of the plunger cooling tube system with and without incorporating the plunger material properties into the CFD analysis. 93
Figure 6.1. Inlet Airflow Velocity Vs Pressure Difference of the plunger cooling tube system design. 95
Figure 6.2. Graph of Inlet Airflow Velocity Vs Heat Absorbed for the current tool design..... 99
Figure 6.3. Graph of Inlet Airflow Velocity Vs Power Applied for the current tool design..... 100
Figure 6.4. Graph of Heat Absorbed Vs. Inlet Airflow Velocity of the plunger cooling tube system. 108

Figure 6.5. Graph of Inlet Airflow Velocity Vs. Power Applied for the plunger cooling tube system. 109
Figure 6.6. Diagram of airflow velocity distribution in the 3-D model of the plunger cooling tube system. Inlet velocity: 105.97 m/s, outlet pressure: 0.4 bar..... 111
Figure 6.7. Diagram of pressure distribution in the 3-D model of the plunger cooling tube system. Inlet velocity: 105.97 m/s, outlet pressure: 0.4 bar. 111
Figure 6.8. Diagram of temperature distribution in the 3-D model of the plunger cooling tube system. Inlet velocity: 105.97 m/s, outlet pressure: 0.4 bar..... 112
Figure 6.9. Diagram of airflow velocity distribution at the first four holes from the plunger tip of the cooling tube. Inlet velocity: 105.97 m/s, outlet pressure: 0.4 bar..... 112
Figure 6.10. Vector diagram of the airflow velocity distribution at the first hole from the cooling tube plunger tip. Inlet velocity: 105.97 m/s, outlet pressure: 0.4 bar..... 113
Figure 6.11. Diagram of pressure distribution at the first four holes from the plunger tip of the cooling tube. Inlet velocity: 105.97 m/s, outlet pressure: 0.4 bar..... 113
Figure 6.12. Diagram of temperature distribution at the first four holes from the plunger tip of the cooling tube. Inlet velocity: 105.97 m/s, outlet pressure: 0.4 bar..... 114
Figure 6.13. Graph of Heat Absorbed Vs. Inlet Airflow Velocity of the plunger cooling tube system. 123
Figure 6.14. Graph of Inlet Airflow Velocity Vs. Power Applied for the plunger cooling tube system. 123
Figure 6.15. Diagram of airflow velocity distribution in the 3-D model of the plunger cooling tube system. Inlet velocity: 105.97 m/s, outlet pressure: 0.4 bar..... 125

Figure 6.16. Diagram of pressure distribution in the 3-D model of the plunger cooling tube system. Inlet velocity: 105.97 m/s, outlet pressure: 0.4 bar. 125
Figure 6.17. Diagram of temperature distribution in the 3-D model of the plunger cooling tube system. Inlet velocity: 105.97 m/s, outlet pressure: 0.4 bar..... 126
Figure 6.18. Diagram of airflow velocity distribution at the first four holes from the plunger tip of the cooling tube. Inlet velocity: 105.97 m/s, outlet pressure: 0.4 bar..... 126
Figure 6.19. Vector diagram of the airflow velocity distribution at the first hole from the cooling tube plunger tip. Inlet velocity: 105.97 m/s, outlet pressure: 0.4 bar..... 127
Figure 6.20. Diagram of pressure distribution at the first four holes from the plunger tip of the cooling tube. Inlet velocity: 105.97 m/s, outlet pressure: 0.4 bar..... 127
Figure 6.21. Diagram of temperature distribution at the first four holes from the plunger tip of the cooling tube. Inlet velocity: 105.97 m/s, outlet pressure: 0.4 bar..... 128
Figure 6.22. Graph of Inlet Airflow Velocity Vs. Power Applied for the plunger cooling tube system. 128
Figure 7.1. Graph of Inlet airflow velocity Vs Pressure Difference of the current cooling tube system design..... 137
Figure 7.2. Graph of Heat absorbed Vs Inlet airflow velocity for the current tool design..... 140
Figure 7.3. Graph of Heat absorbed Vs Inlet airflow velocity for the equal ratio (0.0133 m) spacing distance between the cooling tube holes 140
Figure 7.4. Graph of Heat absorbed Vs Inlet airflow velocity for the 0.75 ratio (0.013 m) spacing distance between the cooling tube holes 141

Figure 7.5. Graph of Heat absorbed Vs Inlet airflow velocity for the 0.5 ratio (0.01 m) spacing distance between the cooling tube holes 141
Figure 7.6. Graph of Heat absorbed Vs Inlet airflow velocity for the 0.25 ratio (0.0068 m) spacing distance between the cooling tube holes 142

LIST OF TABLES

Table 1. Advantages and disadvantages of the Blow and Blow Process 7

Table 2. Advantages and disadvantages of the Narrow Neck Press and Blow Process.....8

Table 3. Different plunger substrate material 13

Table 4. Specifications of the modified Land TI 35 sm [65].....43

Chapter 1 INTRODUCTION

The world glass production has been estimated at 100 million tons for 1996 [1]. The U.K presently produces in the region of 5 billion glass containers annually with an approximate turnover of £500 million [2]. Currently about 30-40 billion glass containers are manufactured in Europe with an estimated £4 billion turnover [2]. It has been established that 78% of the European population selected glass as a packaging material in a recent survey carried out by Glasspac.com- Glass Packaging Communication. This survey showed that glass is accepted as the most environmentally friendly packaging material by 66% of consumers. Glasspac.com also highlighted that another 70% of the population perceived that glass typifies quality, trusting that quality products are stored in glass containers.

The current glass container industry has technically made great strides from its medieval background in improving product quality and lowering manufacturing cost (i.e. lightweighting, energy reduction, man-power reductions, high productivity machines). A better understanding of the glass forming process and advances in technology has altered the primitive physically laborious method of forming glass containers into a mechanical and more efficient process. The advancement from wooden form tools to semi-automatic machines were made in the eighteenth century to assist in the manual blowing of bottles [3]. In the early twentieth century, Michael Owens introduced a fully automatic machine

[4]. Emhart in Switzerland developed an improvement to this machine in 1921. This machine essentially operates in 2 stages, shaping of the parison (blank mould) and formation of the glass container (blow mould). This Individual Section (IS) machine, Figure 1.1 (page 19) has been up to the present time the industry's accepted standard for worldwide glass container production. The essence of this longevity is the smooth working combination between machine and glass combined with the co-ordinated action of the mechanical motion and machine operating time [5]. This is an important pre-requisite for a successful Narrow Neck Press and Blow (NNPB) light weight container-forming process. The IS machine's excellent success over more than 70 years is attributed to the original design that permitted continuous further development in order to increase production capabilities [6]. The advancement of the IS-machine have been in the gob loading mechanism (i.e. feeding hot glass to the blank mould), adopting electronic time control system, increasing the machine sections and the change in the cooling air passage [7,8]. The formation of the glass container by the IS machine is based on two different processes. They are the blow and blow and press and blow processes. The former is used to produce a wide range of glass containers having various shapes and sizes. The press and blow process was originally developed for wide mouth containers (i.e. jars) and was later refined in the late 1960's to produce narrow neck containers employing the narrow neck press and blow (NNPB) process, which produced lightweight containers.

The feeder and forehearth technology advancement in the last twenty years in the IS machine has also assisted in the achievement of better glass container dimensional tolerances. This is seen in the overall reduction of the wall thickness of a one-pint milk bottle in the 1950's weighing 500g having a wall thickness of 4.02 mm to a bottle in the 1990's weighing 225g with a wall thickness of 1.99 mm [9]. This showed that whilst still maintaining the original container strength, a reduction of 45% in container weight together with approximately 50% reduction in wall thickness was achieved. This allowed the achievement of better quality glass containers by optimising the forehearth and feeder operation by controlling the gob weight, glass viscosity/temperature and glass temperature homogeneity. The selection of the glass composition is vital to the smoothness of the pressing operation because the glass has to be supple enough without needing high gob temperatures. Hence increasing the glass container quality. The accuracy of the gob weight has to be within plus or minus one quarter of one percent or better for the production of large containers (>400 g). This is to produce a good final quality container. The variation in gob weight can be caused by:

a) Temperature variance in the glass

b) "Alien" additions in the glass

c) Unstable feeder drive movement

d) Cyclic weight variance

Gob temperature homogeneity is important in achieving a satisfactory gob weight for the production of high quality glass containers of a particular size.

1.1 Blow and blow process

The blow and blow container forming process is illustrated in Figure 1.2 on page 19. The force of the gravity causes a gob of molten glass to drop from the deflectors of the delivery equipment into the blank mould. Under the force of its weight the gob is packed into the blank mould cavity and into the neck ring to shape the needed container "finish" to enable the closure system to be used. This is called the "counter-blow". A tiny opening is left when the plug in the neck ring is removed. Through this opening compressed air is blown shaping the gob into the parison 'preform'. The semi-solid parison carried by the finish is then inverted for the second forming stage. The blow mould halves close to support the parison. This enables the neck ring to open and return to the blank side in order to start the next forming cycle. The blow mould is covered by the blow head, which enables compressed air to blow the parison to its final form. The container is then removed by a set of 'tongs' via the take out mechanism. This container is placed on an air cooled dead plate then onto a belt to be annealed in a lehr. The annealing process reheats the containers and then slowly cools them down. This relieves the residual stresses from the glass container hence increasing container strength.

The glass container formation process relies on the corresponding temperature and viscosity of the molten glass. Sufficient heat must be removed in the blank mould stage from the outer layer of the parison to form a skin. This leaves it in a semi-solid state to facilitate invert. This process also needs the parison's cooled

outer layer to reheat sufficiently from within to facilitate its blowing to the final form. The blow and blow process is advantageous as it is capable of producing containers having various sizes and shapes. It also has higher impact strength hence a longer life span and high durability in returnable containers [10]. One of the difficulties encountered by this process is the inconsistent distribution of glass within the final container. This is caused by the compressed air taking the easiest route during blowing the parison. Uneven glass distribution will result, which can have a wall thickness ratio of about 2:1 (thickest to thinnest). The resulting unevenness in glass distribution in the sidewall of a container does not allow light weighting because of the performance criteria (i.e. strength). This limits the container's weight reduction and raises the production cost as approximately 33% of this cost is attributed to the energy intensive glass melting process [11]. This increase in cost adds to the increase in the transportation and handling cost. The blow and blow process also has a slow production rate. This is caused by the poor conduction of heat by the air bubble within the parison. Hence the air bubble does not extract much heat from the glass [12]. This restricts the cooling effect on the molten glass and consequent shaping of the semi-solid parison skin ready for the invert and parison blowing stage. This restriction increases the glass container production time.

1.2 Narrow Neck Press and Blow (NNPB) Process

The press and blow container forming process is shown in Figure 1.3 on page 20. As with the blow and blow process the gob of glass falls into the blank

mould under the force of gravity. It is forced down onto the tip of the plunger. The baffle then seats on top of the blank mould and the plunger then presses upwards and into the gob distributing the hot glass within the blank mould cavity. This pressing motion ceases when the molten glass takes up the resulting spare volumetric displacement within the equipment. Baffle is removed prior to the blank mould halves opening and the parison is inverted for the second forming stage. The blow mould halves then close around the parison supporting it under the finish. The neck ring mould allows the parison to be inverted. The neck ring then opens and is reverted to the blank side ready to commence the forming cycle. The blow head then covers the blow mould, blowing the parison to its final finished form. When the blow mould opens, a pair of 'tongs' removes the container via the take out mechanism. The container is placed onto an air cooled dead plate prior to being sent to the lehr on a conveyer belt for heat treatment. The various positions of the plunger during the forming process are shown in Figures 1.4 to 1.6 on pages 20 and 21.

The major difference between the press and blow and blow and blow process is the employment of the plunger in the former to produce the parison. The Figure 1.7 on page 22 shows a few narrow glass neck containers. Doyle [13] reported that the blow and blow process produced 152 300g containers per minute and the press and blow process produced 168 containers using an eight section double gob machine. Doyle explained that 192 300g containers could be produced per minute with an increase of 26% if it is produced by the press and

blow process taking into consideration its weight reduction due to the even glass distribution. The narrow neck press and blow (NNPB) process was developed in the late 60's to maximise the effectiveness of the press and blow process which had been originally developed to produce food jars. The NNPB process produced lightweight containers having thin walls and closer dimensional tolerances allowing a reduction in the blow and blow container weight by 15%-30% [10]. Accompanying this there is an increase of between 15%-25% in production speeds [10]. Up to that period containers were produced with inherent disadvantages like inconsistent mould cooling, weight reduction limitations due to inconsistencies in the radial wall thickness and poor dimensional quality by the blow and blow process [10]. Development in the glass container industry has been focused on the increment in production speed and container weight diminution [14,15]. The need to increase container strength in step with container light weighting is paramount to the competitiveness of glass containers in the packaging industry [16].

Process	Advantages	Disadvantages
Blow and Blow Process	1. High impact strength	1. Inconsistent finish quality
	2. Strong enduring reusable containers	2. Uneven glass distribution.
		3. Limited weight reduction
	3. Longer life span in reusable containers	4. Limited manufacturing speed

Table 1. Advantages and disadvantages of the Blow and Blow Process

Process	Advantages	Disadvantages
Narrow Neck Press and Blow Process	1. Containers with thin walls	1. Severe wear on plunger surface
	2. Containers with closer dimensional tolerances	2. Finish container defect
	3. Reduction in gob weight	3. Extended job change set up time.
	4. Increase in production speed	

Table 2. Advantages and disadvantages of the Narrow Neck Press and Blow Process

The advantages and disadvantages of both the Blow and Blow and Narrow Neck Press and Blow Processes are shown in Tables 1 and 2. Cost of mould equipment has risen because it is under increased demand to perform more efficiently as production speeds rise and container flaw rates drop. Ensor [17] informed that the cost of the mould equipment has risen from 2% of the production cost in 1960 to 5% in 1970. Sidler [18] reported that the cost had risen to 9.7% in 1988. The required mould material properties as explained by Ensor below are based on the assumption that the principle mould equipment material is grey cast iron.

a) Density or homogeneity

b) High wear resistance

c) Capable of producing a good surface finish

d) High resistance to oxidation

e) Resistance to thermal checking

f) High graphite particle distribution

g) Low thermal expansion

h) High thermal conductivity

i) Good machinability

j) Resistance to growth

Cast iron has remained the principal mould equipment material although it causes some difficulties brought about by the extreme thermal demands of the forming cycle. The mould tooling has to be capable of performing continuous cycles in contact with hot abrasive glass at temperatures of 1000°C to 1200°C and also be exposed to flowing cool air over the freshly heated surface. Angus [19] informed that the general material composition of grey cast iron glass mould tooling equipment consisted of 3.5-3.77% Carbon, 1.6-2.3% Silicon, 0.45-0.65% Manganese, <0.12% Sulphur and <0.35% Phosphorous together with 0.15-0.25% Titanium. This composition in its fully annealed ferritic form can withstand cracking. If it is annealed to a spheroised pearlite structure then it offers strong opposition to wear and cracking. Ensor [20] explained in detail the different elements that influence the performance of the mould, resistance to dimensional alterations, thermal shock resistance, resistance to oxidation and resistance to surface cracking. The influences of alloy elements (i.e. molybdenum, chromium and vanadium) were discussed by Ensor and the composition of a general iron was presented as 3.3-3.5% Carbon, 2.2-2.4% Silicon, 0.5-0.7% Manganese, <0.1% Sulphur, <0.1% Phosphorus and 0.08-

0.1% Titanium. Ensor also explained the differing thermal qualities of rough and refined grain cast irons in relation to the optimum graphite form and distribution. Ensor concluded that in order to check thermal cracking and the breakdown of the glass contact surface, an adjusted combination of refined and rough graphite form with a low thermal diffusivity is needed. Thermal diffusivity is the property describing the ability of removing heat from the contact surface at the demanded rate. The compromise between the refined and rough graphite form is achieved with the former being used at the glass contact surface whilst the latter is employed at the rear of the mould to aid cooling.

The plunger in the Narrow Neck Press and Blow (NNPB) process ensures accurate distribution of molten glass within the blank mould cavity and removes the thermal energy from the inner wall of the parison. As such the NNPB plunger (Figure 1.8 on page 22) operates both as a heat exchanger and a form tool. The NNPB plunger is made of a steel substrate having a layer of coating material machined to the needed plunger geometric shape. The thermal energy is conducted from the inner wall of the parison to the composite wall of the plunger and is then taken away by the coolant air flowing within the plunger bore. The plunger performs in severe conditions of high cyclic temperatures, thermal impact, high-speed exposure with hot molten glass and mechanical interference with the neck ring mould. The prime function of the plunger is to extract sufficient heat energy from the parison so that it can be inverted prior to the blowing stage. Compressed coolant air is passed through the plunger bore

via a cooling tube to remove the heat energy from the inner plunger wall (Figure 1.9 and 1.10 on page 23). This process also reduces the effects of the high temperatures on the plunger substrate. The process cannot function for more than a few cycles without plunger cooling. The parison must reheat sufficiently to achieve the desired final blow as the heat moves from the inner core to both the internal and external surfaces of the parison. The use of the plunger to form the parison results in micro surface discontinuities causing residual stresses on the internal surface of the NNPB manufactured containers. Annealing relieves these stresses and in so doing increases the residual strength of the containers. The stages of the container forming process are illustrated in Figure 1.11 on page 24.

The problems associated with the NNPB plungers operating under harsh conditions are its wear rates [21], which is the cause of defects in the final product, unstable thermal distribution and plunger distortion. This leads to shorter tool life and process unpredictability. The NNPB plunger works in cycling temperatures of approximately 550°C to 850°C and has sliding contact with hot abrasive glass. This results in plunger wear through abrasion and plunger material being deposited into the final container producing a weaker glass container. Incorrect plunger material preference and the ineffectiveness of the plunger cooling tube system are associated with the wear and failure modes exhibited by the NNPB plungers. There has been little advance made in the type of materials employed for plungers. The NNPB plunger investigated during

this study employed a plain carbon steel substrate as preferred to the cast iron first used when the process was developed. A current leading manufacturer of plungers in the U.K has reported that at present cast iron based plungers are hardly manufactured [22]. Cast iron was used extensively before [19] because of its easy machinabililty, low cost, acceptable thermal properties and some rectification of its defects [23-25]. Demands on the thermal capacity of cast iron have increased tremendously in line with an increase in manufacturing speeds. The hallmark of good mould equipment is its thermal diffusivity. This leading plunger manufacturer concluded that steel had better thermal properties than cast iron from tests carried out at a university in the North East of England. Steel was also found to offer better cost benefit, machinability and coating adhesion. When re-sprayed or modified cast iron plungers also experienced problems in wall thickness due to its expansion rates.

Current plungers are manufactured from plain carbon steel (EN 8, EN 362 and EN 351), hardened by flame sprayed nickel based powder alloy (Colmonoy) and more recently High Velocity Oven Fused (HVOF) spray coated tungsten carbide. The nominal compositions of the plain steel substrates EN 8, EN 362 and EN 351 are specified in Table 3 on page 13. Currently tungsten carbide coatings are being used more than the nickel base materials having a varied 40 to 60RC hardness as container manufacture process speeds up. These tungsten carbide coatings give better quality glass containers and prolong the plunger working life. Presently developed tungsten carbide powder contains

refine-diffused carbides offering greater performance to the previous powders having rough carbides.

	Element	Mass (%)
BS 970:080 – M40 (EN 8)	C	0.36/0.44
	Si	0.1/0.4
	Mn	0.6/1
	P	0.05
	S	0.05
BS 970:805 – A20 (EN 362)	C	0.18/0.23
	Si	0.15/0.35
	Mn	0.7/0.9
	P	0.035
	S	0.04
	Cr	0.4/0.6
	Mo	0.15/0.25
	Ni	0.4/0.7
BS 970:635 – M15 (EN 351)	C	0.12/0.18
	Si	0.1/0.4
	Mn	0.6/0.9
	P	0.04
	S	0.05
	Cr	0.4/0.8
	Mo	0.1
	Ni	0.7/1.1

Table 3. Different plunger substrate material

This causes the wear resistant particles to be better sustained by the matrix and resistant to abrasion by the hot molten glass. Other coating materials have been successfully employed, but only perform satisfactory in a less taxing environment than the NNPB plunger. The employment of the coating material and its blending to the plunger substrate are decisive quantities in porosity development. The leading defect in the present "moderate standard" plunger coating materials is the existence of porosity, which is damaging to the coatings' capability. This causes the primary defects experienced by the NNPB plungers like elevated wear proportions, plunger distortion and plunger material being deposited into the final product. The most prominent failure of the NNPB plunger is the deposit of plunger material into the glass, usually known as "black speck". This critical defect greatly reduces the mechanical properties of the container [26-29]. This problem was overcome by using thin film coatings with a high room temperature hardness, which are widely used on metal working tools. These coatings have a convincing short-term performance when used with a suitable substrate [30,31] but produces less satisfactory results when used together with a cast iron substrate. These materials must resist approximately half a million thermal and mechanical loading cycles, as it is not easily resurfaced.

Current plunger difficulties related to the substrate and coating material also contributed to a build up of an oxide layer on the internal surface of the plunger [32]. The wet compressed air flowing within the plunger cooling tube system

further exacerbated this problem. This oxide layer prevents adequate plunger cooling hence contributing to the machine down time, process unreliability and disappointing final product quality. The loading experienced by the plunger materials caused by the rapid thermal cycling process has not been thoroughly investigated [31] and the preferred plunger materials chosen depending on room temperature and mechanical properties is unconvincing. Earlier trials to increase the NNPB plunger working life have also not closely investigated the process performance attributes and its harsh practical environment. The effect of the cyclic character of the thermal cycle is shown [32] to influence both the plunger coating and substrate structure. This indicates that ageing does occur primarily during a thermal cycle having a structural transformation. This ageing increases ductility and the ability of the plungers to bend during operation if the mechanism was poorly aligned. The Kirkendall effect and the mutual interdiffusion at the coating/substrate interface [33] causing empty lattice areas and fine porosity could affect nickel based coating materials on iron based substrates which suffer from ageing. There is a possibility that unpredictable coating response and local softening of the plunger material could be linked to structural transformations taking place within the plunger operating temperature range. The capability of these coating/substrate systems to resist continuous thermal and mechanical loading must be a development prerequisite when developing this system. This needs a deep understanding of the thermal and mechanical interaction characteristics at the glass/tool interface.

Closer investigation of the plunger surface has ascertained a "hertzian" [34,35] type of sliding contact causing subsurface weakness. This extraction of plunger material sticks to the inside surface of the glass container during the blow stage operation process [36] leading to three important considerations:

a) The NNPB manufactured containers have lower impact resistance

b) The corrupted glass container loses its inertness

c) Noticeable visible defects in remote situations

Lost of plunger material (i.e. craters) and critical container defects like spikes and black specks are caused by the present plunger material (i.e. EN 8 with Colmonoy coating) defectiveness [37,38]. These defects are the result of plunger material being gouged out during the forming process and adhering to the glass causing the production of poor quality containers. This situation is associated to the process temperatures and material phase evolvement. This condition arises because of the thermal cycling taking place during the forming process. The lost of plunger material is partly attributed to the variation in plunger temperature [32,39] along its length (annular rings forming at various sections of the plunger). This clearly indicates that the plunger cooling tube system is operating inefficiently. Hence this causes the ineffective coolant air extraction of the thermal energy, which is transferred from the glass contact surface to the plunger wall by conduction. Preliminary work [40-47] using computational fluid dynamics (CFD) modelling and examination of coolant airflow within the plunger show that the recirculation and choking of the airflow

pattern within the bore corresponds to the areas of poor plunger cooling. This condition is caused by eddies that are formed at various points between the plunger bore and cooling tube resulting in stagnation points.

Currently there is no scientific approach when designing the plunger cooling tube system i.e. size and distribution of radial cooling tube holes, taper dimensions etc. Hence it would be beneficial to explore the full potential of the plunger cooling tube system by further investigating the size and distribution of cooling tube holes, which influences the coolant air circulation. The cooling tube geometry must be designed to optimise the plunger cooling tube system. Hence improving the performance of the container forming process by achieving the required parison profile and temperature for an efficient container product.

1.3 Aims and objectives of the investigation

The effectiveness of the plunger cooling tube system (i.e. cooling tube design) is the removal of sufficient thermal energy as this greatly affects the final container quality and geometry. Model experimentation of the plunger cooling tube system carried out to date have been limited [40,48] but is indicative of the advantages in exploring the full potential of this system.

The aims of this investigation into the plunger cooling tube system design for the NNPB process are to predict a more efficient heat transfer system allowing

a uniform temperature distribution along the plunger surface, increasing tool life and eliminating container defects.

The objectives of this investigation are to assess the cooling tube design, optimise the heat transfer efficiency of the plunger cooling tube system and to allow for an even temperature distribution along the plunger surface. The objectives of this investigation will be accomplished by carrying out the following:

- Design and development of the plunger and cooling tube test rig together with associated experimental work to establish the boundary conditions i.e. airflow velocity and pressure.
- The measurement of the temperature distribution along the plunger and parison surface after the parison forming stage using the thermal imaging technique.
- Investigation of the airflow distribution into the cooling tube of the NNPB plunger using the computational fluid dynamics (CFD) technique with the 2D, axisymmetric and 3D models.

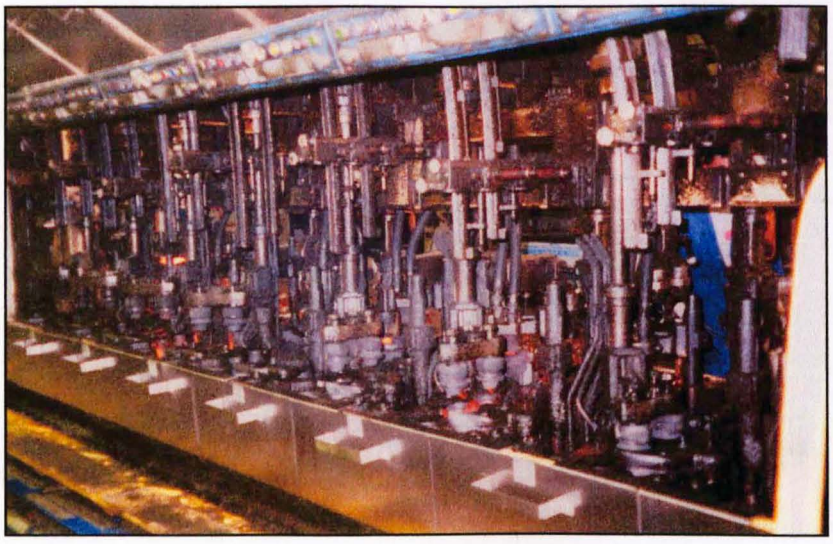

Figure 1.1. IS Machine

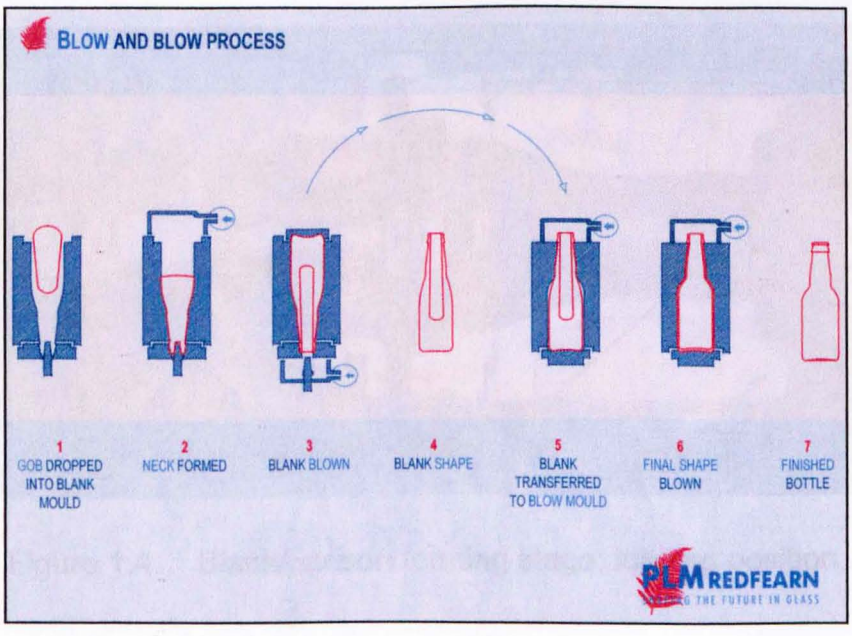

Figure 1.2. Blow and Blow Process

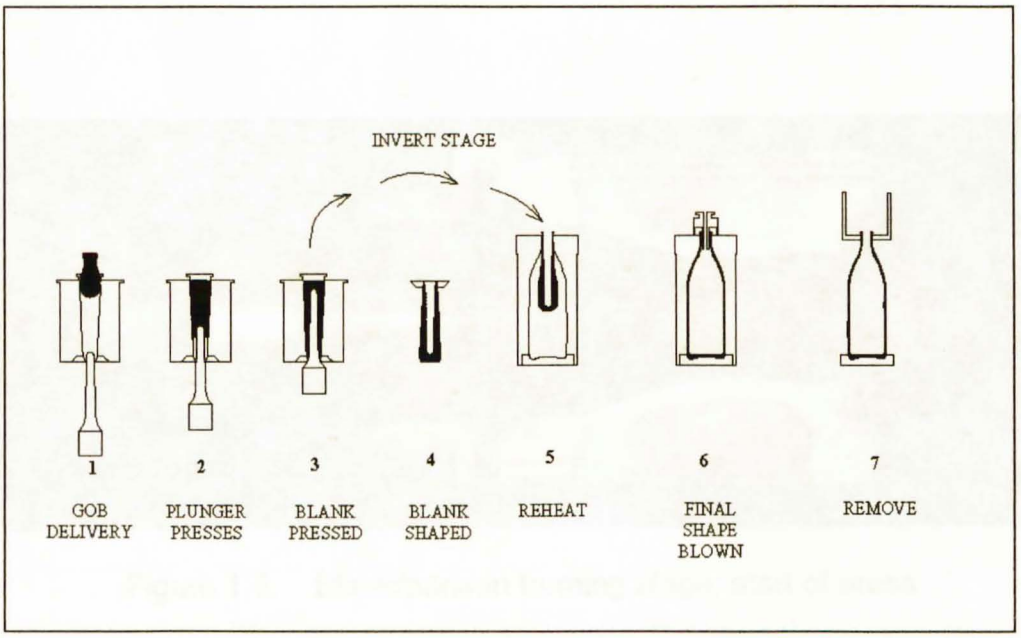

Figure 1.3. Narrow Neck Press and Blow (NNPB) Process

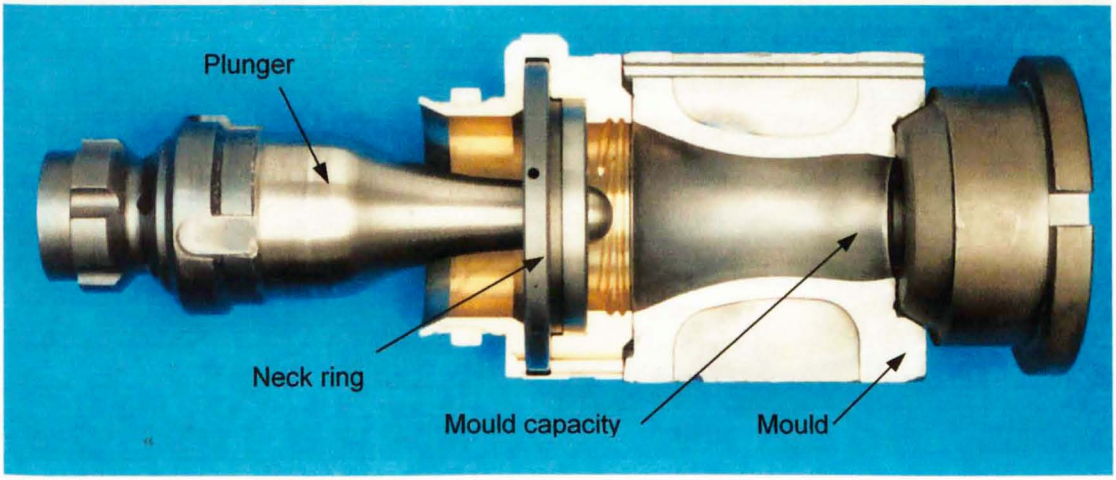

Figure 1.4. Blank/parison forming stage; loading position

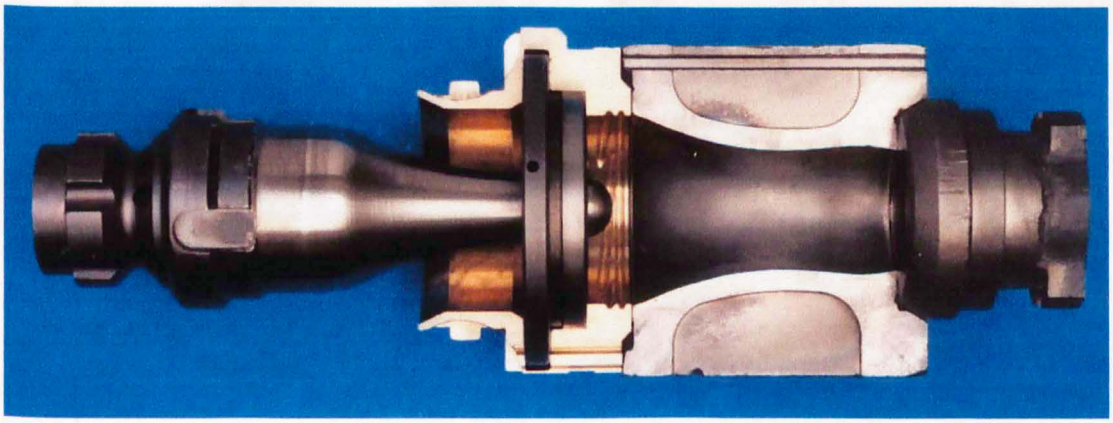

Figure 1.5. Blank/parison forming stage; start of press

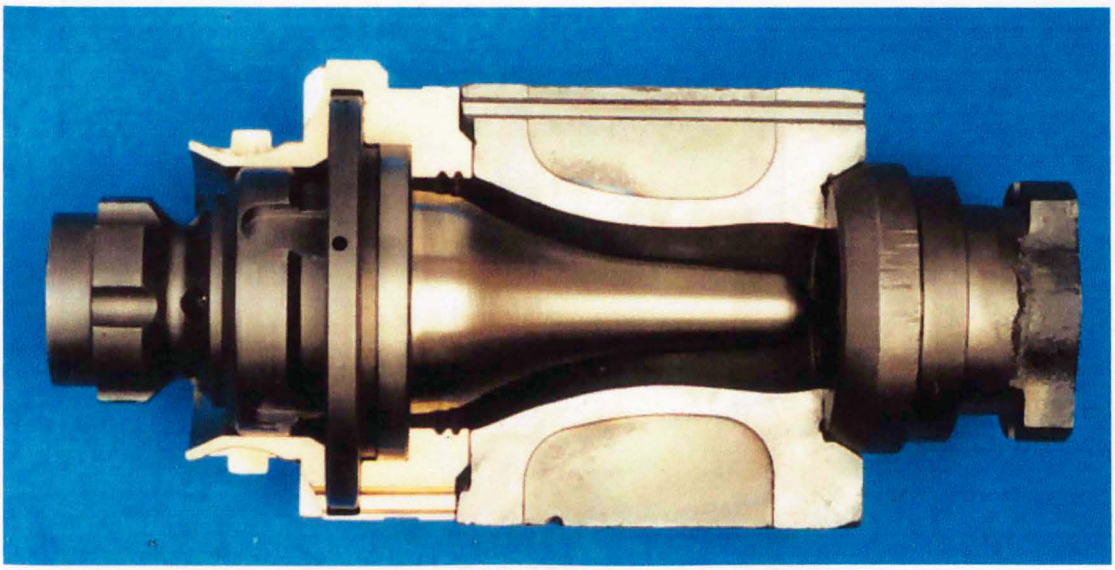

Figure 1.6. Blank/parison forming stage; end of press

Figure 1.7. Narrow neck glass containers

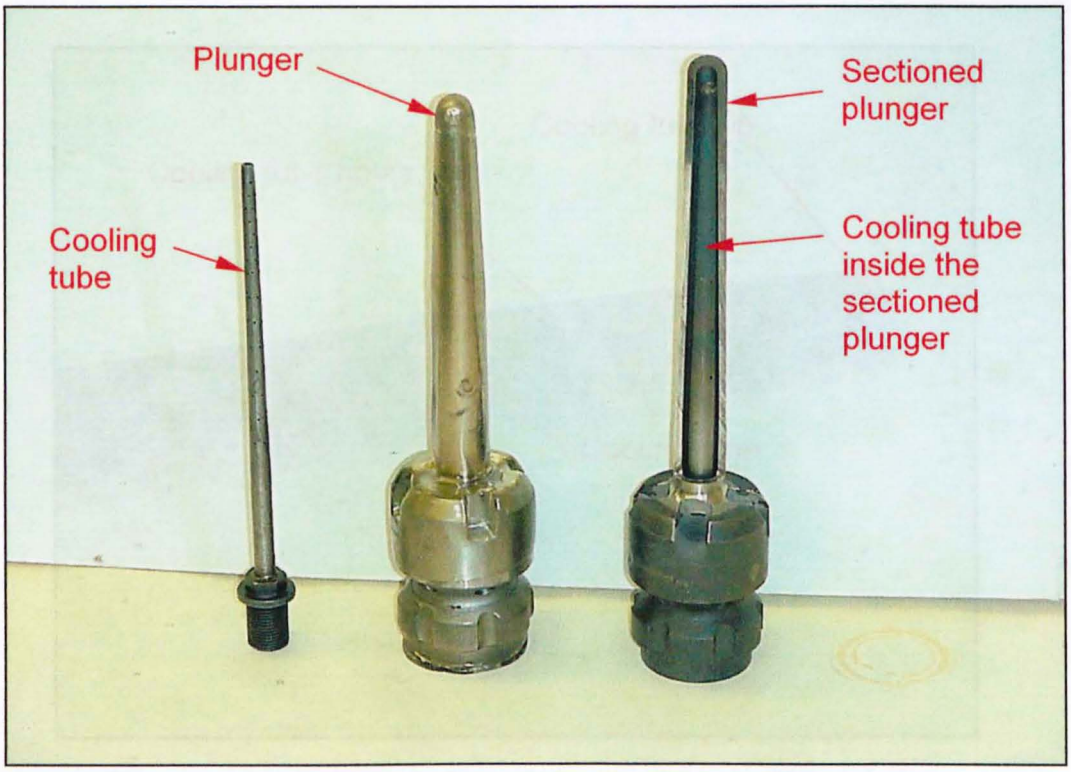

Figure 1.8. The Narrow Neck Press and Blow (NNPB) plunger

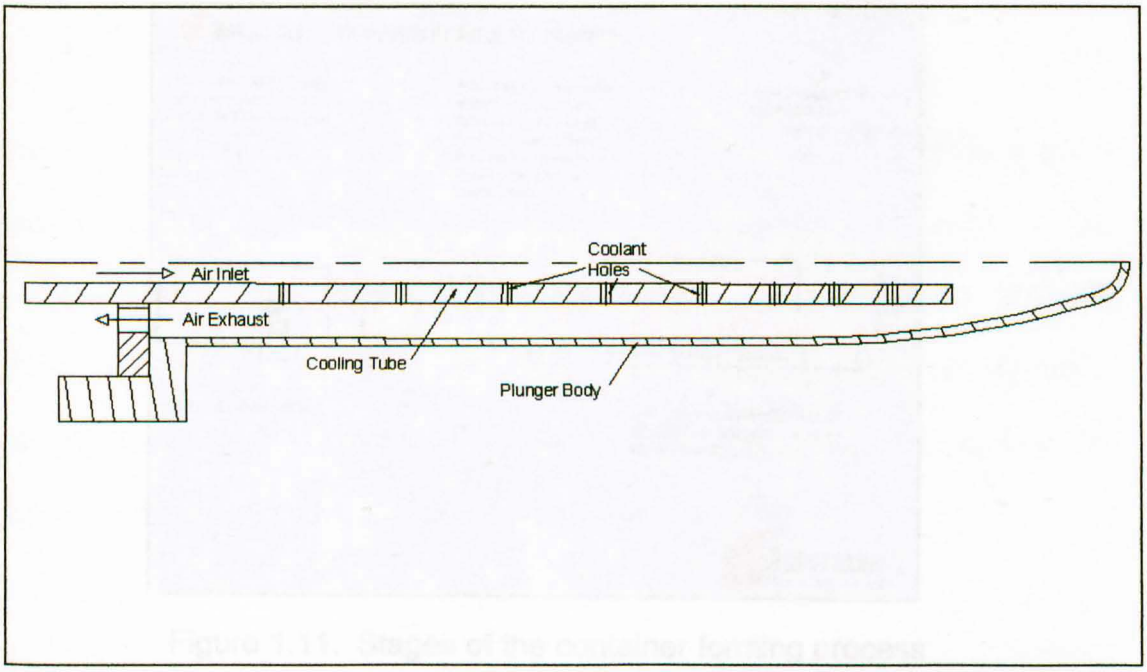

Figure 1.9. Cross section of a typical NNPB plunger and cooling tube

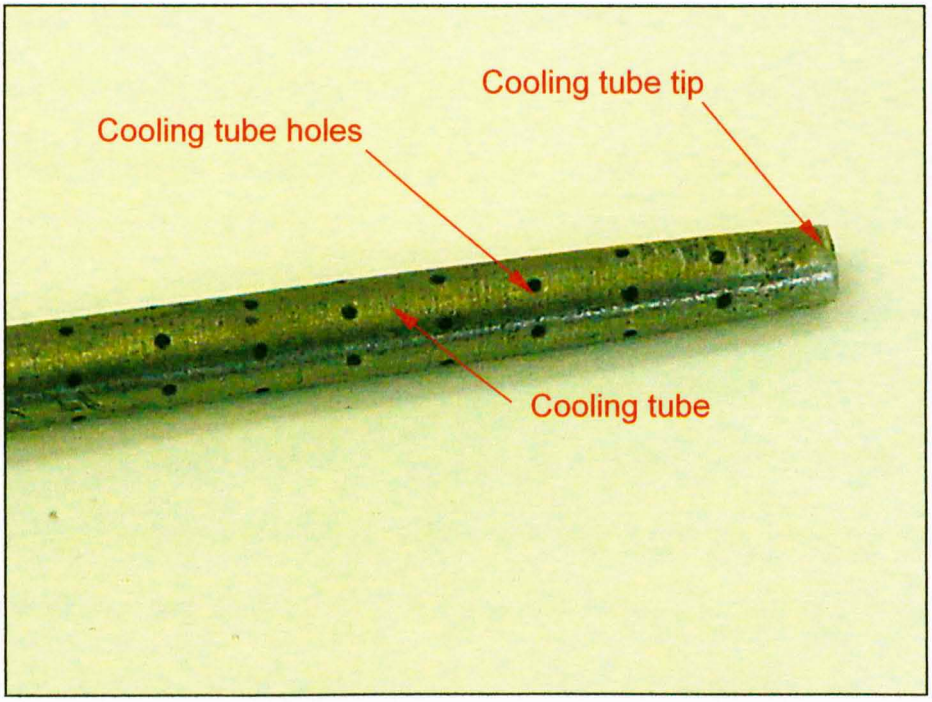

Figure 1.10. Enlarged view of the tip of the cooling tube

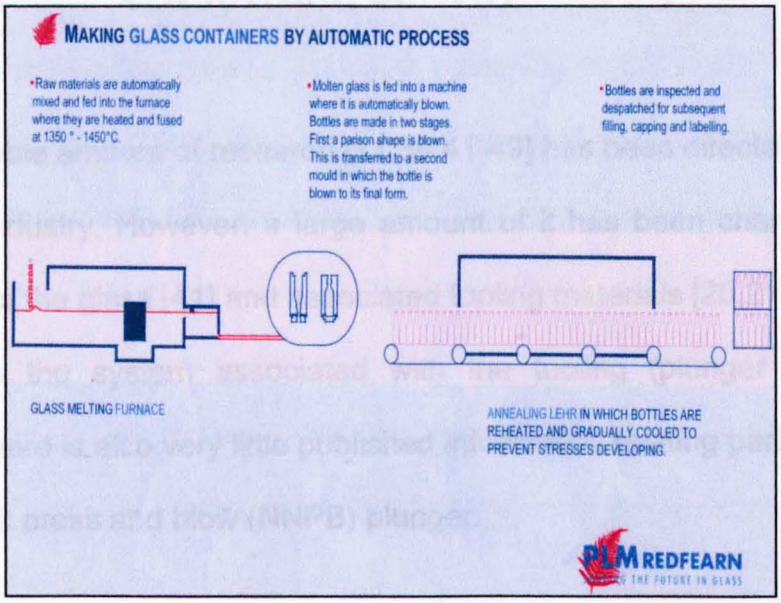

Figure 1.11. Stages of the container forming process

Chapter 2 LITERATURE SURVEY

A considerable amount of research [21,39,41-49] has been directed to the glass container industry. However, a large amount of it has been channelled to the properties of the glass [41] and associated tooling materials [20,21,32,39,50-54] rather than the system associated with the tooling (plunger cooling tube system). There is also very little published information relating particularly to the narrow neck press and blow (NNPB) plunger.

Trier [55,56] reports the possibility of using water as an alternative medium to compressed air for the plunger cooling tube system and the difficulties encountered. Seidel [49,57] identifies the prominent role of the plunger in producing lightweight containers and process monitoring of the cyclic operation to increase production efficiency.

The quest for super light weight containers and the push for higher production rates is due to the increasing cost of raw materials. Cerbone and Alvigi [51] stressed the importance of producing a durable plunger to achieve this quest. It was strongly implied that plunger characteristics such as plunger material, coatings and plunger defects have to be continuously researched in order to improve and produce high quality NNPB plungers.

Kent [58] stresses the importance of effectively controlling the forming process to increase production speeds and light weighting of the ware. Kent reported that the plunger operating temperature significantly influences the heat transfer from the molten glass. Kent explains that adjusting the amount of cooling airflow into the plunger can control the heat transfer. Hence identifying that when the tool temperature increases the rate of heat transfer from the molten glass decreases. Kent also showed that the usage of lubricant in the IS machine blank mould does suppress the heat transferred from the parison.

Edgington [59] reports that apart from improving the glass composition and glass conditioning control, plunger design and material should also be given equal attention. Edgington highlighted that plunger wear and damage does contribute to a poor container finish. To overcome this anomaly, Edgington suggests that further investigation be taken into increasing the plunger cooling efficiency, comprehension of the heat transfer process and developing a detailed conception of the entire NNPB process.

Penlington, Sarwar and Armitage [48] emphasised the need to better understand and improve the efficiency of the plunger cooling tube system to prevent container defects, increase tool life and enhance process performance. Penlington, Sarwar, Marshall, Cockerham and Lewis [38] have linked the NNPB plunger performance deficiencies to the heat transfer capabilities and geometry of the plunger. Following this, the oxide residue on the inside surfaces of the

plunger is indicated as the cause of premature plunger failure and poor tool life. Penlington, Sarwar, Marshall, Cockerham and Lewis [21,39], Rawson [46], Winther and Schaeffer [47] have all identified deficiencies in the NNPB plunger performance (i.e. plunger distortion, high plunger wear rates and plunger material being deposited into the glass) and their relationship with defects in containers.

Ensor [20], Wasylyk [60] and Lubitz [61] have shown that container defects i.e. spikes and black specks can arise due to plunger material adhering to the glass causing the production of a poor quality container. This loss of material is partly attributed to the variation in plunger temperature [32,39] along its length (annular rings forming at various parts of the plunger). This clearly indicates that the plunger cooling tube system is operating inefficiently because the thermal energy that is transferred from the glass contact surface to the plunger wall by conduction, is not effectively being removed by the cooling medium within the plunger bore.

Preliminary work using computational fluid dynamics (CFD) modelling and examination of the coolant flow within the plunger have been carried out by Penlington, Sarwar and Armitage [48], Penlington and Sarwar [41], and Anon [40] and the results show that the recirculation and choking of the airflow pattern within the bore corresponds to the areas of poor cooling. This situation is

caused by eddies that are formed at various points between the plunger bore and cooling tube leading to stagnation points.

Cesar de Sa [62] demonstrated the capabilities of numerical modelling in simulating the glass forming process providing important information in improving the actual forming process (i.e. plunger and mould design, optimum pressure and blow times). Stork and Loyd [63] used a numerical model (one dimensional) to analyse the heat transfer in the plunger, glass and blank mould during parison formation of an NNPB process. It is reported that the temperature of the plunger and the blank mould at the glass contact interface does affect the temperature distribution in the parison. Hence the cooling of the mould and plunger is important.

It was emphasised by Babcock and M^{c}Graw [64] that to completely comprehend the container shaping operation, the following have to be known:

- The glass and mould metal existing temperatures and temperature time distributions during the shaping operation.
- The stress concentrating at all points in the glass during all cycle stages.
- The results exhibited on the final container (i.e. strength and physical appearance) by the temperature and forces acting on the glass during the shaping operation.

Chapter 3 DESIGN AND DEVELOPMENT OF THE PLUNGER AND COOLING TUBE TEST RIG AND EXPERIMENTAL WORK

3.1 Introduction

The laboratory experiment was devised to simulate the IS machine conditions for the plunger cooling tube system. The purpose of this experiment was to ensure that the boundary conditions (P_{out}, V_{in}) used with the CFD model would be representative of the actual working system. These boundary conditions were vital for both the ANSYS 5.4 (used for analysing the 2D and axisymmetric models) and CFX 5.3 (used for analysing the 3D model) software to proceed with the CFD mathematical modelling of the plunger cooling tube system. The laboratory experiment was carried out under room temperature. The test rig was built incorporating the plunger cooling tube system. Controlled compressed air was circulated within the plunger and cooling tube during this experiment. The compressed airflow was controlled to maintain the pressure difference values (between 0.5 bar to 3 bar) used on the shop floor.

3.2 Test rig

The experimental set-up of the plunger cooling tube system is shown in Figure 3.1 on page 30. An enlarged picture of the plunger enclosed in the casing is shown in Figure 3.2 on page 31. Figure 3.3 on page 31 shows the schematic layout of this experimental set-up. An air compressor was installed at the start

of the piping that carried the compressed air. An inlet control valve was installed at the end of this pipe. This pipe was connected with a control valve, airflow meter and pressure gauge linked with a reinforced PVC hose. This PVC hose was then installed to the inlet of the cooling tube. This connection was enclosed in the casing. The cooling tube was inserted into the plunger. An outlet was made on the casing and was installed with another reinforced PVC hose. A control valve and pressure gauge was connected to this hose. The pressure gauges and control valves were installed at both the inlet and outlet sections of the cooling tubes to maintain the current pressure difference (between 0.5 bar to 3 bar) used on the shop floor.

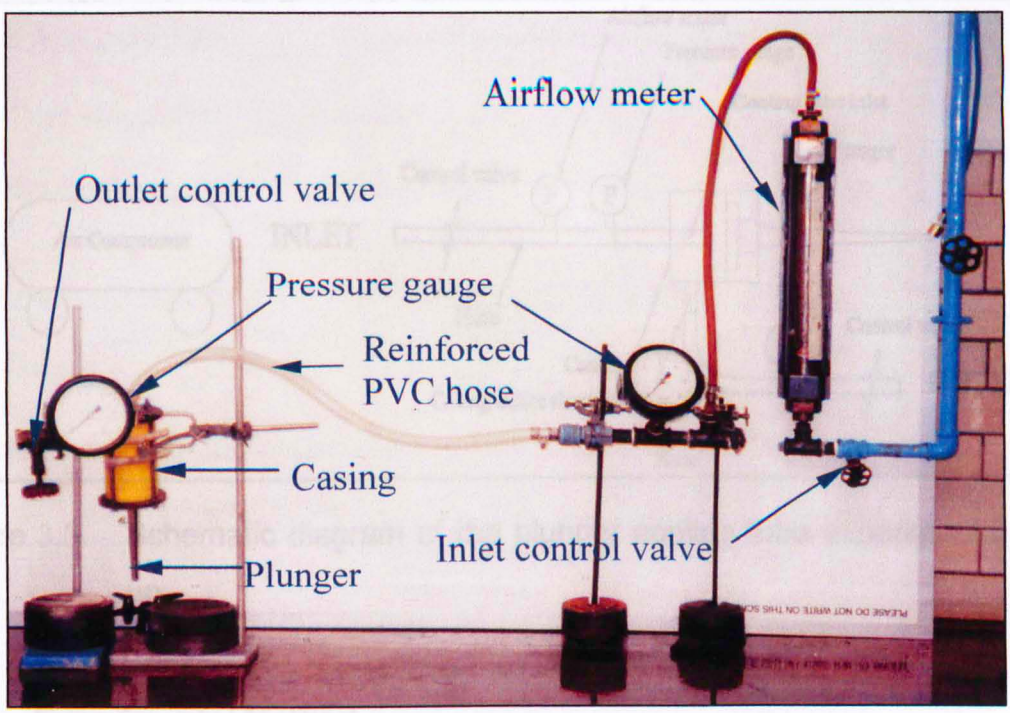

Figure 3.1. Experimental set-up of the plunger cooling tube system

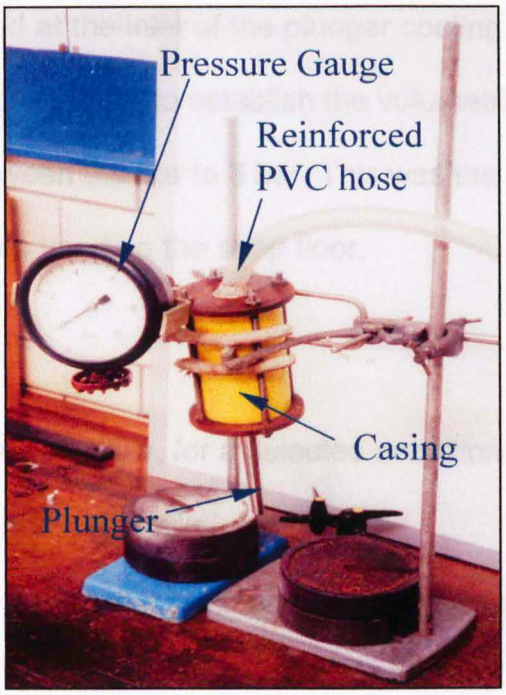

Figure 3.2. Enlarged view of the plunger cooling tube enclosed in the casing

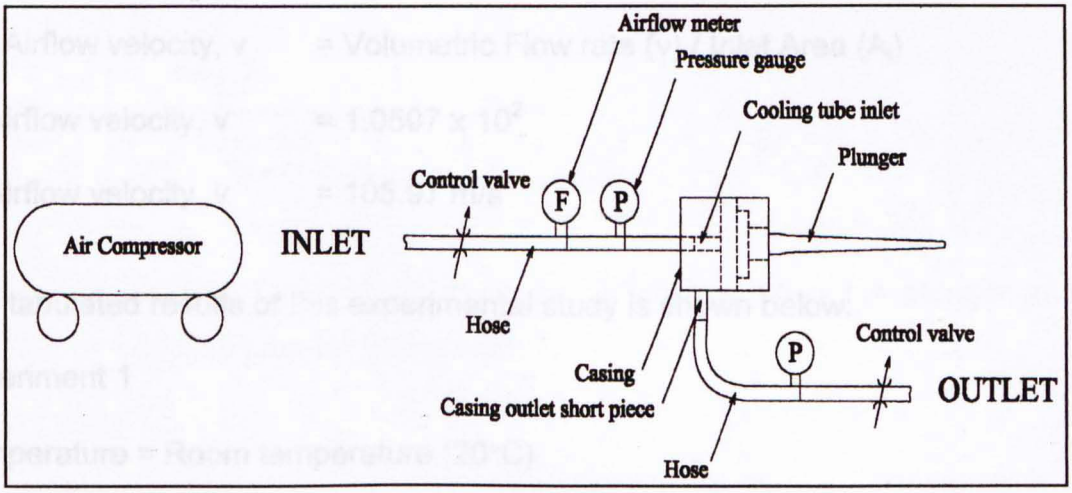

Figure 3.3. Schematic diagram of the plunger cooling tube experimental set-up

3.3 Experimental Method

The volumetric airflow into this system was measured to determine the inlet airflow velocity within the plunger cooling tube system. The volumetric airflow

meter that was installed at the inlet of the plunger cooling tube system recorded this data. Tests were carried out to establish the volumetric airflow at a pressure difference ranging between 0.5 bar to 3 bar. This was the actual compressed air pressure range that was used on the shop floor.

3.4 Results

Determining the airflow velocity v, for a selected condition: -

Volumetric airflow, $\dot{v}= 2.8 \times 10^{-3}$ m^3/s

Inlet pressure P_{in} =1.5 bar; Outlet pressure P_{out} =0.4 bar; Inlet diameter $D_i = 5.8 \times 10^{-3}$ m

Volumetric airflow, $\dot{v}$ = Inlet Area (A_i) x Airflow velocity (v)

$\therefore$ Airflow velocity, v = Volumetric Flow rate ($\dot{v}$) / Inlet Area (A_i)

Airflow velocity, v = 1.0597×10^2

Airflow velocity, v = 105.97 m/s

The tabulated results of this experimental study is shown below:

Experiment 1

Temperature = Room temperature (20°C)

For a given exit pressure, i.e. P_{out} = 0 bar

$\Delta P = P_{in} - P_{out}$ where

ΔP = Difference between the inlet pressure and outlet pressure
P_{in} = Inlet pressure (bar)
P_{out} = Outlet pressure (bar)

P_{in} (bar)	Actual P_{out} (bar)	ΔP (bar)	Volumetric airflow (10^{-3} m^3/s)	Airflow velocity (m/s)	Remarks
0.5	0.0	0.5	2.0	75.7	
1.0	0.2	1.0	2.45	92.73	Outlet c/valve fully open
1.5	0.4	1.5	2.8	105.97	``
2.0	0.6	2.0	3.1	117.33	``
2.5	0.7	2.5	3.35	126.79	``
3.0	1.0	3.0	3.58	135.5	``

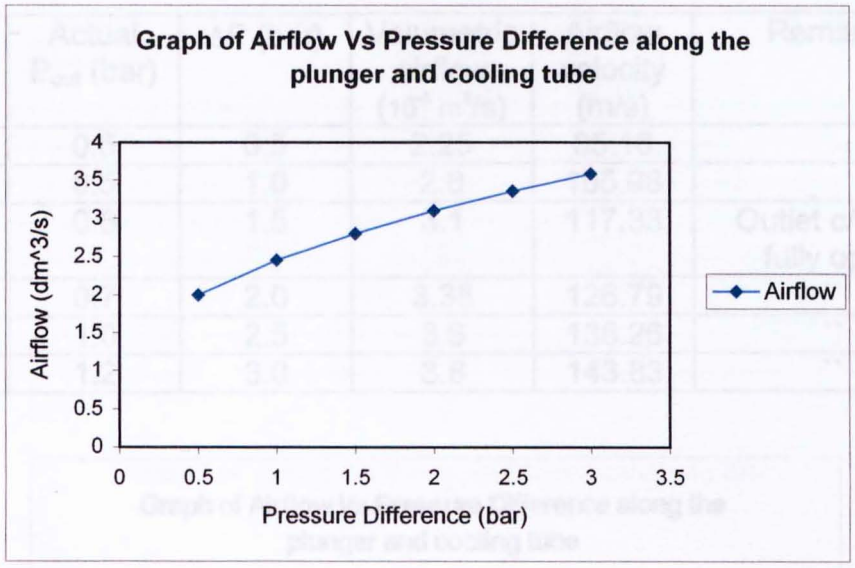

Figure 3.4. Graph of Airflow Vs Pressure Difference along the plunger and cooling tube for Experiment 1.

Experiment 2

Temperature = Room temperature (20°C)

For a given exit pressure, i.e. P_{out} = 0.5 bar

$\Delta P = P_{in} - P_{out}$ where

ΔP = Difference between the inlet pressure and outlet pressure
P_{in} = Inlet pressure (bar)
P_{out} = Outlet pressure (bar)

P_{in} (bar)	Actual P_{out} (bar)	ΔP (bar)	Volumetric airflow (10^{-3} m^3/s)	Airflow velocity (m/s)	Remarks
1.0	0.5	0.5	2.25	85.16	
1.5	0.5	1.0	2.8	105.98	
2.0	0.6	1.5	3.1	117.33	Outlet c/valve fully open
2.5	0.7	2.0	3.35	126.79	``
3.0	1.0	2.5	3.6	136.26	``
3.5	1.2	3.0	3.8	143.83	``

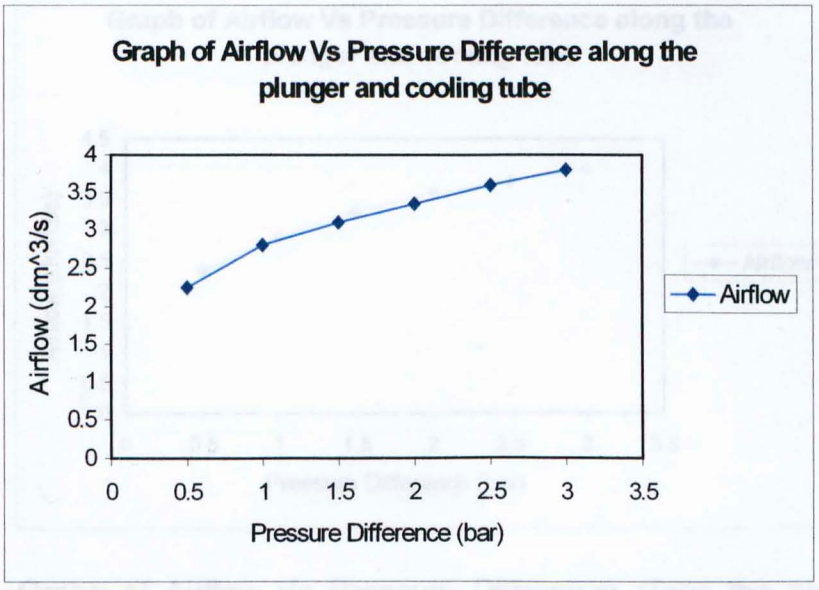

Figure 3.5. Graph of Airflow Vs Pressure Difference along the plunger and cooling tube for Experiment 2.

Experiment 3

Temperature = Room temperature (20°C)

For a given exit pressure, i.e. P_{out} = 1.0 bar

$\Delta P = P_{in} - P_{out}$ where

ΔP = Difference between the inlet pressure and outlet pressure
P_{in} = Inlet pressure (bar)
P_{out} = Outlet pressure (bar)

P_{in} (bar)	Actual P_{out} (bar)	ΔP (bar)	Volumetric airflow (10^{-3} m^3/s)	Airflow velocity (m/s)	Remarks
1.5	1.0	0.5	2.33	88.19	
2.0	1.0	1.0	2.9	109.76	
2.5	1.0	1.5	3.3	124.9	
3.0	1.0	2.0	3.6	136.26	
3.5	1.2	2.5	3.8	143.83	Outlet c/valve fully open
4	1.4	3.0	4.0	151.4	``

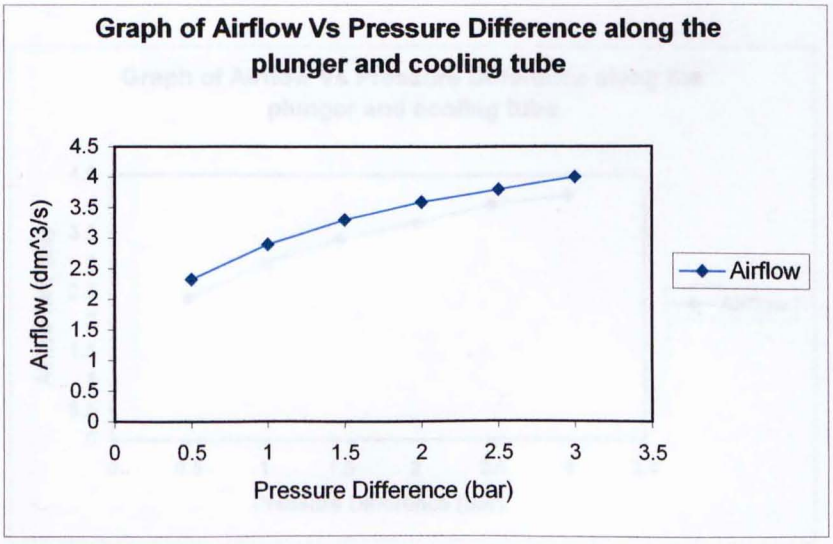

Figure 3.6. Graph of Airflow Vs Pressure Difference along the plunger and cooling tube for Experiment 3.

Experiment 4

Temperature = Room temperature (20°C)

For a given exit pressure, i.e. P_{out} = 1.5 bar

$\Delta P = P_{in} - P_{out}$ where

ΔP = Difference between the inlet pressure and outlet pressure
P_{in} = Inlet pressure (bar)
P_{out} = Outlet pressure (bar)

P_{in} (bar)	Actual P_{out} (bar)	ΔP (bar)	Volumetric airflow (10^{-3} m^3/s)	Airflow velocity (m/s)	Remarks
2.0	1.5	0.5	2.4	90.84	
2.5	1.5	1.0	3.0	143.83	
3.0	1.5	1.5	3.43	129.82	
3.5	1.5	2.0	3.7	140.04	
4	1.5	2.5	4.0	151.4	
4.5 (4.3)	1.5	3.0	4.15	157.07	Inlet valve fully open. Press=4.3 bar

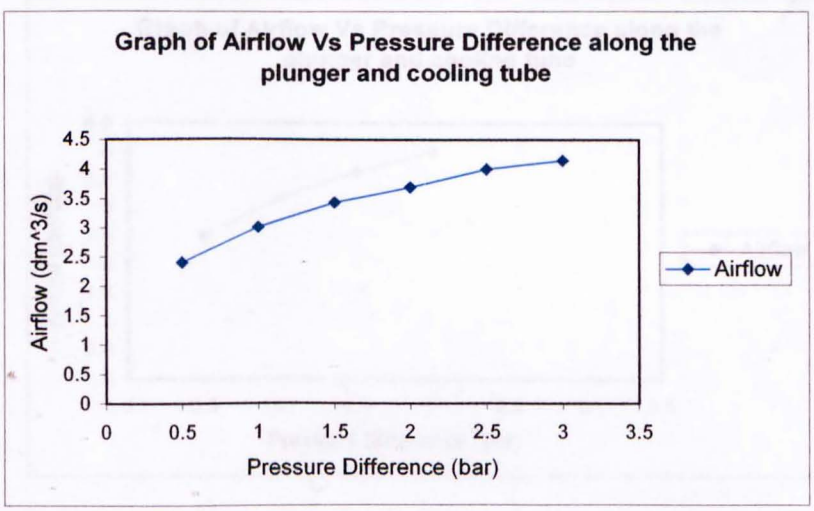

Figure 3.7. Graph of Airflow Vs Pressure Difference along the plunger and cooling tube for Experiment 4.

Experiment 5

Temperature = Room temperature (20°C)

For a given exit pressure, i.e. P_{out} = 2.0 bar

$\Delta P = P_{in} - P_{out}$ where

ΔP = Difference between the inlet pressure and outlet pressure
P_{in} = Inlet pressure (bar)
P_{out} = Outlet pressure (bar)

P_{in} (bar)	Actual P_{out} (bar)	ΔP (bar)	Volumetric airflow (10^{-3} m^3/s)	Airflow velocity (m/s)	Remarks
2.5	2.0	0.5	2.5	94.62	
3.0	2.0	1.0	3.15	119.22	
3.5	2.0	1.5	3.58	135.5	
4	2.0	2.0	3.9	147.61	
4.5 (4.4)	2.0	2.5	4.1	155.18	Inlet valve fully open. Press=4.4 bar
5 (4.4)	2.0	3.0			``

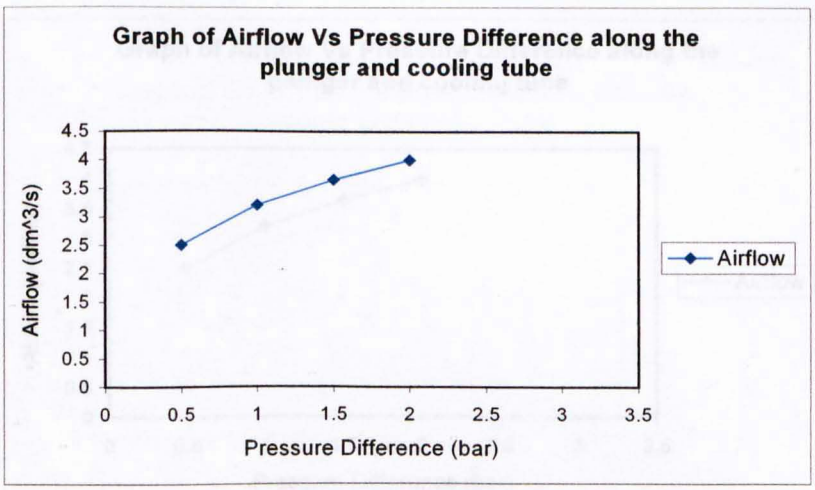

Figure 3.8. Graph of Airflow Vs Pressure Difference along the plunger and cooling tube for Experiment 5.

Experiment 6

Temperature = Room temperature (20°C)

For a given exit pressure, i.e. P_{out} = 2.5 bar

$\Delta P = P_{in} - P_{out}$ where

ΔP = Difference between the inlet pressure and outlet pressure
P_{in} = Inlet pressure (bar)
P_{out} = Outlet pressure (bar)

P_{in} (bar)	Actual P_{out} (bar)	ΔP (bar)	Volumetric airflow (10^{-3} m^3/s)	Airflow velocity (m/s)	Remarks
3.0	2.5	0.5	2.5	94.62	
3.5	2.5	1.0	3.2	121.12	
4	2.5	1.5	3.65	138.15	
4.5 (4.5)	2.5	2.0	4.0	151.4	Inlet valve fully open. Press=4.5 bar
5 (4.5)	2.5	2.5			``
5.5 (4.5)	2.5	3.0			``

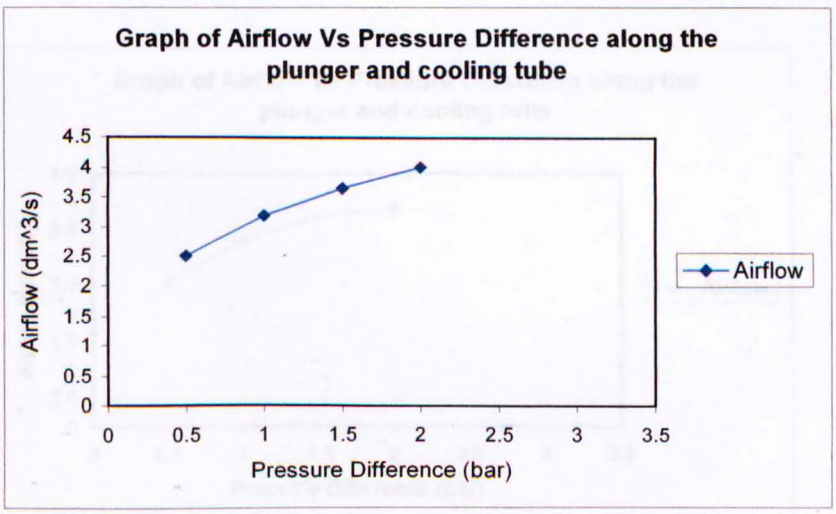

Figure 3.9. Graph of Airflow Vs Pressure Difference along the plunger and cooling tube for Experiment 6.

Experiment 7

Temperature = Room temperature (20°C)

For a given exit pressure, i.e. P_{out} = 3 bar

$\Delta P = P_{in} - P_{out}$ where

ΔP = Difference between the inlet pressure and outlet pressure
P_{in} = Inlet pressure (bar)
P_{out} = Outlet pressure (bar)

P_{in} (bar)	Actual P_{out} (bar)	ΔP (bar)	Volumetric airflow (10^{-3} m^3/s)	Airflow velocity (m/s)	Remarks
3.5	3.0	0.5	2.55	96.51	
4.0	3.0	1.0	3.3	124.9	
4.5	3.0	1.5	3.75	141.93	
5.0 (4.7)	3.0	2.0	3.9	147.61	Inlet valve fully open. Press=4.7 bar
5.5 (4.7)	3.0	2.5			``
6.0 (4.7)	3.0	3.0			``

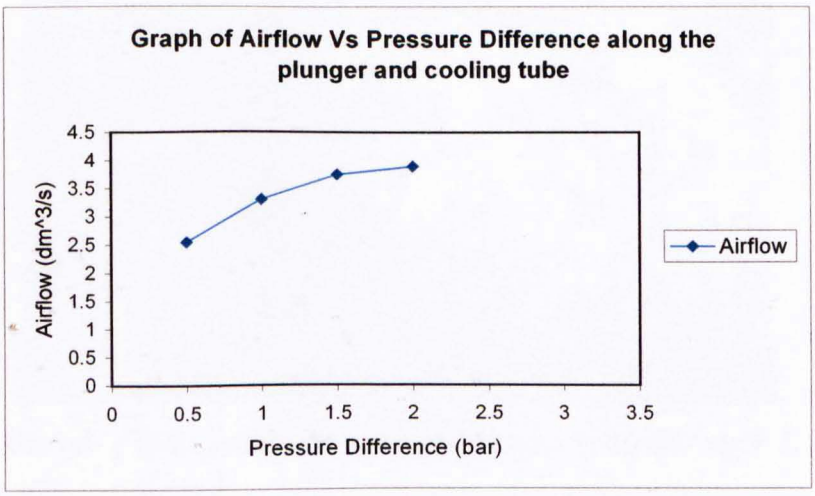

Figure 3.10. Graph of Airflow Vs Pressure Difference along the plunger and cooling tube for Experiment 7.

3.5 Observation

The laboratory experiments showed that some of the exit pressure could not be maintained as specified in the experimental layout. For example, in experiment 1, the exit pressure of 0 bar could not be achieved for the inlet pressure range of 1 to 3 bar. This was with the outlet control valve fully open. The same was experienced with experiment 2 and 3. In experiments 4 to 7, the inlet pressures of between 4.5 bar to 6 bar could not be achieved. This was with the inlet control valve being fully open.

The airflow velocity was calculated from data (i.e. experiment 1) using the inlet diameter of the cooling tube (i.e. 5.8E-03 m) obtained from the engineering drawings provided by the industrial collaborating company. The calculated inlet airflow velocity was 105.97 m/s.

Chapter 4 THERMAL IMAGING STUDY FOR THE TEMPERATURE DISTRIBUTION IN THE PLUNGER AND PARISON

4.1 Introduction

The thermal imaging analysis of the plunger and parison was carried out on the shop floor as seen in Figure 4.1 below. This exercise recorded the temperature distribution in the plunger and parison at the blank mould open stage immediately after the invert. This information was required to establish the temperature boundary conditions, representative of the actual working system. The temperature boundary condition was then used in the CFD modelling.

Figure 4.1 Carrying out the thermal imaging analysis on the shop floor

4.2 Thermal imaging equipment [65]

The thermal imaging system consists of a scanner, infrared detector, computer based processor, display device and output instruments (monitor and printer). A schematic diagram of the scanner and detector arrangement used in this project (Land TI 35 sm) shows the principle of the technique, Figure.4.2 on page 44.

Infrared radiation emitted by the subject passes through the window of the scanner unit and strikes one of the surfaces of the rotating polygon mirror. As the mirror rotates, radiation from different points on the subject is reflected by the eight surfaces, which scan the subject horizontally and vertically as shown in Figure.4.2 (page 44). Radiation reflected from the surfaces of the polygon mirror then passes through a lens. For focusing purposes, the lens is moved by a motor. After being transmitted by the lens, the radiation passes through the chopper, which is connected to the polygon mirror and rotates to chop (momentarily interrupt) the radiation reflected by the mirror. When the chopper interrupts the radiation from the subject, the radiation emitted by the chopper itself is incident on the detector.

Interference filters are placed in front of the detectors to limit the range of wavelengths to which the detector is sensitive. One of three different interference filters can be used, depending on the range selected by the user, 3.5 μm to 5μm for -20 °C to 120 °C and 3.9 μm for 100 °C to 1500 °C. A wider band of wavelengths is chosen at lower temperatures in order to increase the

intensity of the infrared radiation. The detector is positioned so that the radiation focused by the lens forms 12 scan lines. Each complete revolution of the eight-sided polygon mirror produces 96 scan lines (12 scan lines × 8 mirror surfaces) to create one image. The radiation striking each element of the detector is converted into an analogue signal proportional to the intensity of the radiation. This analogue signal is then used for image processing.

The temperature measurement system is calibrated automatically every time the instrument is switched on. An accurately known temperature source is moved into the detector's view field whose output is measured. The system calculates and stores the calibration constants for the system in the memory of the imager.

Table 4. Specifications of the modified Land TI 35 sm [65]

Feature	Specification
Manufacturer / model	Land Infrared Ltd / Land TI 35 sm
Temperature range	-20 to 1500 °C blackbody temperature
Focusing range	0.105 m to infinity
Frame frequency	25 Hz
Field of view	16 ° × 16 °
Detector	Thermoelectrically cooled HgCdTe
Spectral response	-20 to 120 °C: 3.5 μm to 5μm
	100 to 1500 °C: 3.9 μm
Correction factors	Emissivity
	Background temperature
	Target distance
	Atmospheric absorption coefficient

4.3 Window and offset controls of the thermal imager

The correct selection of window and offset control is essential to measure the temperature with the thermal imaging system. Land TI 35 sm has three temperature measurement ranges: Low (0°C-120°C), Middle (100°C-350°C) and High range (300°C-1500°C). The window control sets the temperature difference between the white and black part of the grey scale.

The offset control sets the difference between an internal reference temperature and the temperature, which is displayed as black in the image. Since the radiation from a body is extremely non-linear with temperature, the window and offset controls are also non-linear. In short, the window control determines the range of temperature coverage for a particular measurement and the offset control determines the range it is located.

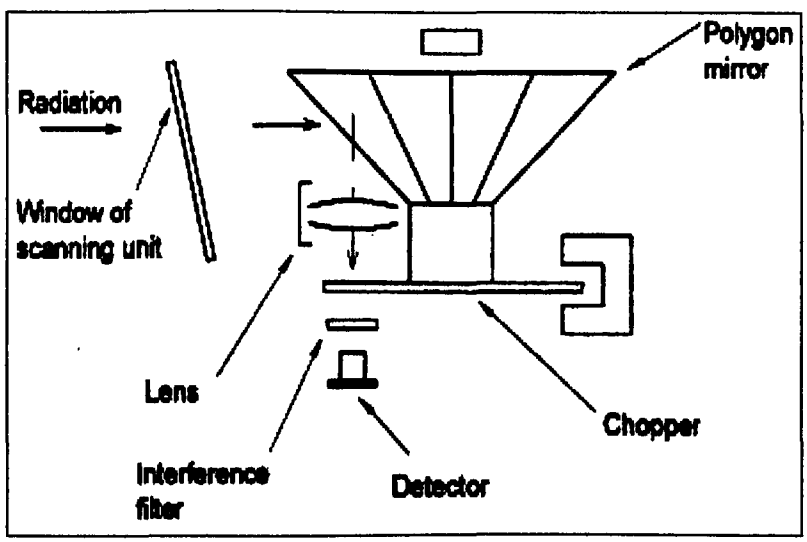

Figure 4.2. Schematic diagram of the thermal imager Land TI 35 sm [66]

4.4 Experimental Study

The thermal imager was calibrated by assessing the temperature of steam (100°C). The images of the temperature distribution along the plunger and parison were recorded approximately between 0.8 to 1 second after the blank mould opening stage. This was in synchronise with the machine cycle times. These images were captured consecutively from the blank mould open stage to the parison invert stage at time intervals of 80 milliseconds between each frame. This helped to facilitate the selection of the plunger and parison at the precise moment immediately after the invert. This was important as it reduces the margin of error caused by the heat transfer from the plunger to the surroundings by conduction, convection and radiation.

4.5 Results

4.5.1 Plunger Temperature

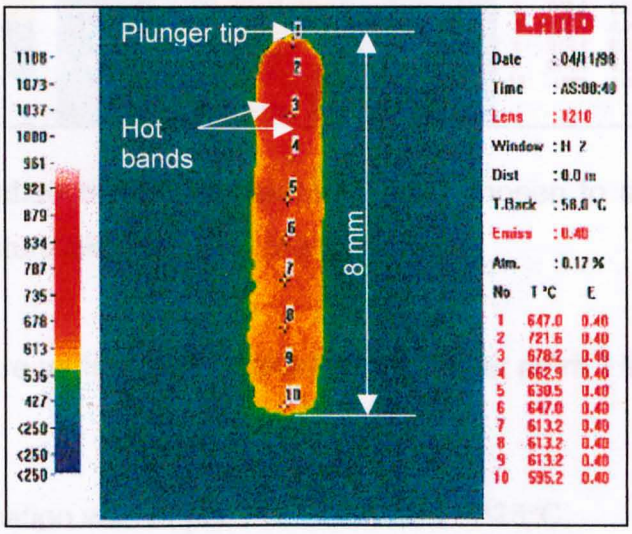

Figure 4.3. The location of the temperature points chosen to investigate the temperature distribution in the plunger.

- The temperature varies from a value of 721.6 °C at point 2 to a temperature of 595.2°C at point 10
- The hottest location was at point 2, which was at a value of 721.6°C.
- The coolest location was at point 10,which was at a value of 595.2°C.
- The average temperature of the 10 points along the plunger was 642.2°C.

4.5.2 Parison Temperature

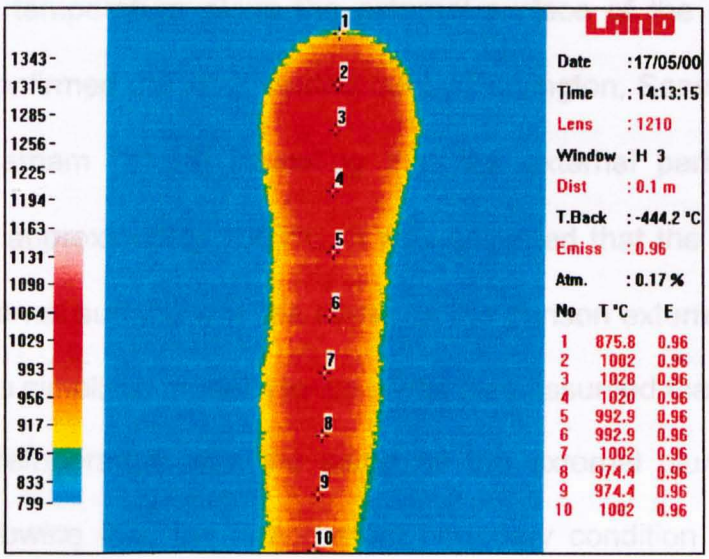

Figure 4.4. The location of the temperature points chosen to investigate the temperature distribution in the parison.

- The temperature varies from a value of 875.8°C at point 1 to 1028°C at point 3.
- The hottest location was at point 3, which was 1028°C.
- The coolest location was at point 1, which was 875.8°C.

- The average temperature of the 10 points along the parison was 986.44°C

4.6 Observation

The average temperature of the plunger recorded was 642.2°C at the blank mould open stage. This confirmed the previously reported result [21,38] confirming the NNPB operating temperatures were in a range of 600°C to 800°C. Following the thermal imaging experiment of the parison, it was shown that the average temperature along the external surface of the parison was 986.44°C. This confirmed the work carried out by Penlington, Sarwar, Marshall, Lewis and Cockerham [21,38] indicating that the external parison surface temperature was approximately 1000°C. It was assumed that the temperature of the parison internal surface was the same as the parison external surface in order to produce a simplistic model. Hence it was also assumed that the parison internal surface temperature was the same as the external plunger surface temperature. Following this, the temperature boundary condition (i.e. uniform temperature T= 1000°C) was assumed along the length of the external plunger surface for the purpose of the computational fluid dynamics (CFD) modelling.

Chapter 5 ASSESSING THE AIRFLOW DISTRIBUTION IN THE 2D AND AXISYMMETRIC MODEL OF THE NNPB PLUNGER COOLING TUBE SYSTEM USING THE CFD ANALYSIS TECHNIQUE

5.1 Introduction

ANSYS 5.4, the computational fluid dynamics (CFD) software package was used to analyse both the 2D and axisymmetric models of the plunger cooling tube system. ANSYS has more than 31 years of experience in the computer-aided engineering (CAE) industry. The ANSYS programme was initially a finite element analysis code, which acquired the FLOTRAN programme, a computer fluid dynamics (CFD) package. This acquisition into the ANSYS product fold complemented the current ANSYS programme. The ANSYS programme has diverse designs resolving usage, ranging from common everyday products to sophisticated high technology systems. ANSYS present customer base boast of more than 4,100 commercial licenses and 10,000 university licenses worldwide.

The model of the plunger cooling tube system to produce a 330 ml beer bottle was built initially in 2D then in axisymmetric according to the dimensions in the engineering drawings provided by the collaborating establishment (Appendix 1). Initial CFD investigation was carried out on both these models using the boundary conditions (P_{in}, P_{out}) established from the laboratory experimental study (Chapter 3). Both the models were assessed using the steady state,

turbulent and compressible conditions. The steady state condition was selected because it constituted the all-constant condition anywhere in the airflow stream of the plunger cooling tube system with respect to time but the conditions might differ at various points. The turbulent condition was chosen because of the airflow irregular movement. Turbulent flow is characterised by the altering velocity at different points in the flow field. The compressible condition was preferred because it takes into consideration the change in the airflow density within the plunger cooling tube system. The airflow through the cooling tube system (i.e. long pipe) was flowing at high velocities and the drop in pressure may alter the airflow density. The laws of conservation of mass, momentum and energy define the fluid flow problem. These laws are expressed in terms of partial differential equations, which are discretized with a finite element based technique. The assumptions about the fluid and analysis are as follows:

1. The fluid is Newtonian
2. There is only one phase
3. The problem domain does not change
4. The user must determine:
   a) if the problem is laminar or turbulent
   b) if the incompressible or the compressible algorithm must be invoked

The principal equations on which the ANSYS software is based are the continuity, momentum and compressible energy equations.

The continuity equation is expressed as:

$$\frac{\partial}{\partial t}\rho + \frac{\partial}{\partial x}(\rho V_x) + \frac{\partial}{\partial y}(\rho V_y) + \frac{\partial}{\partial y}(\rho V_z) = 0$$

where V_x, V_y, V_z = components of the velocity vector in the x, y and z directions respectively

ρ = density

x, y, z = global Cartesian coordinates

t = time

The momentum equation is expressed as:

$$\tau_{ij} = -P\sigma_{ij} + \mu\left(\frac{\partial}{\partial x_j}u_i + \frac{\partial}{\partial x_i}u_j\right) + \sigma_{ij}\lambda\frac{\partial}{\partial x_i}u_i$$

where τ_{ij} = stress tensor

u_i = orthogonal velocities ($u1 = V_x$, $u2 = V_y$, $u3 = V_z$)

μ = dynamic viscosity

λ = second coefficient of viscosity

In terms of the total temperature, the compressible energy equation is:

$$\frac{\partial}{\partial t}(\rho C_p T_o) + \frac{\partial}{\partial x}(\rho V_x C_p T_o) + \frac{\partial}{\partial y}(\rho V_y C_p T_o) + \frac{\partial}{\partial z}(\rho V_z C_p T_o) = \frac{\partial}{\partial x}\left(K\frac{\partial}{\partial x}T_o\right) +$$

$$\frac{\partial}{\partial y}\left(K\frac{\partial}{\partial y}T_o\right) + \frac{\partial}{\partial z}\left(K\frac{\partial}{\partial z}T_o\right) + W^v + E^\kappa + Q_v + \phi + \frac{\partial P}{\partial t}$$

where C_p = specific heat

T_o = total temperature

K = thermal conductivity

W^v = viscous work term

Q_v = volumetric heat source

ϕ = viscous heat generation term

E^K = kinetic energy

V_x, V_y, V_z = components of the velocity vector in the x, y and z directions respectively

P = pressure

Further numerical algorithms associated with these equations can be found in the ANSYS Theory Manual [67].

The purpose of this investigation was to assess the inlet airflow velocity and airflow pattern of both these models. This assessment showed that the predicted inlet airflow velocity was more accurate in the 2D model than the axisymmetrical model. This was deduced when the inlet airflow velocity of both these models were compared with resultant inlet airflow velocity of the laboratory experiment found in Experiment 1 of Chapter 3. As an example, a particular case having an inlet pressure (P_{in}) of 1.5 bar and outlet pressure (P_{out}) of 0.4 bar was assessed. The approximate average inlet airflow velocity for the 2D and axisymmetric models were 166.66 m/s and 8 m/s respectively. The laboratory experimental inlet airflow velocity for this case was 105.97 m/s Hence the 2D model had an approximate accuracy of 57% as compared to the axisymmetric model's 7.6% accuracy. The CFD results of the 2D model (Figures 5.1 to 5.3) and axisymmetric model (Figures 5.4 and 5.5) are shown below. Additional observations of this investigation can be found in Appendix 2.

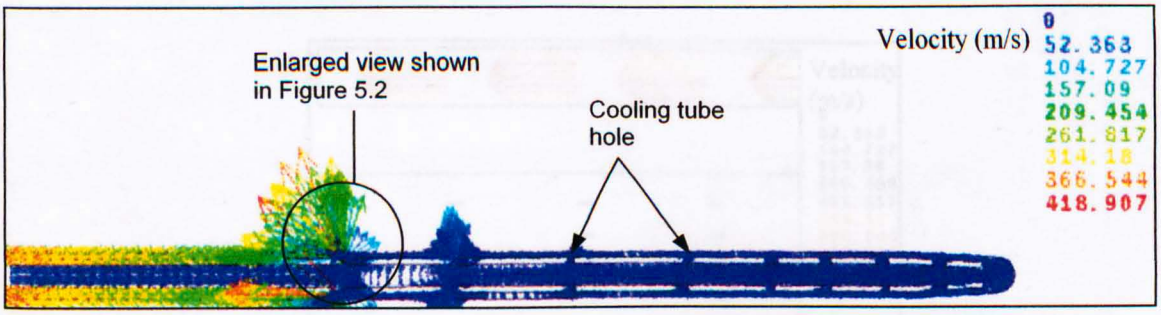

Figure 5.1. Diagram of airflow through the 2 dimensional model of the cooling tube. Inlet pressure: 1.5 bar, outlet pressure: 0.4 bar, iteration: 1200 and is compressible.

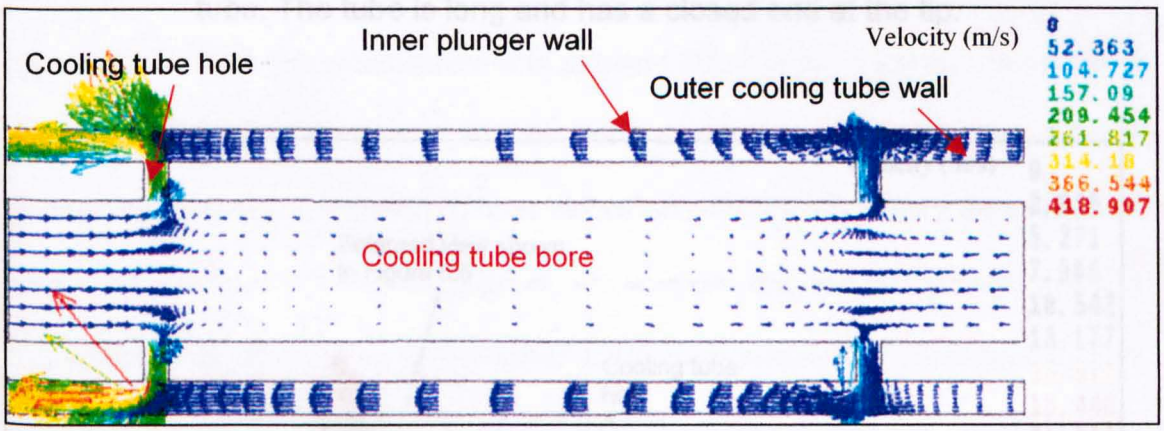

Figure 5.2. An enlarged sectional view of the airflow patterns after the first hole along the cooling tube. The tube is long and has a closed end.

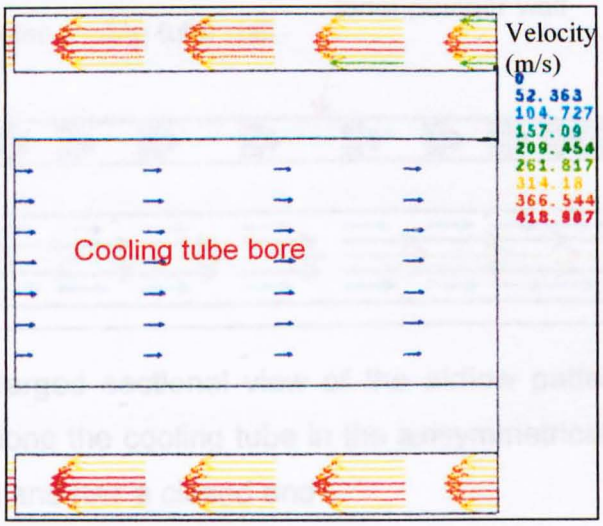

Figure 5.3. An enlarged view of the airflow patterns at the inlet of the cooling tube. The tube is long and has a closed end at the tip.

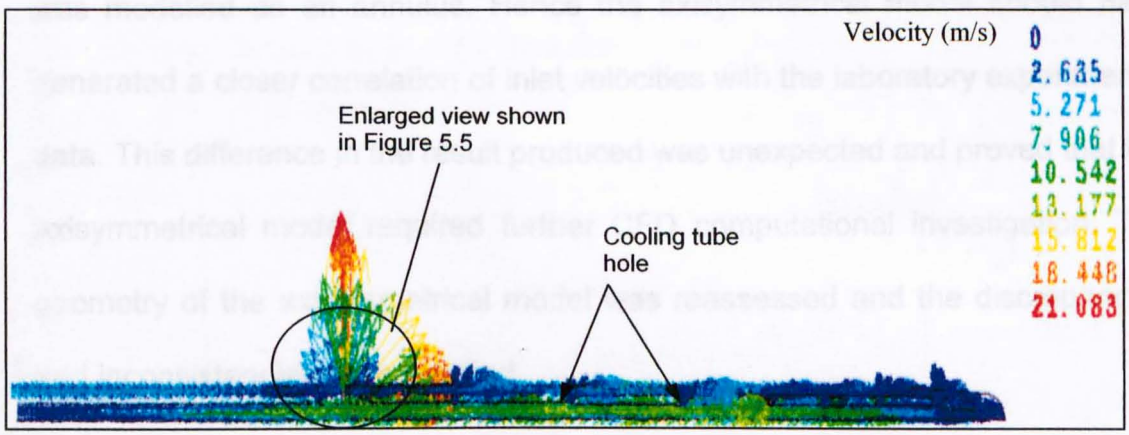

Figure 5.4. Diagram of the airflow through the axisymmetric model of the cooling tube. Inlet pressure: 1.5 bar, outlet pressure: 0.4 bar, iteration: 1200 and is compressible.

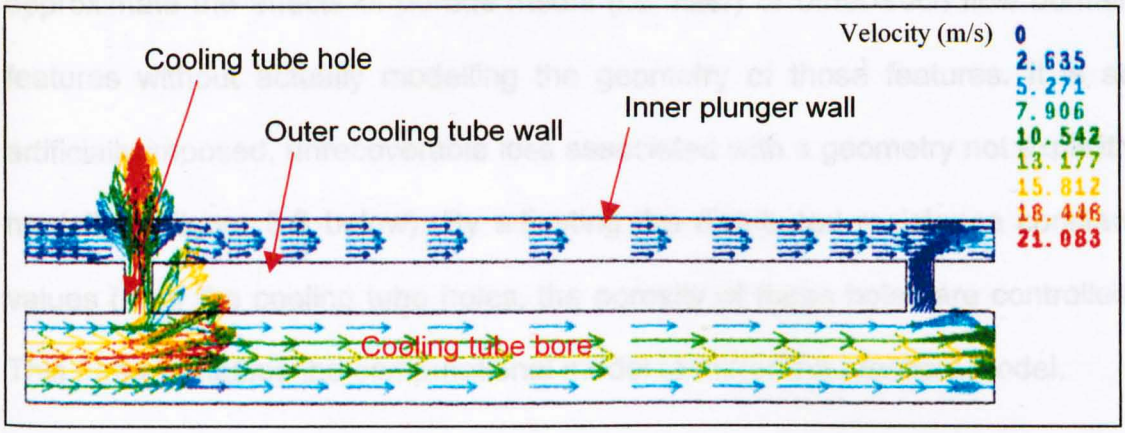

Figure 5.5. An enlarged sectional view of the airflow patterns after the first hole along the cooling tube in the axisymmetrical model. The tube is long and has a closed end.

The CFD axisymmetrical model was actually a closer geometrical representation of the practical NNPB plunger cooling tube system because it was modelled as an annulus. Hence the axisymmetrical model should have generated a closer correlation of inlet velocities with the laboratory experimental data. This difference in the result produced was unexpected and proved that the axisymmetrical model required further CFD computational investigation. The geometry of the axisymmetrical model was reassessed and the discrepancies and inconsistencies were rectified.

In the axisymmetrical model, the plunger cooling tube system was modelled as an annulus. Following this the cooling tube holes in the axisymmetrical model were essentially slots and therefore they were porous. The porosity of these holes was determined by the distributed resistance constant value (k) that was applied to the holes. The distributed resistance is a convenient way to

approximate the effects of porous media (i.e. filter) or other such flow domain features without actually modelling the geometry of those features. It is an artificially imposed, unrecoverable loss associated with a geometry not explicitly modelled (Figure 5.6 below). By adjusting the distributed resistance constant values (k) of the cooling tube holes, the porosity of these holes are controlled. This further enables the computational model to mirror the practical model.

The total pressure gradient is shown below for the X direction.

$$\frac{\partial p}{\partial X_{\text{resistance}}} = \{k\rho V_X |V|\}$$

where k = distributed resistance constant value

ρ = density

V_X = Velocity in the x direction

$|V|$ = Magnitude of velocity

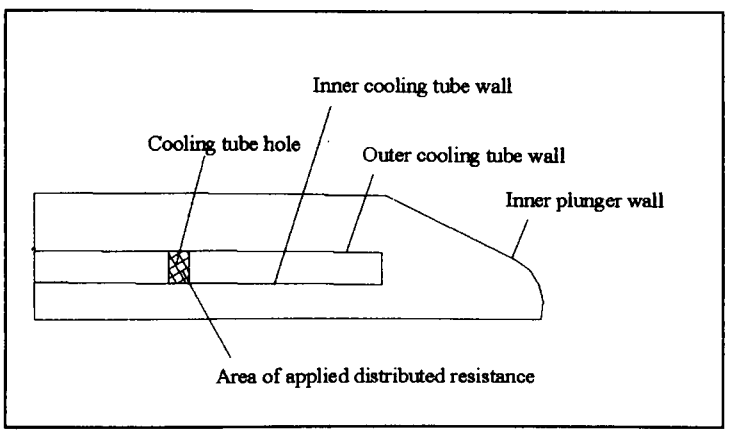

Figure 5.6. Diagram showing the plunger tip and cooling tube with the area of the applied distributed resistance.

The iterative method of solution was employed to obtain the distributed resistance constant value (*k*) for these cooling tube holes. The investigation was carried out using the exit pressure (P_{out}) and inlet velocity (V_{in}) as the boundary conditions instead of the inlet pressure (P_{in}) and outlet pressure (P_{out}) used in the initial investigation. This was because the CFD software package (ANSYS 5.4) recommended using this combination of boundary conditions. This package works at its optimum capability when used with these boundary conditions (P_{out}, V_{in}), producing a stable solution with minimal error. The corrected axisymmetrical model was subjected to an exit pressure (P_{out}) of 0.4 bar and an inlet velocity (V_{in}) of 105.97 m/s for 5000 iterations under a compressible condition. The compressible condition was chosen because the air flows within an enclosed area (i.e. plunger cooling tube system) hence making it possible for the air to be in a compressed condition. The distributed resistance constant value (*k*) of 1.5×10^4 was assumed for the cooling tube holes. This CFD investigation predicted an inlet pressure ($P_{in\ CFD'}$) of 1.58 bar. When comparing this computational result with the experimental pressure ($P_{in\ exp}$) of 1.5 bar, it was shown that the inlet pressure ($P_{in\ CFD'}$) of the axisymmetrical model was x1.05 of the experimental result ($P_{in\ exp}$) i.e. ($P_{in\ CFD'} = 1.05\ P_{in\ exp}$). The CFD results and observations are shown in Figures 5.7 to 5.11 on pages 57 to 60. This showed that the improved axisymmetrical model was predicting a more accurate result. Following this, to further refine the axisymmetric model to replicate the actual working model, the porosity of the cooling tube holes had to be further controlled. Hence the porosity of these holes had to be adjusted to

accurately predict the corresponding inlet pressures for the pressure difference (0.5 bar to 3 bar) used on the shop floor. The temperature boundary condition was only added to this CFD model for further investigation when the model was working satisfactorily.

Graph of Pressure Vs Vertical distance along the inlet of the cooling tube

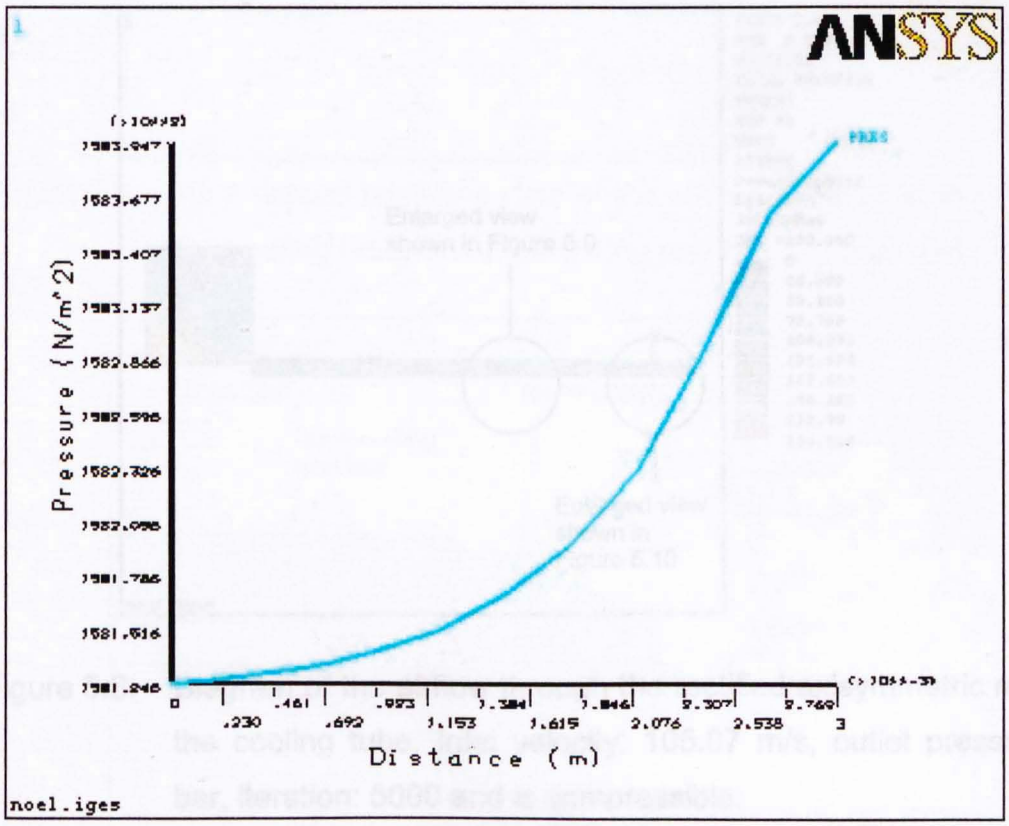

Figure 5.7. Graph of Pressure Vs Vertical distance along the inlet of the cooling tube. Inlet velocity: 105.97 m/s, outlet pressure: 0.4 bar, iteration: 5000 and is compressible

- There was a gradual increase in the airflow pressure from 1.581 bar at the inlet of the cooling tube along the axis. It reached a peak of 1.583 bar at the tip of the cooling tube.

- The lowest pressure value was 1.581 bar which was at the inlet of the cooling tube along the axis.
- The pressure range was between 1.581 bar to 1.583 bar.
- The average inlet pressure along the cooling tube was 1.58 bar.

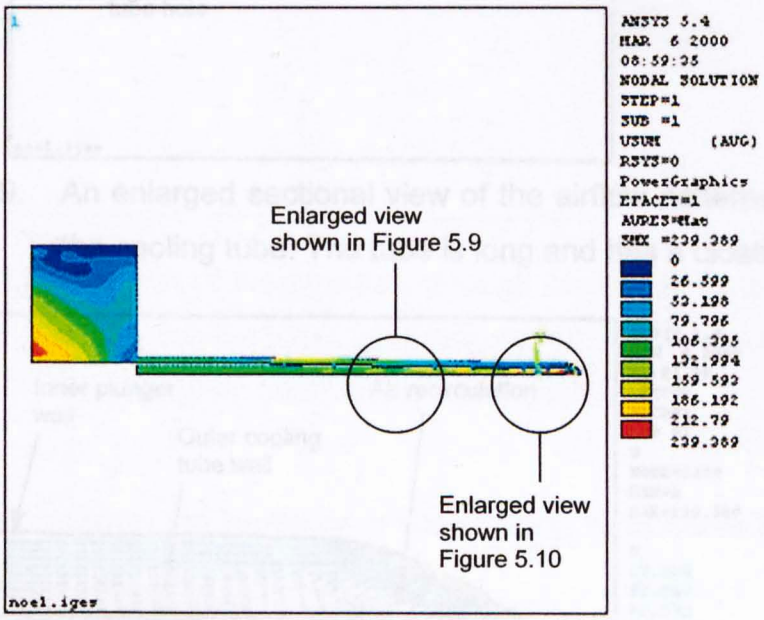

Figure 5.8. Diagram of the airflow through the rectified axisymmetric model of the cooling tube. Inlet velocity: 105.97 m/s, outlet pressure: 0.4 bar, iteration: 5000 and is compressible.

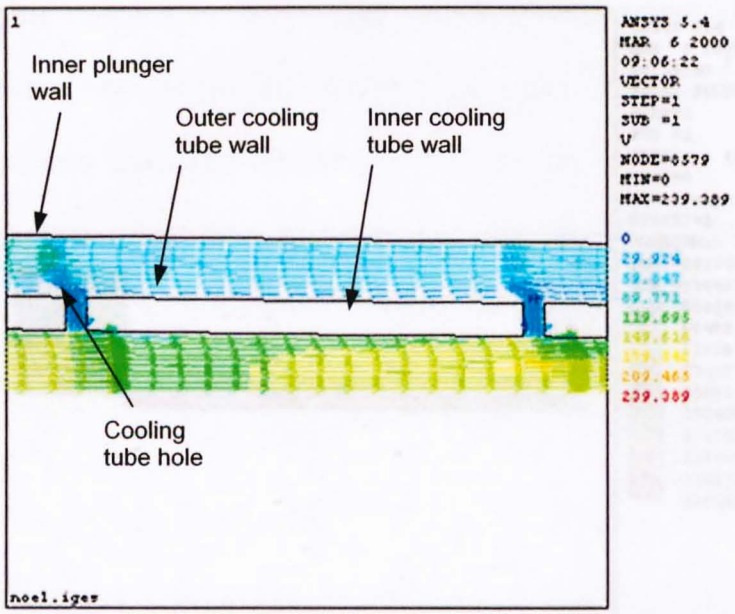

Figure 5.9. An enlarged sectional view of the airflow patterns at the center of the cooling tube. The tube is long and has a closed end.

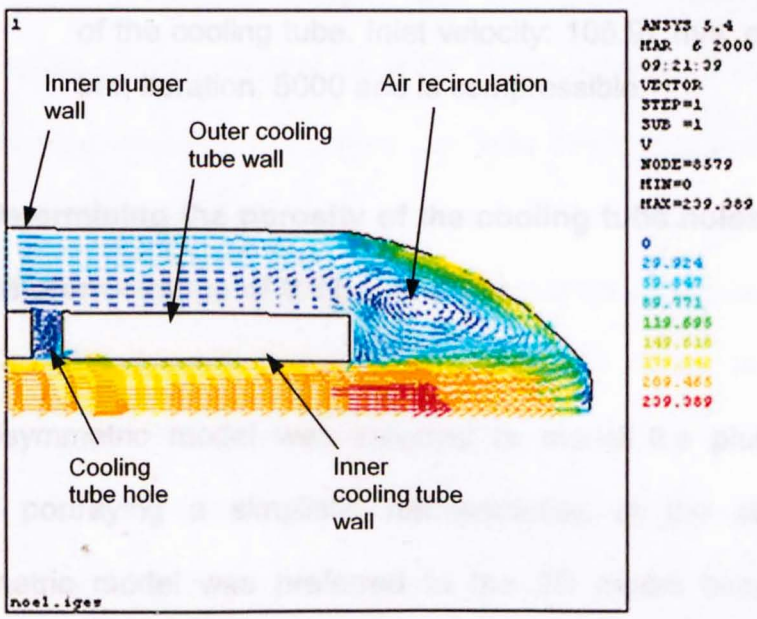

Figure 5.10. An enlarged sectional view of the airflow patterns at the tip of the cooling tube. The tube was long and had a closed end.

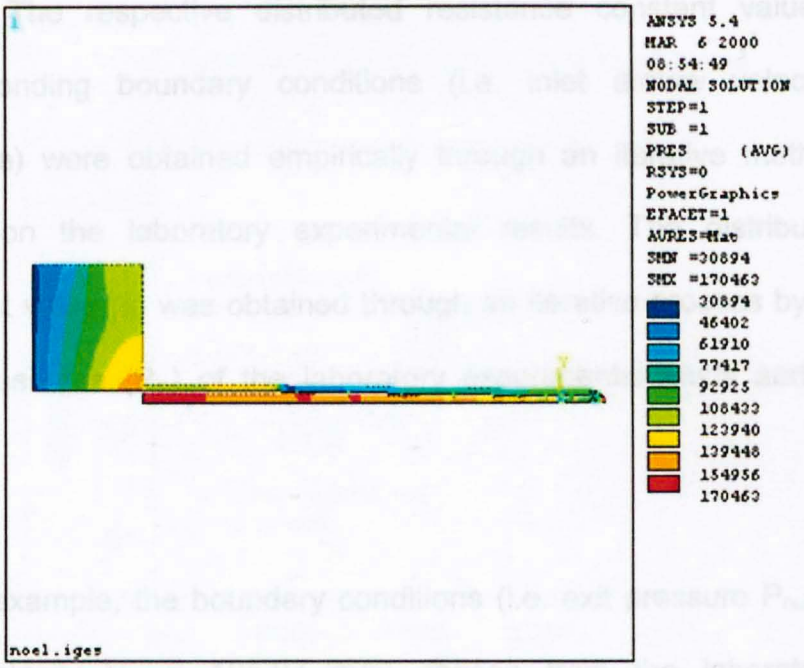

Figure 5.11. Diagram of the pressure through the rectified axisymmetric model of the cooling tube. Inlet velocity: 105.97 m/s, outlet pressure: 0.4 bar, iteration: 5000 and is compressible.

5.2 Determining the porosity of the cooling tube holes for the pressure difference range of 0.5 bar to 3 bar

The axisymmetric model was selected to model the plunger cooling tube system, portraying a simplistic representative of the actual model. The axisymmetric model was preferred to the 2D model because of its better accuracy in replicating the actual working model. Following this, the cooling tube holes, which were essentially slots, were porous. The porosity of the cooling tube holes was controlled by adjusting the distributed resistance constant values (k) enabling the CFD model to replicate the actual working

model. The respective distributed resistance constant values (k) for the corresponding boundary conditions (i.e. inlet airflow velocity and outlet pressure) were obtained empirically through an iterative method of solution based on the laboratory experimental results. The distributed resistance constant value (k) was obtained through an iterative process by comparing the inlet pressures (P_{in}) of the laboratory experimental study and computational results.

As an example, the boundary conditions (i.e. exit pressure P_{out} = 0.4 bar and inlet velocity V_{in} = 105.97 m/s) chosen from the laboratory experiment (Experiment 1 in Chapter 3) were used in this investigation to determine the distributed resistance constant value (k). When a constant value of 1.5×10^4 for the distributed resistance constant (k) was assumed, a computational inlet pressure ($P_{in\ CFD'}$) of 1.58 bar was predicted. This value was compared with the experimental inlet pressure ($P_{in\ exp}$) of 1.5 bar. Following this, it was shown that the computational inlet pressure ($P_{in\ CFD'}$) was 1.05 times the experimental inlet pressure ($P_{in\ exp}$). This showed that the assumed k value for this particular case had produced a computational model that closely replicated the actual model. This is shown in Figure 5.12 on page 62.

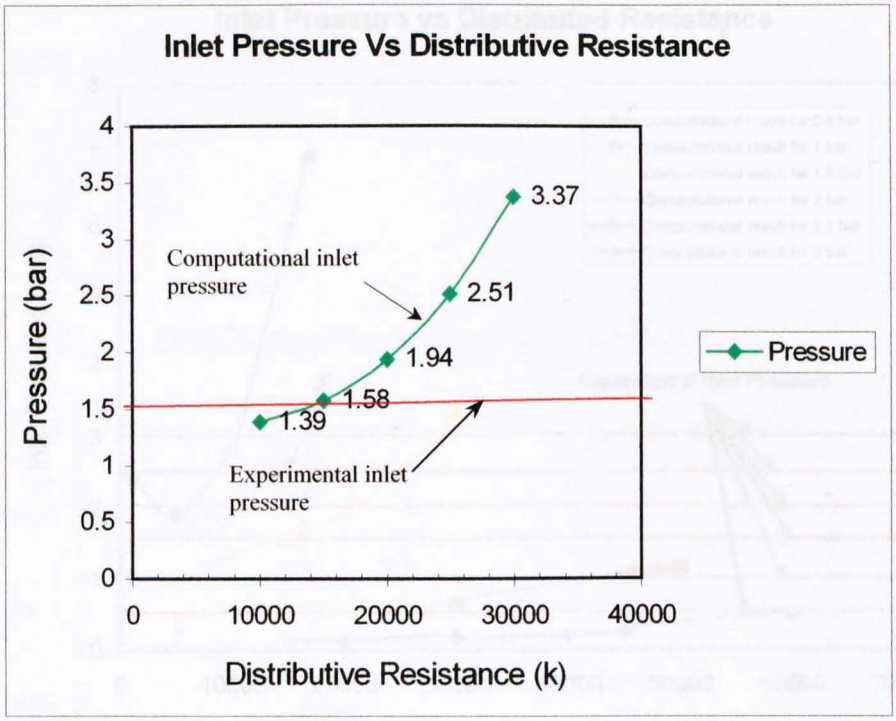

Figure 5.12. Graph of Inlet Pressure Vs Distributed resistance for an inlet pressure of 1.5 bar. (Boundary conditions used were exit pressure P_{out} =0.4 bar and inlet velocity V_{in} =105.97 m/s)

This investigation was repeated to obtain the approximate distributed resistance constant values (*k*) for the respective inlet pressure in the range of 0.5 bar to 3 bar (Figure 5.13 on page 63). The relationship between the inlet pressure (0.5 bar to 3 bar) and the distributed resistance constant value (*k*) for the axisymmetrical model of the plunger cooling tube system was determined from this investigation (Figure 5.14 on page 64). Figure 5.14 showed that the distributed resistance constant value (*k*) decreased gradually as the inlet pressure increased. The curve started to level and stabilised when the inlet pressure reached 1.5 bar.

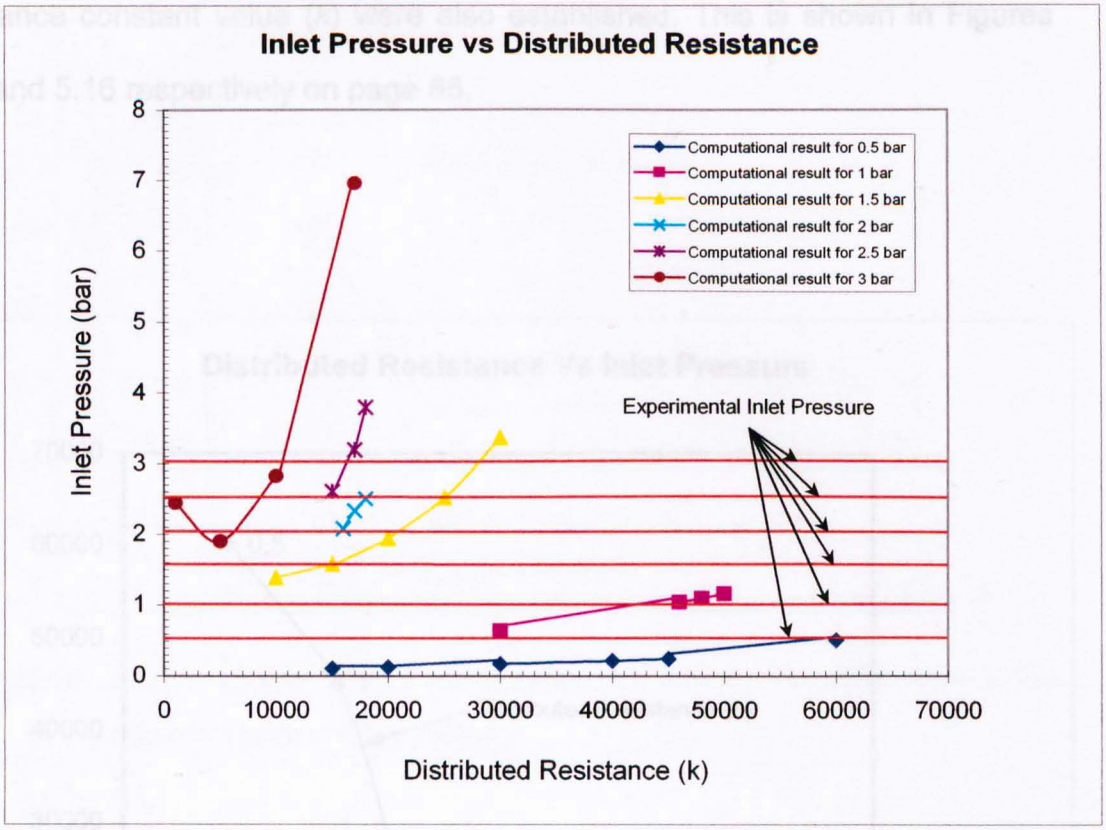

Figure 5.13. Graph of Inlet Pressure (0.5 bar to 3 bar) Vs Distributed Resistance of the plunger cooling tube system

A possible explanation for the decrease in the distributed resistance constant value (*k*) could be due to the recirculation and choking of the airflow at the tip of the plunger when the inlet pressure was increased. When the airflow at the tip of the plunger was blocked, the air was forced by the increased inlet pressure to flow through the cooling tube holes. Following this, the cooling tube holes must have a low distributed resistance constant value (*k*) to allow sufficient air to flow through the plunger cooling tube system. The relationships between the boundary conditions (i.e. outlet pressure and inlet velocity) and the distributed

resistance constant value (k) were also established. This is shown in Figures 5.15 and 5.16 respectively on page 65.

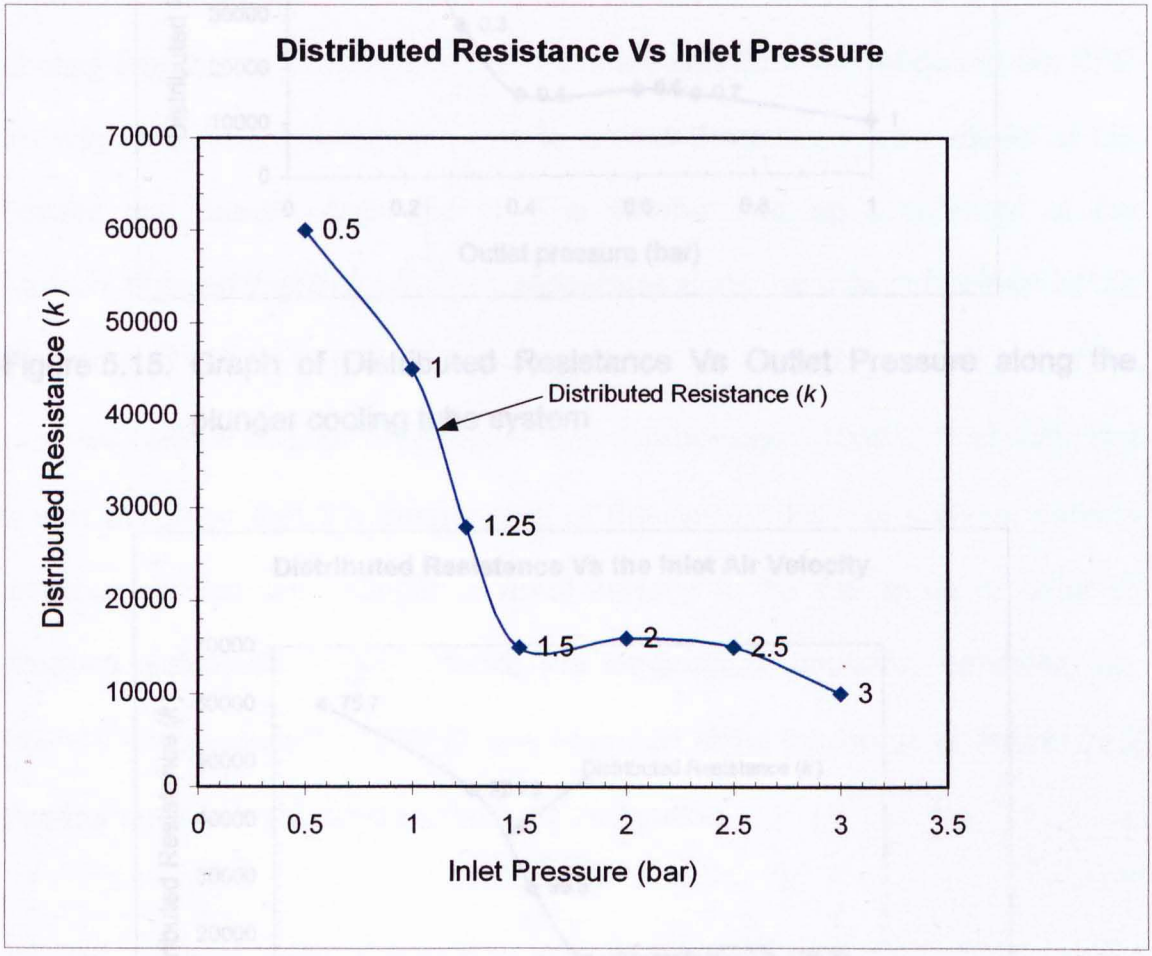

Figure 5.14. Graph of the Distributed Resistance Vs Inlet Pressure along the plunger cooling tube system

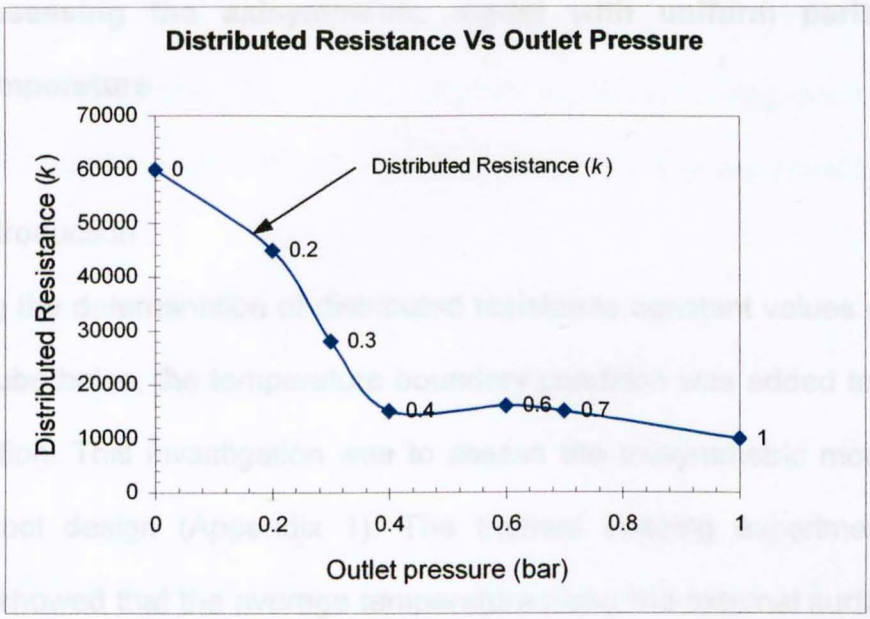

Figure 5.15. Graph of Distributed Resistance Vs Outlet Pressure along the plunger cooling tube system

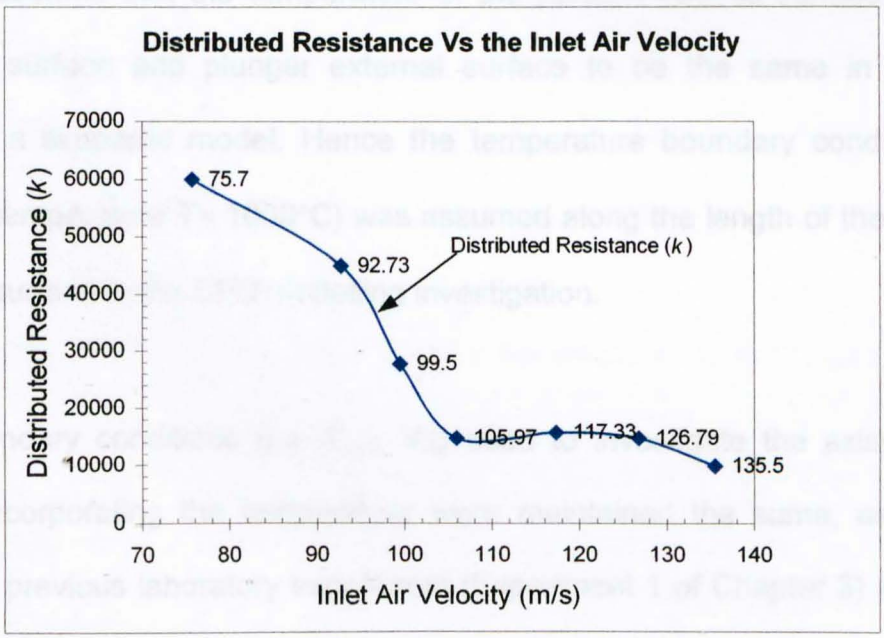

Figure 5.16. Graph of Distributed Resistance Vs Inlet Velocity along the plunger cooling tube system

5.3 Assessing the axisymmetric model with uniform parison skin temperature

5.3.1 Introduction

Following the determination of distributed resistance constant values (*k*) for the cooling tube holes, the temperature boundary condition was added to the CFD investigation. This investigation was to assess the axisymmetric model of the current tool design (Appendix 1). The thermal imaging experiment of the parison, showed that the average temperature along the external surface of the parison was 986.44°C [67]. This supports previous work [21] indicating that the external parison surface temperature was approximately 1000°C. Following this it was assumed that the temperature of the parison internal surface, parison external surface and plunger external surface to be the same in order to produce a simplistic model. Hence the temperature boundary condition (i.e. uniform temperature T= 1000°C) was assumed along the length of the external plunger surface in the CFD modelling investigation.

The boundary conditions (i.e. P_{out}, V_{in}) used to investigate the axisymmetric model incorporating the temperature were maintained the same, as chosen from the previous laboratory experiment (Experiment 1 of Chapter 3) and used in the initial computational work. This investigation was repeated for each of the chosen boundary conditions. Following this investigation the CFD software computated the inlet temperature (T_{inlet}), outlet temperature (T_{outlet}) and density

(ρ) values of air flowing through the plunger cooling tube system. This data enabled the calculation of the mass flow rate ($\dot{m}$) of air flowing into the cooling tube system and the approximate amount of heat that was extracted by the air.

5.3.2 Results

The calculation of a selected result is shown below:

Case 1

The boundary conditions used were: V_{in} = 75.7 m/s; P_{out} = 0 bar; actual P_{in} = 0.51 bar; k = 6 x 10^4;

The assumed CFD software generated data were: $C_{p\ air}$ = 1.004 x 10^3 J/kg K; ρ = 1.925 kg/m^3; T_{inlet} = 290 K; T_{outlet} = 499.2 K

$\dot{m}$ = (πr^2) V_{in} x ρ

$\dot{m}$ = 4.12 x 10^{-3} kg/s

Heat absorbed ($\dot{Q}$) = Mass flow rate ($\dot{m}$) x Specific heat of air ($C_{p\ air}$) x Temperature Difference ($\Delta T_{average}$)

= 865.4W

The tabulated results of this investigation are shown below:

Case	V_{in} (m/s)	P_{out} (bar)	P_{in} (bar)	k	$C_{p\ air}$ (Jkg/)	ρ (kg/m^3)	T_{inlet} (K)	T_{outlet} (K)	$\dot{m}$ (kg/s)	Q (W)
1	75.7	0	0.51	6×10^4	1.004×10^3	1.925	290	499.2	4.12×10^{-3}	865.4
2	86	0.12	1.09	5.2×10^4	1.004×10^3	3.034	289	469.5	7.955×10^{-3}	1441.5
3	92.73	0.2	1.27	4.5×10^4	1.004×10^3	2.903	288	466.8	8.13×10^{-3}	1458.7
4	105.97	0.4	1.58	1.5×10^4	1.004×10^3	2.52	287.7	466.1	7.551×10^{-3}	1352.4
5	117.33	0.6	2.27	1.6×10^4	1.004×10^3	3.488	286	450	0.0116×10^{-3}	1905.3
6	126.79	0.7	2.86	1.5×10^4	1.004×10^3	4.392	285	436.6	0.0157	2395.7
7	135.5	1	3.09	1×10^4	1.004×10^3	4.673	284	431.1	0.0179	2644.1

5.3.3 Discussion

The relationship between the heat absorbed and the inlet airflow velocity is shown in Figure 5.17 on page 69. The graph showed that there was a gradual increase in the amount of heat absorbed from the plunger wall with an increase in the airflow velocity up to the point where the inlet airflow velocity was 92.73 m/s. When the inlet airflow velocity was between 92.73 m/s to 105.97 m/s there was a slight decrease in the heat absorption rate. This could be due to one or a combination of factors i.e. recirculation of air, choking of the airflow pattern, insufficient quantity of cooling tube holes that prevented the smooth and

efficient extraction of heat from the parison. The heat absorption gradually increased again when the inlet airflow velocity was between 105.97 m/s to 135.5 m/s. It showed that generally a greater amount of heat was absorbed from the plunger wall with an increase in the airflow velocity into the plunger cooling system. The same was also true when the graph of heat absorbed versus the inlet pressure (Figure 5.18 on page 70) was examined. The amount of heat absorbed increased with an increase in the inlet pressure except when the inlet pressure was between 1.27 bar and 1.58 bar.

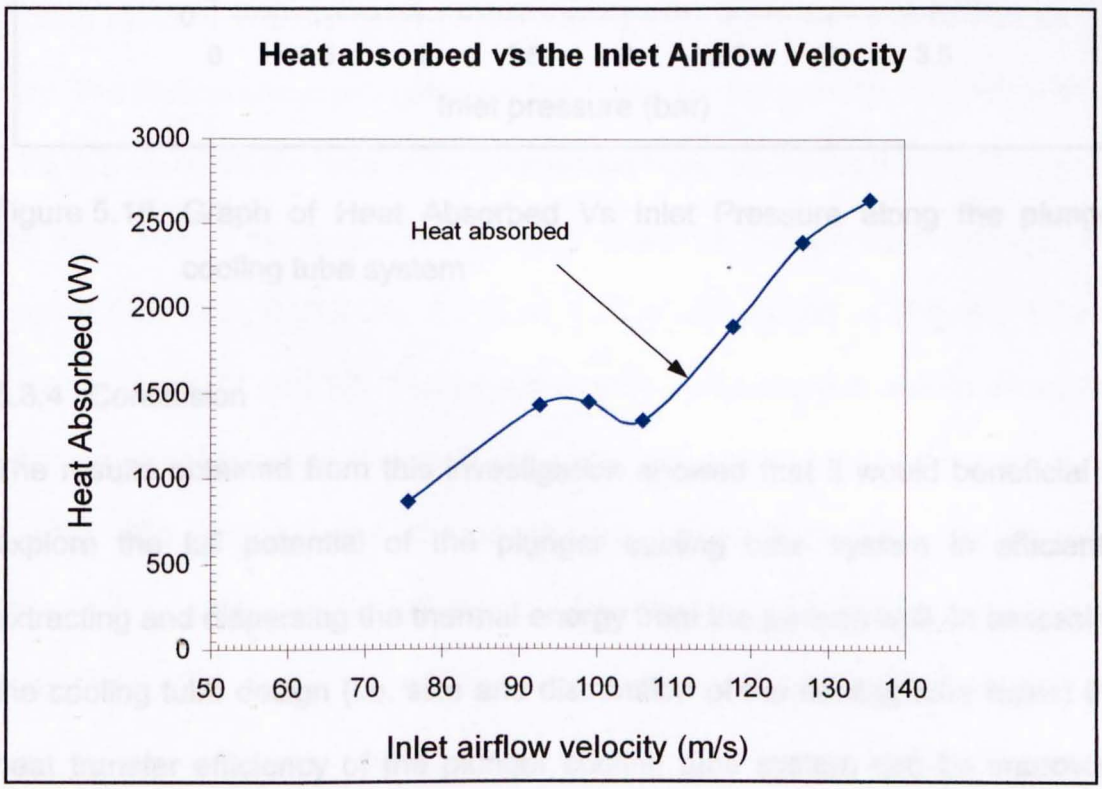

Figure 5.17. Graph of Heat Absorbed Vs Inlet Airflow Velocity along the plunger cooling tube system

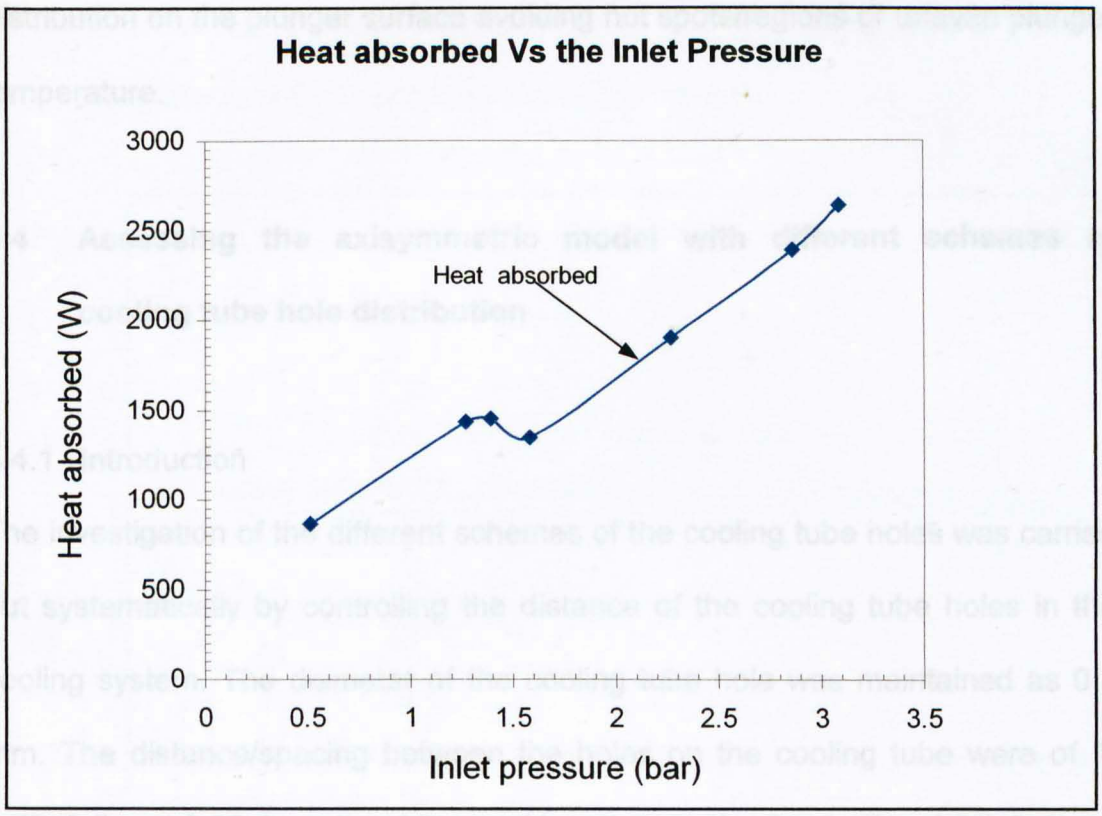

Figure 5.18. Graph of Heat Absorbed Vs Inlet Pressure along the plunger cooling tube system

5.3.4 Conclusion

The results obtained from this investigation showed that it would beneficial to explore the full potential of the plunger cooling tube system in efficiently extracting and dispersing the thermal energy from the parison wall. In assessing the cooling tube design (i.e. size and distribution of the cooling tube holes) the heat transfer efficiency of the plunger cooling tube system can be improved. This improvement should eliminate/reduce the recirculation and choking of the airflow pattern within the cooling tube, thus allowing for an even temperature

distribution on the plunger surface avoiding hot spots/regions or uneven plunger temperature.

5.4 Assessing the axisymmetric model with different schemes of cooling tube hole distribution

5.4.1 Introduction

The investigation of the different schemes of the cooling tube holes was carried out systematically by controlling the distance of the cooling tube holes in the cooling system. The diameter of the cooling tube hole was maintained as 0.7 mm. The distance/spacing between the holes on the cooling tube were of 1, 0.75, 0.5 and 0.25 the ratio of the total length from the first to the eighth hole on the tube. Hence the respective spacing distances between the holes on the cooling tube were 0.0133 m, 0.013 m, 0.01m and 0.0068 m (Figures 5.19 to 5.22 on pages 72 and 73). The objective of this investigation was to determine the amount of heat extracted from the parison by controlling the distance of the cooling tube holes in the plunger cooling tube system. The parison was assumed to have an internal surface temperature of 1000°C as previously established [21]. Following this the computational axisymmetrical model was subjected to a uniform temperature boundary condition of 1000°C along the length of the external plunger surface, which was essentially the internal surface temperature of the parison. This was in line with the assumption that the

temperature of the parison internal surface was the same as the parison external surface in order to produce a simplistic model.

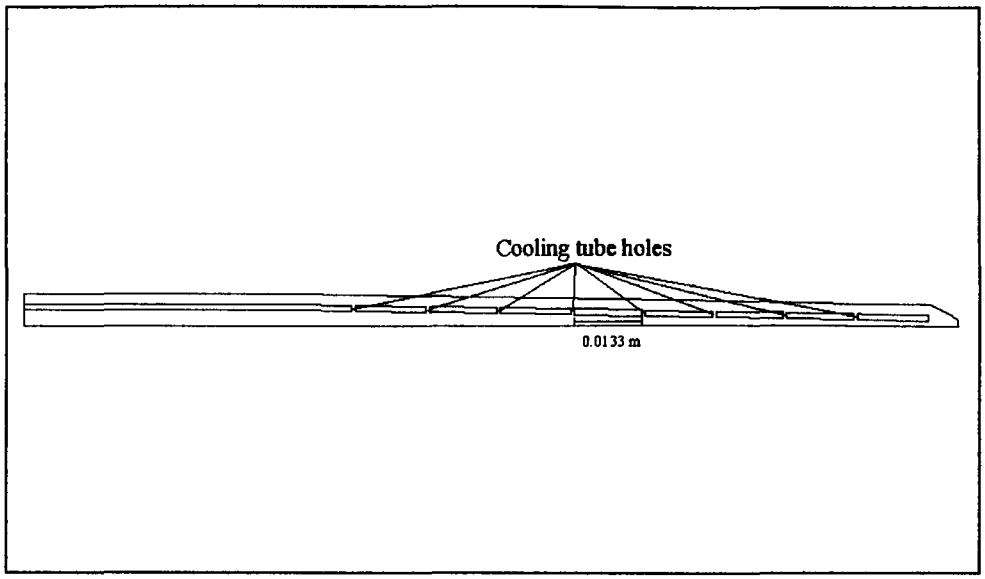

Figure 5.19. Diagram of the plunger cooling tube system showing the distance of 0.0133 m (1 spacing ratio) between the cooling tube holes

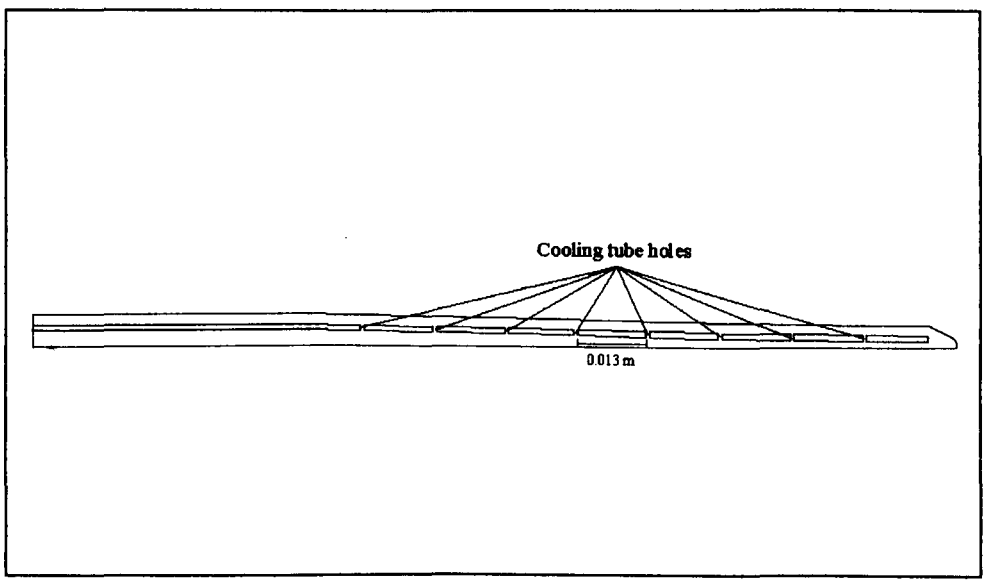

Figure 5.20. Diagram of the plunger cooling tube system showing the distance of 0.013 m (0.75 spacing ratio) between the cooling tube holes

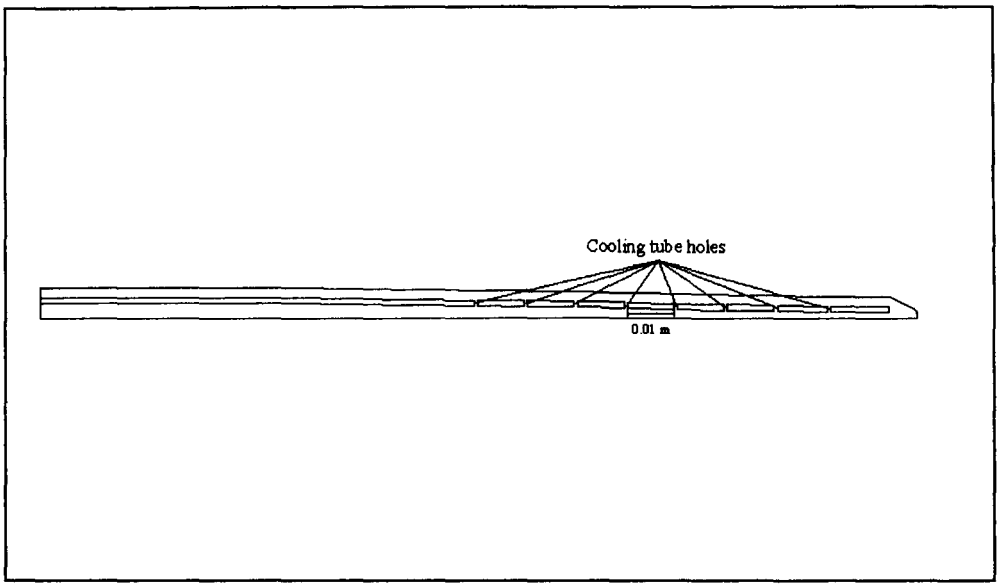

Figure 5.21. Diagram of the plunger cooling tube system showing the distance of 0.01 m (0.5 spacing ratio) between the cooling tube holes

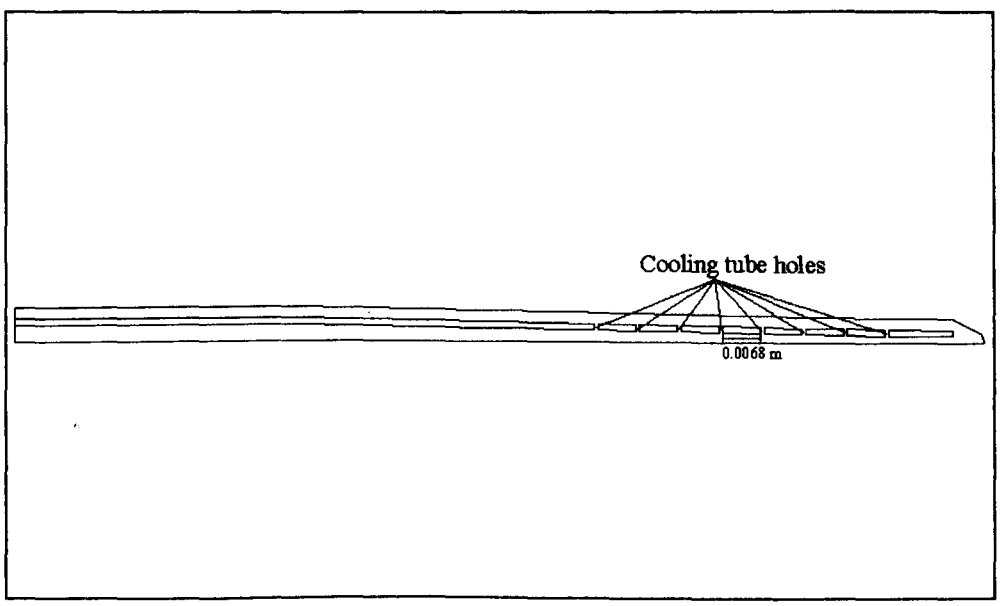

Figure 5.22. Diagram of the plunger cooling tube system showing the distance of 0.0068 m (0.25 spacing ratio) between the cooling tube holes

5.4.2 Results

The boundary conditions (i.e. $P_{out,}$ V_{in}) used in this investigation were maintained the same, as chosen from the previous laboratory experimental results (Experiment 1 of Chapter 3) and used in previous computational work. This investigation was repeated for each of the chosen boundary conditions with different locations of the cooling tube holes.

Following this investigation, the CFD software computated the inlet temperature (T_{inlet}), outlet temperature (T_{outlet}) and mass flow rate ($\dot{m}$) of air flowing through the plunger cooling tube system. This data allowed the calculation of the approximate amount of heat that was extracted by the plunger cooling tube system having different sets of cooling tube hole locations. The calculation of a selected result of this investigation is shown below:

Case 1 (current cooling tube design)

The boundary conditions used were: V_{in} = 75.7 m/s; P_{out} = 0 bar; actual P_{in} = 0.51 bar; k = 6×10^4;

The assumed CFD software generated data were: $C_{p\ air}$ = 1.004×10^3 J/kg K; ρ = 1.925 kg/m^3; T_{inlet} = 290 K; T_{outlet} = 499.2 K

$\dot{m}$ = $(\pi r^2)\ V_{in} \times \rho$

$\dot{m}$ = 4.12×10^{-3} kg/s

Heat absorbed ($\dot{Q}$) = Mass flow rate ($\dot{m}$) x Specific heat of air ($C_{p\ air}$) x Temperature Difference ($\Delta T_{average}$)

= 865.4 W

The tabulated results of this investigation are shown below:

Current cooling tube design

Case	V_{in} (m/s)	P_{out} (bar)	P_{in} (bar)	k	$C_{p\ air}$ (Jkg/K)	ρ (kg/m^3)	T_{inlet} (K)	T_{outlet} (K)	$\dot{m}$ (kg/s)	$\dot{Q}$ (W)
1	75.7	0	0.51	6×10^4	1.004×10^3	1.925	290	499.2	4.12×10^{-3}	865.4
2	86	0.12	1.09	5.2×10^4	1.004×10^3	3.034	289	469.5	7.955×10^{-3}	1441.5
3	92.73	0.2	1.27	4.5×10^4	1.004×10^3	2.903	288	466.8	8.13×10^{-3}	1458.7
4	105.97	0.4	1.58	1.5×10^4	1.004×10^3	2.52	287.7	466.1	7.551×10^{-3}	1352.4
5	117.33	0.6	2.27	1.6×10^4	1.004×10^3	3.488	286	450	0.01157×10^{-3}	1905.3
6	126.79	0.7	2.86	1.5×10^4	1.004×10^3	4.392	285	436.6	0.01574	2395.7
7	135.5	1	3.09	1×10^4	1.004×10^3	4.673	284	431.1	0.0179	2644.1

1 ratio spacing (equal spacing)

Case	V_{in} (m/s)	P_{out} (bar)	P_{in} (bar)	k	$C_{p\ air}$ (Jkg/K)	ρ (kg/m^3)	T_{inlet} (K)	T_{outlet} (K)	$\dot{m}$ (kg/s)	$\dot{Q}$ (W)
1	75.7	0	0.51	6×10^4	1.004×10^3	1.73	290	501.5	3.703×10^{-3}	786.3
2	92.73	0.2	1.27	4.5×10^4	1.004×10^3	2.457	289	477	6.442×10^{-3}	1215.9
3	105.97	0.4	1.58	1.5×10^4	1.004×10^3	2.291	288	469	6.864×10^{-3}	1247.4

4	117.33	0.6	2.27	1.6×10^4	1.004×10^3	3.193	287	444	0.0106	1669.7
5	126.79	0.7	2.86	1.5×10^4	1.004×10^3	3.642	284	419	0.0131	1769.6
6	135.5	1	3.09	1×10^4	1.004×10^3	4.251	286	453	0.0163	2730.7

0.75 ratio spacing

Case	V_{in} (m/s)	P_{out} (bar)	P_{in} (bar)	k	$C_{p\ air}$ (Jkg/K)	ρ (kg/m^3)	T_{inlet} (K)	T_{outlet} (K)	$\dot{m}$ (kg/s)	Q (W)
1	75.7	0	0.51	6×10^4	1.004×10^3	1.748	290	501	3.741×10^{-3}	792.6
2	92.73	0.2	1.27	4.5×10^4	1.004×10^3	2.484	289	477	6.513×10^{-3}	1229.3
3	105.97	0.4	1.58	1.5×10^4	1.004×10^3	2.29	288	468	6.861×10^{-3}	1240
4	117.33	0.6	2.27	1.6×10^4	1.004×10^3	2.967	287	456	9.843×10^{-3}	1670.1
5	126.79	0.7	2.86	1.5×10^4	1.004×10^3	3.834	285	440	0.0137	2139
6	135.5	1	3.09	1×10^4	1.004×10^3	5.601	284	412	0.0215	2757.7

0.5 ratio spacing

Case	V_{in} (m/s)	P_{out} (bar)	P_{in} (bar)	k	$C_{p\ air}$ (Jkg/K)	ρ (kg/m^3)	T_{inlet} (K)	T_{outlet} (K)	$\dot{m}$ (kg/s)	Q (W)
1	75.7	0	0.51	6×10^4	1.004×10^3	2.082	290	550	4.46×10^{-3}	1163.3
2	92.73	0.2	1.27	4.5×10^4	1.004×10^3	3.718	289	514	9.75×10^{-3}	2202.1
3	105.97	0.4	1.58	1.5×10^4	1.004×10^3	3.246	288	499	9.73×10^{-3}	2060.3
4	117.33	0.6	2.27	1.6×10^4	1.004×10^3	6.008	287	462	0.0199	3501.9
5	126.79	0.7	2.86	1.5×10^4	1.004×10^3	9.531	285	436	0.0342	5180
6	135.5	1	3.09	1×10^4	1.004×10^3	13.639	284	404	0.0523	6295.5

0.25 ratio spacing

Case	V_{in} (m/s)	P_{out} (bar)	P_{in} (bar)	k	$C_{p\ air}$ (Jkg/K)	ρ (kg/m^3)	T_{inlet} (K)	T_{outlet} (K)	$\dot{m}$ (kg/s)	$\dot{Q}$ (W)
1	75.7	0	0.51	6×10^4	1.004×10^3	2.476	290	504	5.3×10^{-3}	1138.6
2	92.73	0.2	1.27	4.5×10^4	1.004×10^3	5.077	289	461	0.0133	2298.7
3	105.97	0.4	1.58	1.5×10^4	1.004×10^3	6.694	288	465	0.02	3564.3
4	117.33	0.6	2.27	1.6×10^4	1.004×10^3	15.258	287	385	0.051	4980.3
5	126.79	0.7	2.86	1.5×10^4	1.004×10^3	33.574	285	330	0.12	5437.8
6	128	0.73	2.9	1.4×10^4	1.004×10^3	37.757	285	311	0.1366	3567
7	131	0.83	3.0	1.3×10^4	1.004×10^3	49.946	285	303.3	0.185	3400
8	135.5	1	3.09	1×10^4	1.004×10^3	72.316	284	297	0.2771	3616.1

5.4.3 Discussion

The relationship between the heat absorbed and the inlet airflow velocity for the different distances between the cooling tube holes is shown in Figure 5.23 on page 78. This graph showed that the average amount of heat absorbed from the plunger wall was proportional to the increase in the airflow velocity of the cooling tube with the original design, 1 spacing ratio (0.0133 m spacing) and 0.75 spacing ratio (0.013 m spacing) between cooling tube holes.

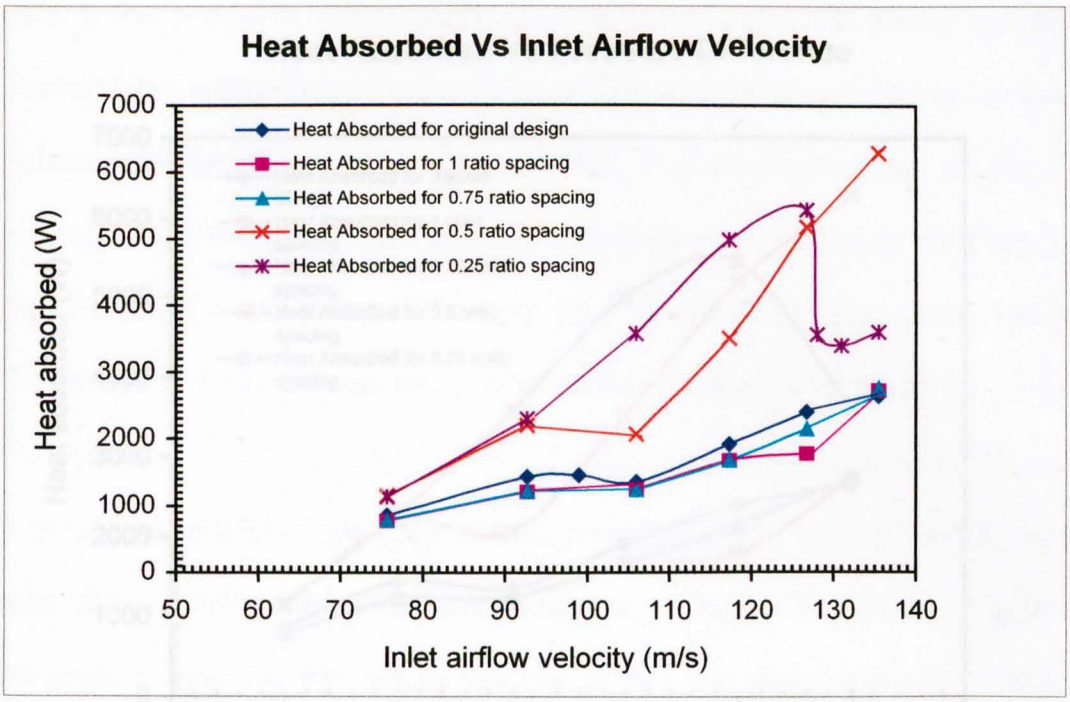

Figure 5.23. Graph of Heat Absorbed Vs Inlet Airflow Velocity of the plunger cooling tube system

In the case of the cooling tube with the 0.5 ratio spacing (0.01 m spacing) between the holes, the amount of heat absorbed was influenced by an increase in the inlet airflow velocity except between the inlet velocities of 92.73 m/s and 105.97 m/s. It experienced a slight drop in the absorption rate. For the cooling tube holes having the 0.25 spacing ratio (0.0068 m spacing), the heat absorption increased steeply to a point where the inlet airflow velocity was 126.79 m/s. When the inlet airflow velocity increased from 126.79 m/s to 131 m/s, the heat absorption then decreased. The heat absorption rate for this particular cooling tube hole configuration then increased again slightly when the inlet airflow velocity increased from 131 m/s to 135.5 m/s.

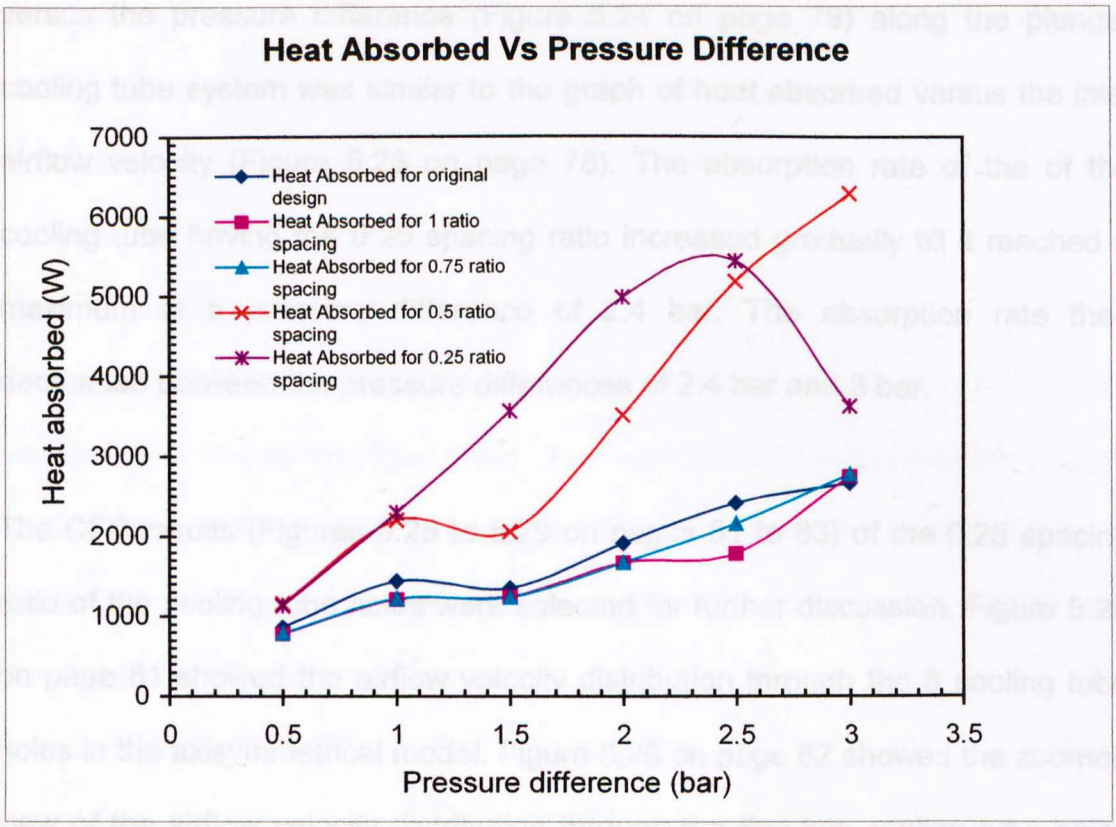

Figure 5.24. Graph of Heat Absorbed Vs Pressure Difference of the plunger cooling tube system

A possible explanation for the decrease in the heat absorption rate of cooling tube with the 0.25 spacing ratio (0.0068 m spacing) between the holes was that since the holes were spaced closer together this caused a choking of the airflow pattern during high inlet airflow velocities. When the inlet airflow velocity was between 126.79 m/s to 131 m/s, choking was brought about by the stagnation of air in the cooling tube holes (Figure 5.27 on page 82). This greatly reduced the extraction of heat from the parison. As the inlet airflow velocity increased from 131 m/s to 135.5 m/s, the air was forced through the holes hence increasing the extraction of heat. The results of the graph of heat absorbed

versus the pressure difference (Figure 5.24 on page 79) along the plunger cooling tube system was similar to the graph of heat absorbed versus the inlet airflow velocity (Figure 5.23 on page 78). The absorption rate of the of the cooling tube having the 0.25 spacing ratio increased gradually till it reached a maximum at a pressure difference of 2.4 bar. The absorption rate then decreased between the pressure differences of 2.4 bar and 3 bar.

The CFD results (Figures 5.25 to 5.29 on pages 81 to 83) of the 0.25 spacing ratio of the cooling tube holes were selected for further discussion. Figure 5.25 on page 81 showed the airflow velocity distribution through the 8 cooling tube holes in the axisymmetrical model. Figure 5.26 on page 82 showed the zoomed view of the airflow velocity distribution through the first two cooling tube holes from the plunger tip. The zoomed view of airflow velocity distribution through the first cooling tube hole from the plunger tip was shown in Figure 5.27 on page 82. Figures 5.28 and 5.29 on page 83 respectively showed the zoomed view of the pressure and temperature distribution at the first cooling tube hole from the plunger tip. When comparing Figure 5.26 (page 82) with Figure 5.28 (page 83), it showed that areas of low airflow velocity correspond to the areas having low-pressure distribution. The diagram of temperature distribution in Figure 5.29 (page 83) showed that the temperature of the air gradually increased as it neared the inner wall of the parison. Hot areas along the inner wall of the parison can also be seen.

It can be inferred from the result shown in Figure 5.23 (page 78), that the cooling tube with the configuration of 0.5 spacing ratio (0.01 m spacing) between the cooling holes has so far provided the best heat absorption rate.

5.4.4 Conclusion

The result obtained from this investigation showed that by controlling the distribution of the cooling tube holes, the heat transfer efficiency of the plunger cooling tube system could be improved. Following this, the next step was to investigate the effects of the plunger material on the heat transfer efficiency of the plunger cooling tube system.

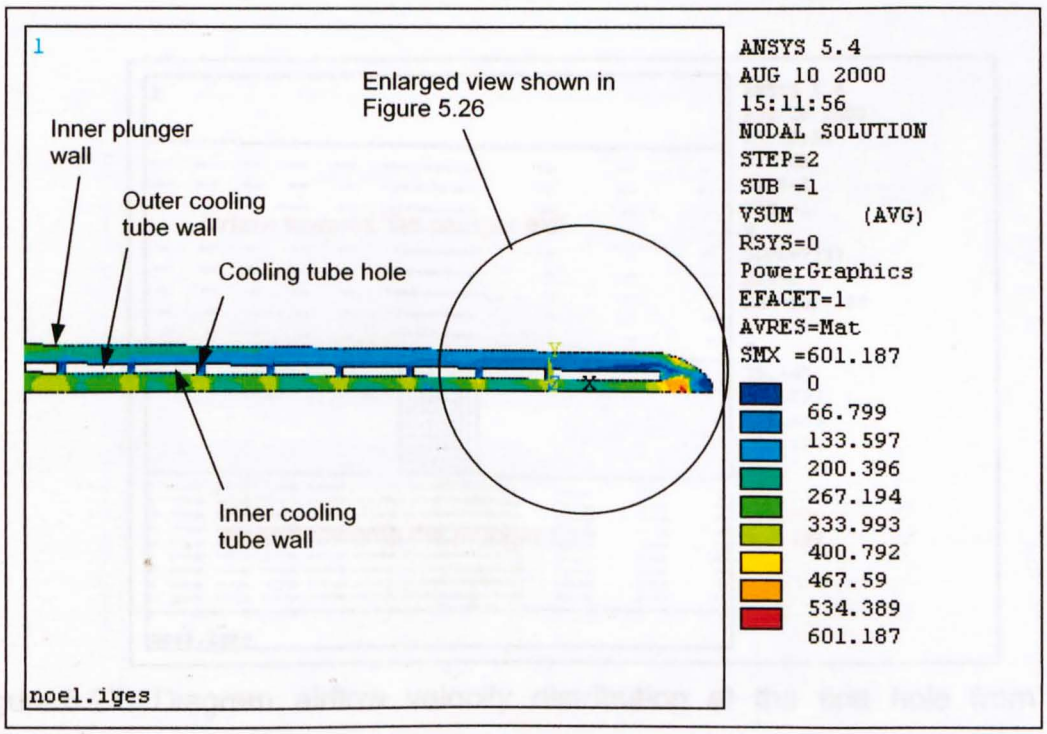

Figure 5.25. Diagram airflow velocity distribution in the axisymmetrical model of the cooling tube. Inlet velocity: 131 m/s, outlet pressure: 0.83 bar.

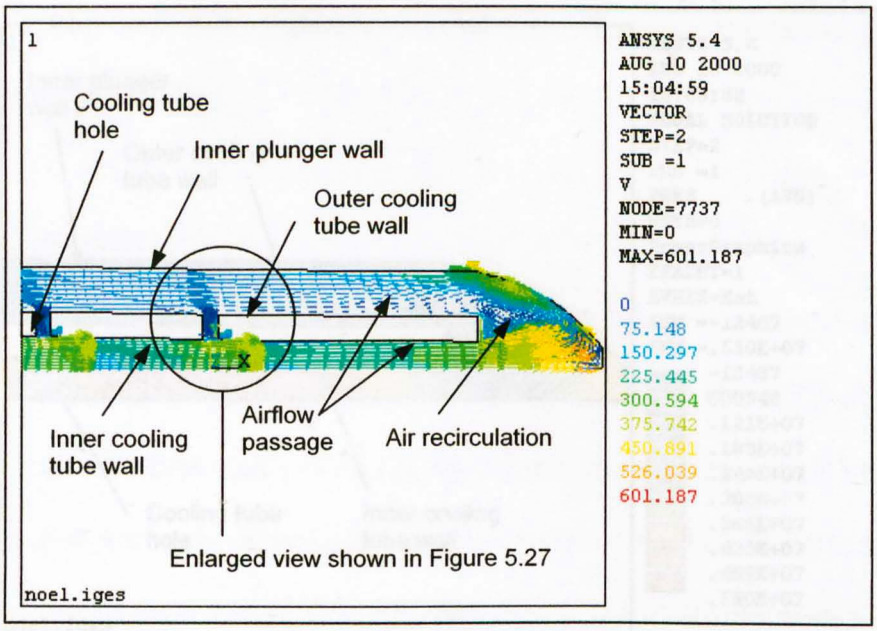

Figure 5.26. Diagram airflow velocity distribution at the plunger tip of the cooling tube. Inlet velocity: 131 m/s, outlet pressure: 0.83 bar.

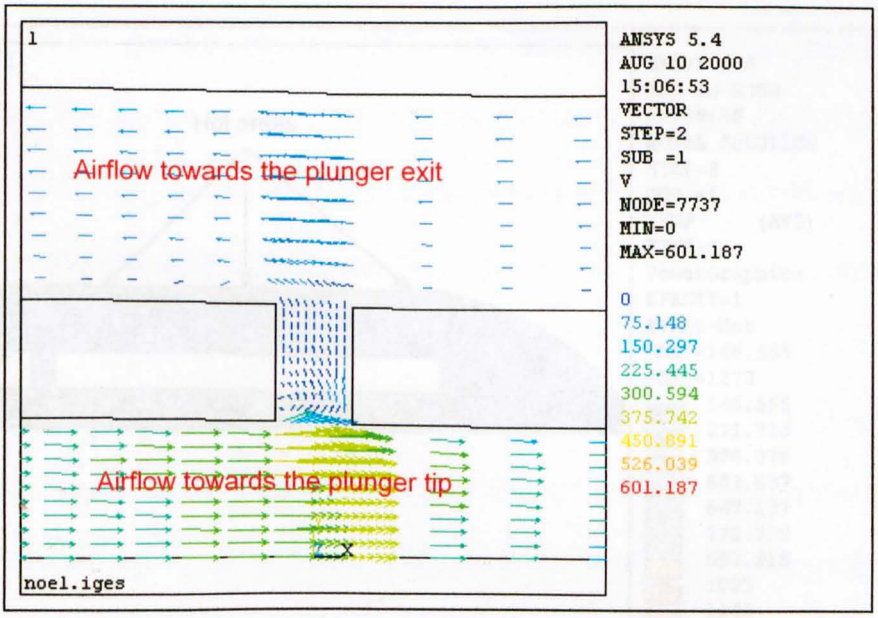

Figure 5.27. Diagram airflow velocity distribution at the first hole from the plunger tip of the cooling tube. Inlet velocity: 131 m/s, outlet pressure: 0.83 bar.

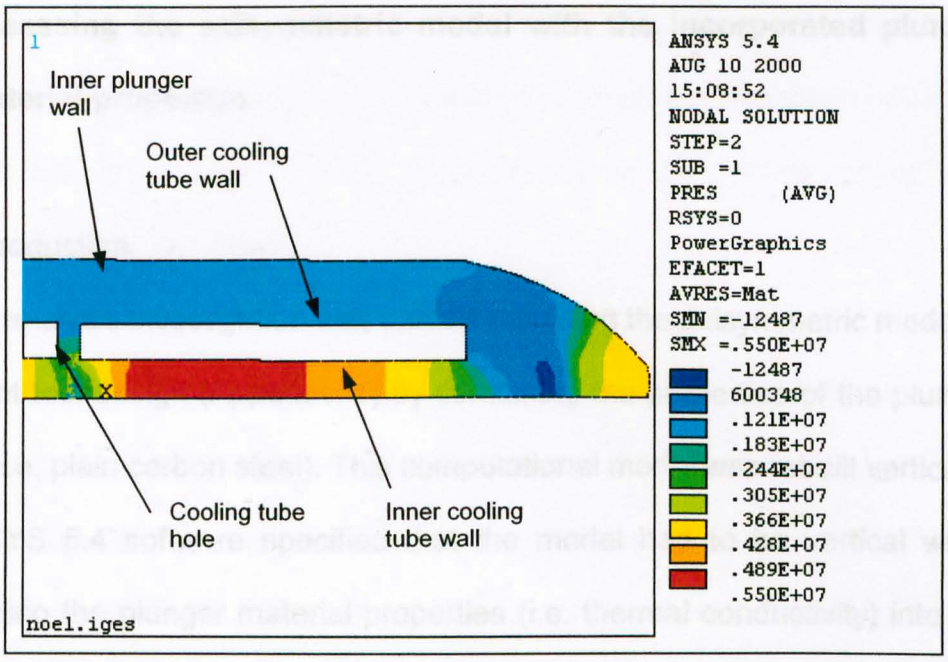

Figure 5.28. Diagram pressure distribution at the plunger tip of the cooling tube. Inlet velocity: 131 m/s, outlet pressure: 0.83 bar.

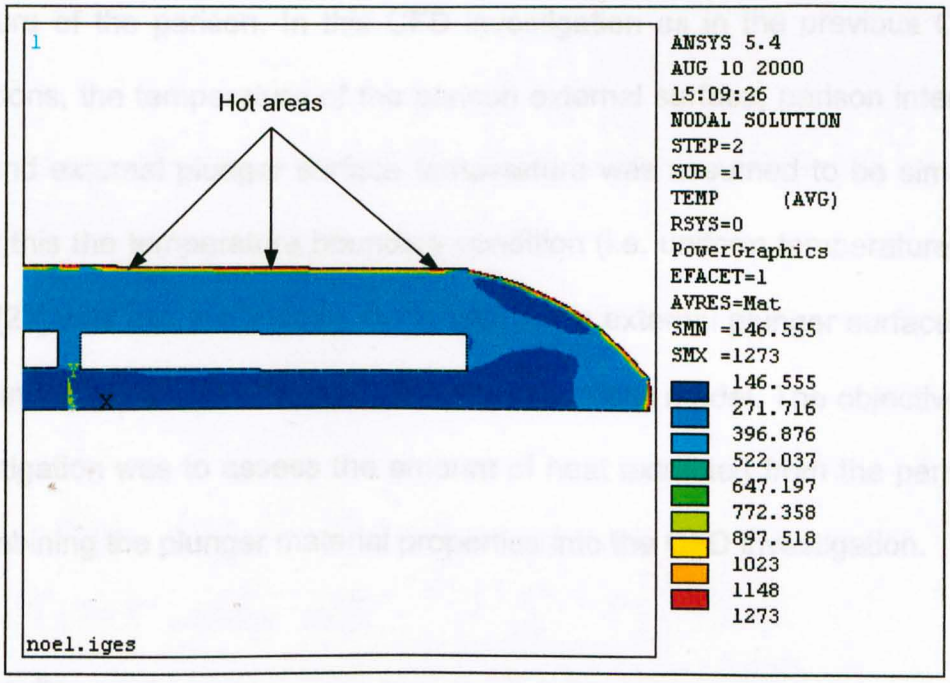

Figure 5.29. Diagram temperature distribution at the plunger tip of the cooling tube. Inlet velocity: 131 m/s, outlet pressure: 0.83 bar.

5.5 Assessing the axisymmetric model with the incorporated plunger material properties

5.5.1 Introduction

The CFD analysis investigation was carried out using the axisymmetric model of the current tool design (Appendix 1) by combining the properties of the plunger material (i.e. plain carbon steel). This computational model was rebuilt vertically. The ANSYS 5.4 software specified that the model had to be vertical when incorporating the plunger material properties (i.e. thermal conductivity) into the CFD investigation. This model was subjected to a uniform temperature boundary condition of 1000°C, which was essentially the external surface temperature of the parison. In this CFD investigation as in the previous CFD investigations, the temperature of the parison external surface, parison internal surface and external plunger surface temperature was assumed to be similar. Following this the temperature boundary condition (i.e. uniform temperature T= 1000°C) [21] was assumed along the length of the external plunger surface for this CFD investigation. This was to produce a simplistic model. The objective of this investigation was to assess the amount of heat extracted from the parison when combining the plunger material properties into the CFD investigation.

5.5.2 Results

The boundary conditions (i.e. P_{out}, V_{in}) used in this investigation were maintained the same, as chosen from previous laboratory experimental results

(Experiment 1 of Chapter 3) and used in the previous computational investigations. This investigation was repeated for each of the chosen boundary conditions with the plunger material properties using the current cooling tube design in the CFD investigation.

Following this investigation, the inlet temperature (T_{inlet}), outlet temperature (T_{outlet}), inlet mass flow rate ($\dot{m}_{inlet}$) and outlet mass flow rate ($\dot{m}_{outlet}$) of air flowing through the plunger cooling tube system were obtained. This data enabled the calculation of the approximate amount of heat extracted by the cooling tube system. The calculation of a selected result of this investigation is shown below:

Case 1

Boundary Conditions were: V_{in} = 75.7 m/s; P_{out} = 0 bar; actual P_{in} = 0.51 bar; $k = 6 \times 10^4$;

Assumed constant $C_{p\ air}$ = 1.004×10^3 J/kg K; constant density ρ_{inlet} = 1.966 kg/m^3; T_{inlet} = 290 K; T_{outlet} = 668 K

$$\dot{m} = (\pi r^2)\, V_{in} \times \rho$$

$$= \pi\, (3 \times 10^{-3})^2 \times 75.7 \times 1.966$$

$$\dot{m} = 4.208 \times 10^{-3} \text{ kg/s}$$

Heat absorbed ($\dot{Q}$) = Mass flow rate ($\dot{m}$) x Specific heat of air ($C_{p\ air}$) x

Temperature Difference ($\Delta T_{average}$)

$= 4.208 \times 10^{-3} \times 1.004 \times 10^{3} \times (668-290)$

Heat absorbed ($\dot{Q}$) = 1597 W

The tabulated results of this investigation are shown below:

Case	V_{in} (m/s)	P_{out} (bar)	P_{in} (bar)	k	$C_{p\ air}$ (Jkg/K)	ρ (kg/m^3)	T_{inlet} (K)	T_{outlet} (K)	$\dot{m}$ (kg/s)	$\dot{Q}$ (W)
1	75.7	0	0.51	6×10^4	1.004×10^3	1.966	290	668	4.208×10^{-3}	1597
2	92.73	0.2	1.27	2.8×10^4	1.004×10^3	3.176	289	606	8.327×10^{-3}	2650.2
3	100	0.31	1.4	4.5×10^4	1.004×10^3	2.909	288	604.5	8.225×10^{-3}	2613.6
4	105.97	0.4	1.58	1.5×10^4	1.004×10^3	2.553	288	606	7.65×10^{-3}	2442.2
5	113	0.52	1.95	1.4×10^4	1.004×10^3	2.95	287	590.5	9.425×10^{-3}	2872
6	117.33	0.6	2.27	1.6×10^4	1.004×10^3	3.598	287	576	0.0119	3463.3
7	122	0.64	2.5	1.6×10^4	1.004×10^3	4.219	286	560	0.01455	4003.6
8	126.79	0.7	2.86	1.5×10^4	1.004×10^3	6.257	285	517	0.0224	5224.7
9	131	0.83	3.0	1.3×10^4	1.004×10^3	8.389	285	477.3	0.03107	5999.1
10	135.5	1	3.09	1×10^4	1.004×10^3	4.704	284	546	0.018	4740.6

5.5.3 Discussion

The relationship between the heat absorbed and the inlet airflow velocity for this exercise is shown in Figure 5.30 on page 87. This graph showed that the inlet airflow velocity influences the amount of heat absorbed from the plunger wall.

The heat absorption rate dropped considerably when the inlet velocity was between 131 m/s and 135.5 m/s.

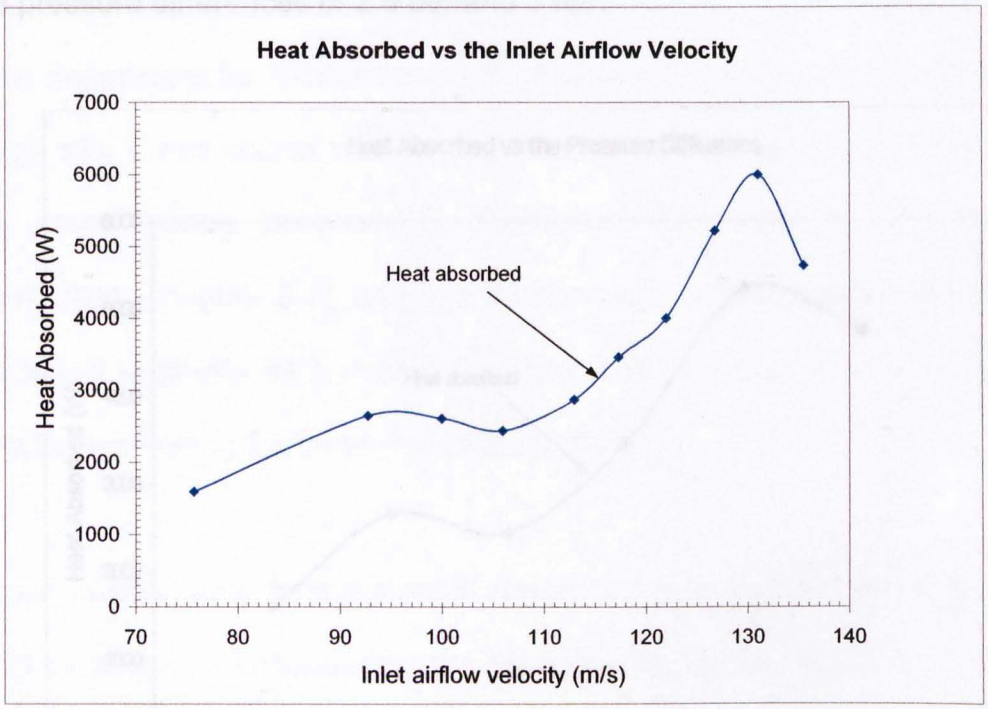

Figure 5.30. Graph of Heat Absorbed Vs Inlet Airflow Velocity of the plunger cooling tube system

A possible explanation for the decrease in the heat absorption rate could be due to the high velocity of inlet air, which causes choking, local recirculation and stagnation. This reduces the smooth and efficient heat extraction from the plunger wall. When the inlet airflow velocity was between 131 m/s to 135.5 m/s, choking was brought about by the stagnation of air in the cooling tube holes (Figure 5.34 on page 92). This greatly reduced the extraction of heat from the parison. The results of the graph of heat absorbed versus the inlet airflow

velocity along the plunger cooling tube system shown in Figure 5.30 on page 87 was quite similar to the graph of heat absorbed versus the pressure difference in Figure 5.31 below. The absorption rate of the cooling tube dropped between the pressure differences of 2.5 bar and 3 bar.

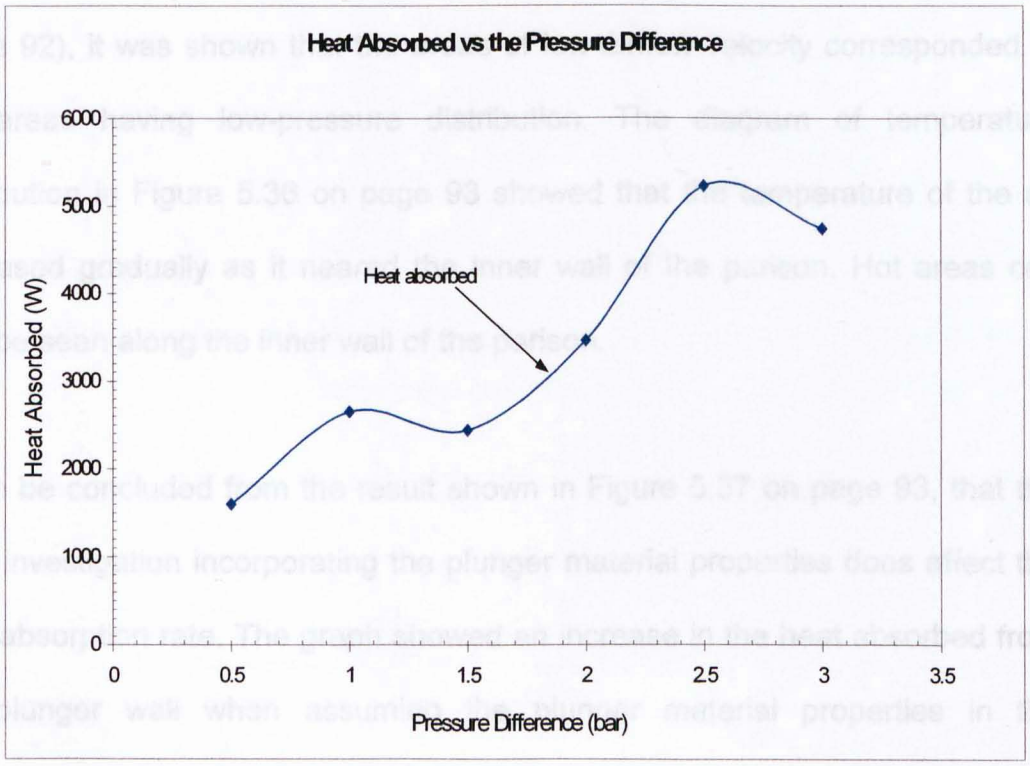

Figure 5.31. Graph of Heat Absorbed Vs Inlet Pressure Difference of the plunger cooling tube system

The CFD results (Figures 5.32 to 5.36 on pages 91 to 93) of the inlet airflow velocity of 135.5 m/s were selected for further discussion. Figure 5.32 on page 91 showed the airflow velocity distribution through the 8 cooling tube holes in the axisymmetrical model. Figure 5.33 on page 91 showed the zoomed view of airflow velocity distribution through the first two cooling tube hole from the

plunger tip. The zoomed view of the airflow velocity distribution through the first cooling tube hole from the plunger tip is shown in Figure 5.34 on page 92. Figures 5.35 and 5.36 respectively on pages 92 and 93 showed the zoomed view of the pressure and temperature distribution at the first cooling tube hole from the plunger tip. When comparing Figure 5.33 (page 91) with Figure 5.35 (page 92), it was shown that the areas of low airflow velocity corresponded to the areas having low-pressure distribution. The diagram of temperature distribution in Figure 5.36 on page 93 showed that the temperature of the air increased gradually as it neared the inner wall of the parison. Hot areas can also be seen along the inner wall of the parison.

It can be concluded from the result shown in Figure 5.37 on page 93, that the CFD investigation incorporating the plunger material properties does affect the heat absorption rate. The graph showed an increase in the heat absorbed from the plunger wall when assuming the plunger material properties in the investigation. This confirms the work carried out by Penlington, Sarwar, Marshall, Cockerham and Lewis [38]. They indicated that the thermal conductivity of the plunger material and the heat transfer coefficients at the interfaces are one of the possible factors affecting the rate of heat transfer through the plunger wall and into the cooling medium.

5.5.4 Conclusion

The result obtained from this investigation showed that the plunger material properties are one of the factors that influence the heat transfer efficiency of the plunger cooling tube system. Following this, the heat transfer effectiveness of the plunger cooling tube system with the CFD 3D model was investigated.

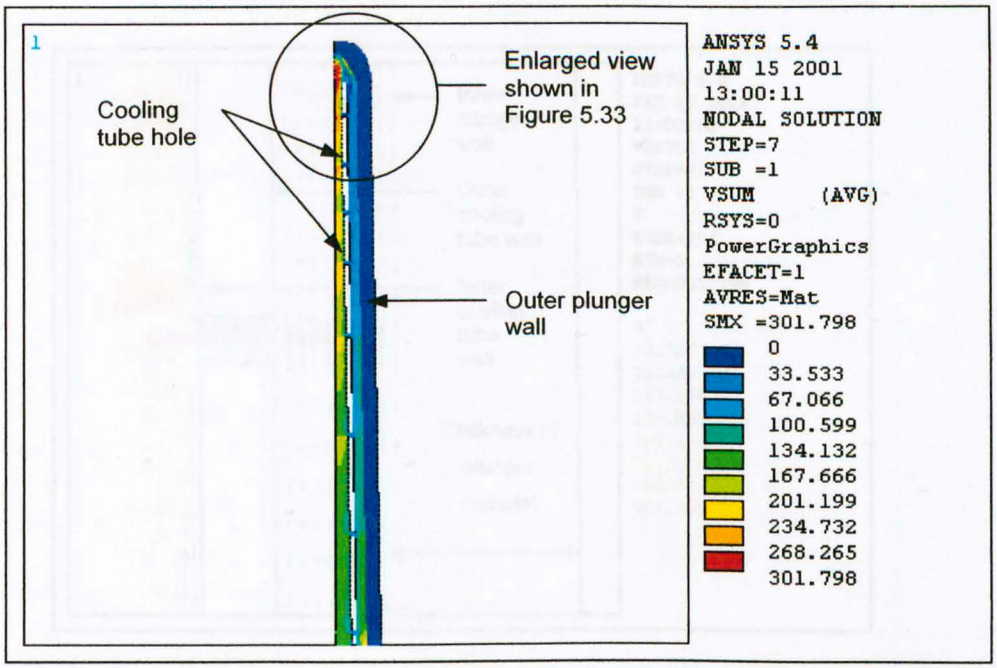

Figure 5.32. Diagram of airflow velocity distribution in the axisymmetrical model of the cooling tube. Inlet velocity: 135.5 m/s, outlet pressure: 1 bar.

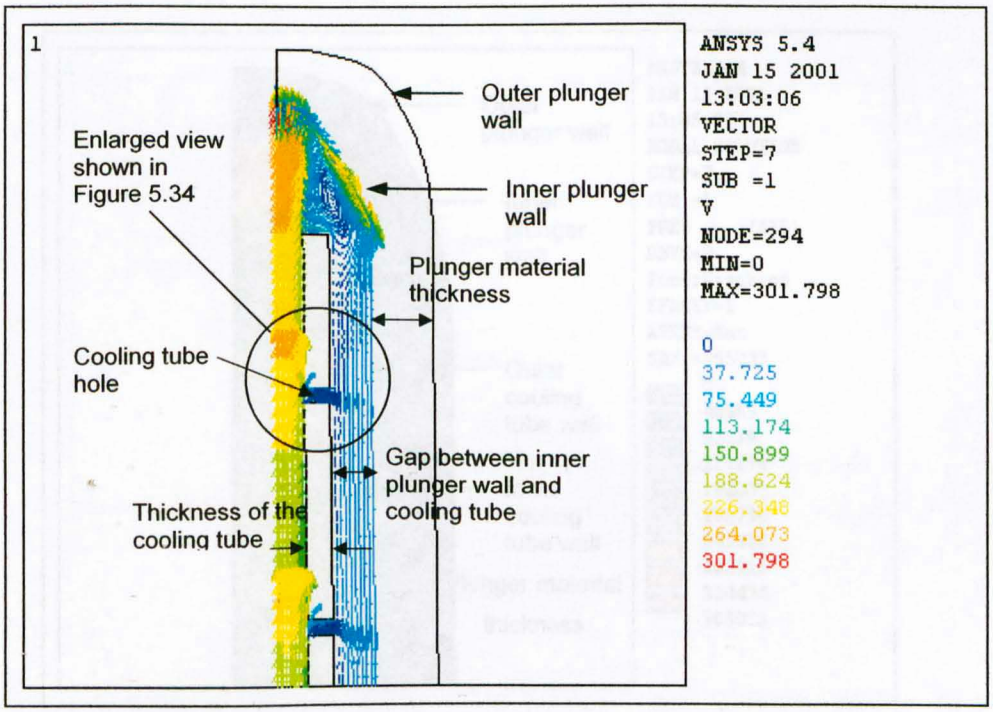

Figure 5.33. Diagram of airflow velocity distribution at the plunger tip of the cooling tube. Inlet velocity: 135.5 m/s, outlet pressure: 1 bar.

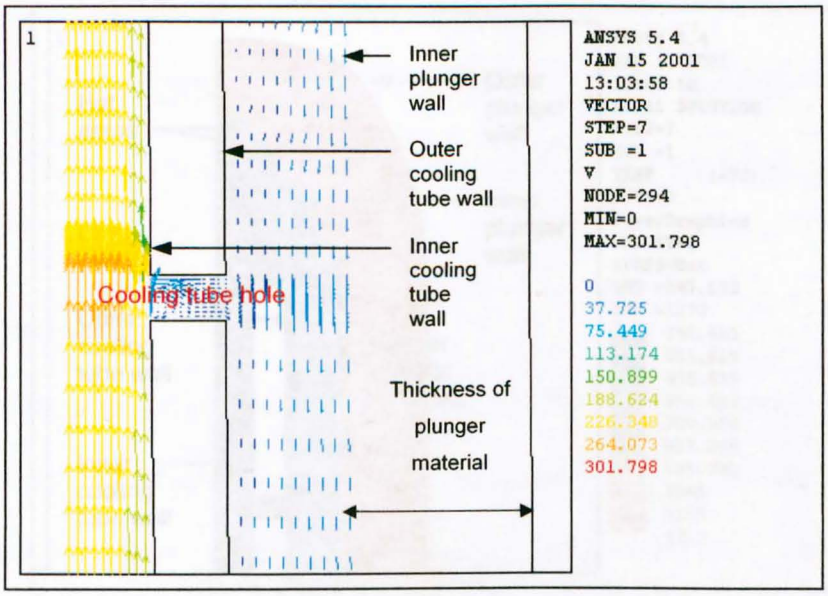

Figure 5.34. Diagram of airflow velocity distribution at the first hole from the plunger tip of the cooling tube. Inlet velocity: 135.5 m/s, outlet pressure: 1 bar.

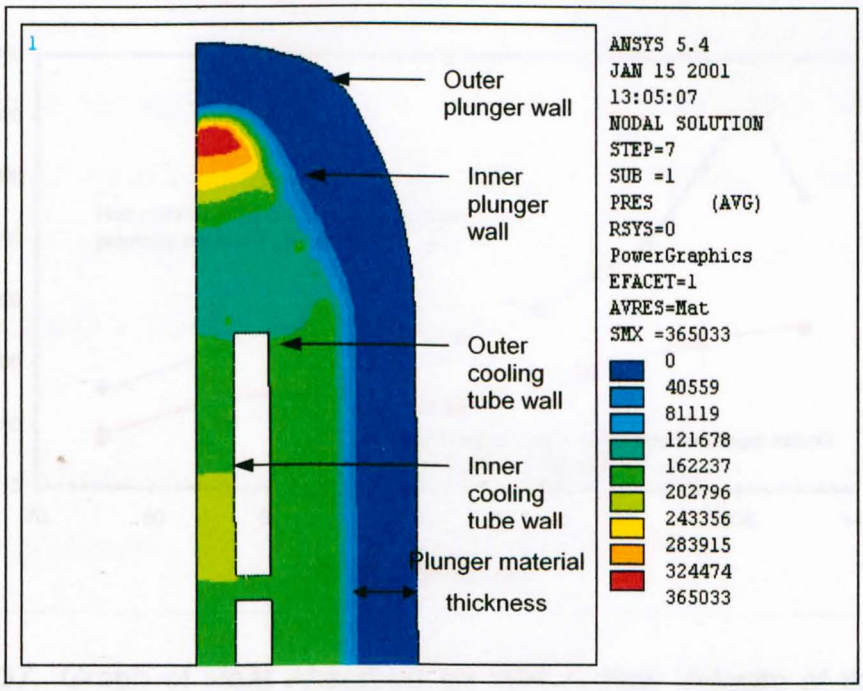

Figure 5.35. Diagram of pressure distribution at the plunger tip of the cooling tube. Inlet velocity: 135.5 m/s, outlet pressure: 1 bar.

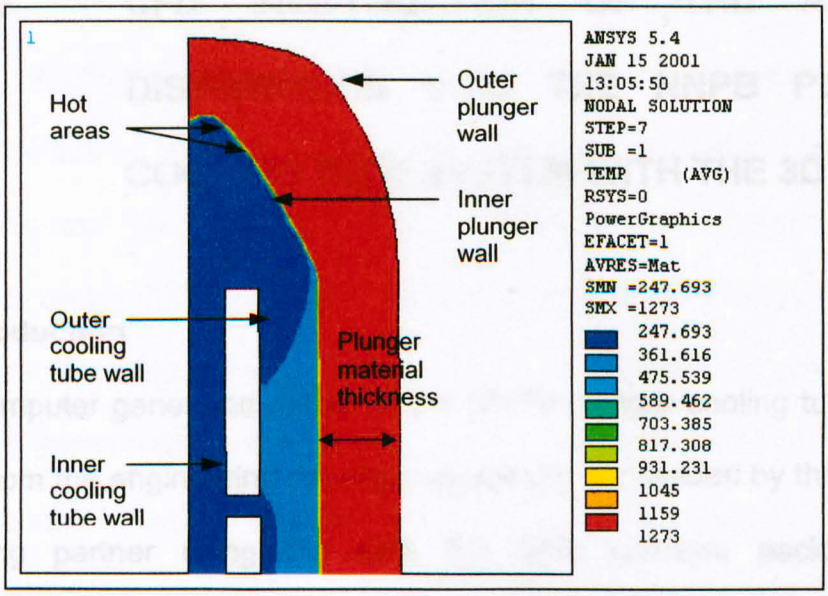

Figure 5.36. Diagram of temperature distribution at the plunger tip of the cooling tube. Inlet velocity: 135.5 m/s, outlet pressure: 1 bar.

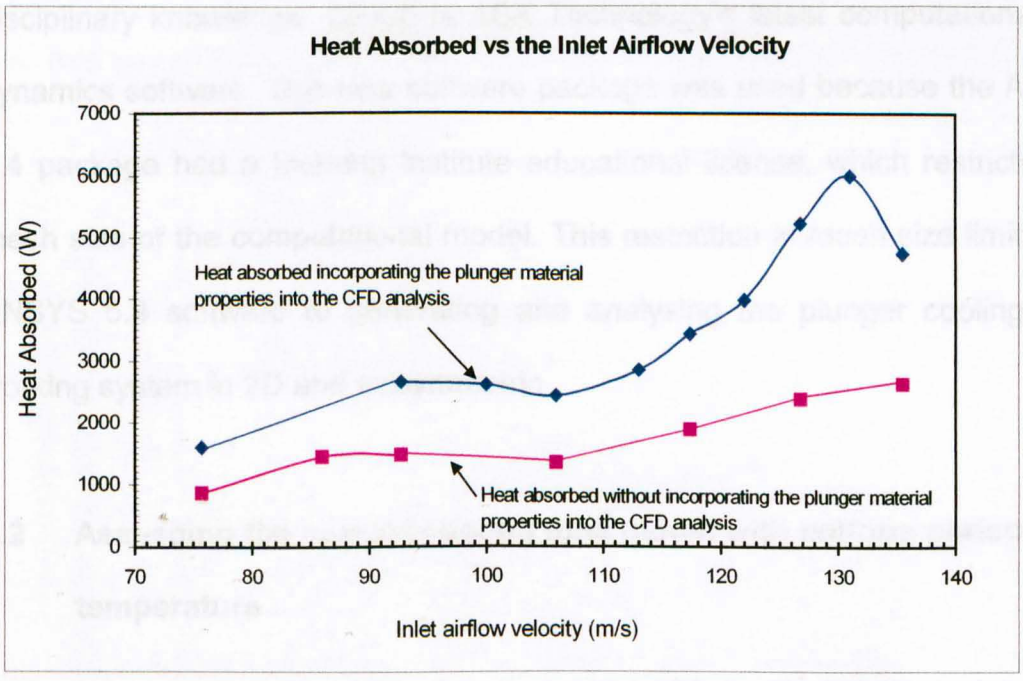

Figure 5.37. Graph of Heat Absorbed Vs Inlet Airflow Velocity of the plunger cooling tube system with and without incorporating the plunger material properties into the CFD analysis.

Chapter 6 CFD INVESTIGATION OF THE AIRFLOW DISTRIBUTION INTO THE NNPB PLUNGER COOLING TUBE SYSTEM WITH THE 3D MODEL

6.1 Introduction

The 3D computer generated model of the NNPB plunger cooling tube system was built from the engineering drawings (Appendix 1) provided by the industrial collaborating partner using the CFX 5.3 CFD software package. AEA Technology developed the CFX software. AEA Technology is an international company with engineering skills, experimental validation facilities and multi-disciplinary knowledge. CFX-5 is AEA Technology's latest computational fluid dynamics software. This new software package was used because the ANSYS 5.4 package had a learning institute educational license, which restricted the mesh size of the computational model. This restriction in mesh size limited the ANSYS 5.4 software to generating and analysing the plunger cooling tube-working system in 2D and axisymmetric.

6.2 Assessing the current cooling tube model with uniform parison skin temperature

6.2.1 Introduction

The model of the current plunger cooling tube system was built in 3D following the dimensions taken from the engineering drawings shown in Appendix 1. The

cooling tube hole diameter size was 0.7 mm as shown in the engineering drawings. The CFD investigation was carried out on the 3D model using the boundary conditions ($P_{out,}$ V_{in}) established from the laboratory experimental study (Experiment 1 of Chapter 3). The aim of this investigation was to assess the accuracy of this CFD investigation of the 3D model with the results from the experimental laboratory study. This assessment showed that there was an accuracy of approximately 52.6% between the CFD results of the 3D model when compared with the experimental laboratory study results (Figure 6.1 below). The cooling tube hole size was then investigated under the electro-microscope to ascertain its actual size. All the 15 holes along the length of the cooling tube were measured both vertically and horizontally across its centre. The average of both these sums were 0.63 mm and approximated to 0.6 mm.

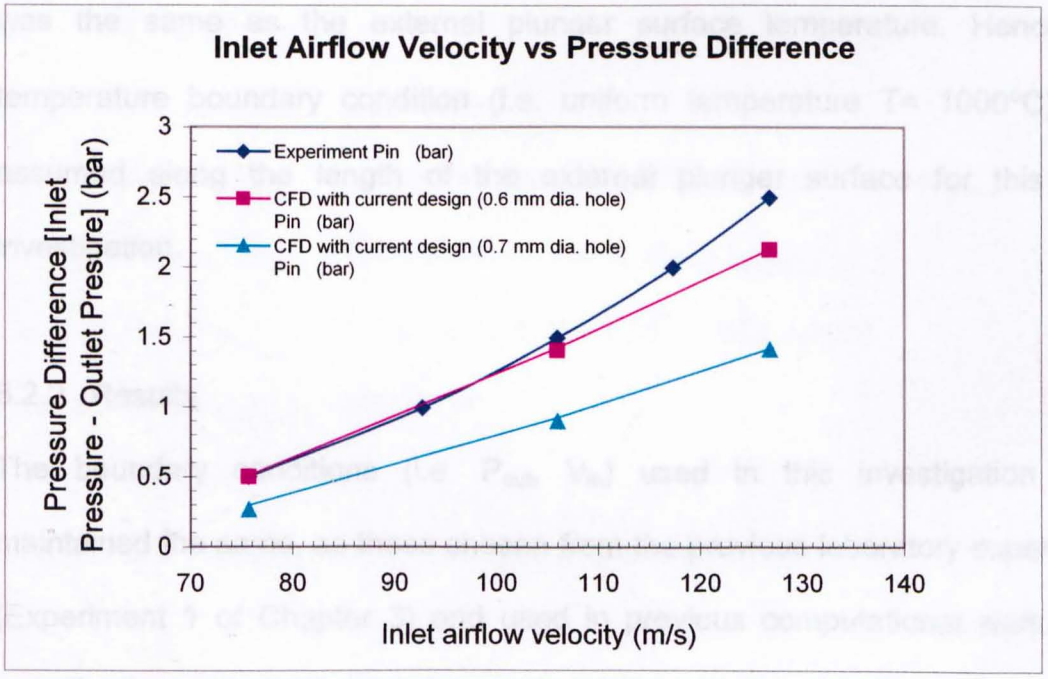

Figure 6.1. Inlet Airflow Velocity Vs Pressure Difference of the plunger cooling tube system design.

The 3D model of the cooling tube was rebuilt using the practical cooling tube hole diameter size of 0.6 mm and reinvestigated using the CFD software. This assessment showed that the new 3D model with the practical cooling tube hole diameter size of 0.6 mm was a closer representation of the laboratory experimental study results (Figure 6.1 on page 95). Hence 0.6 mm was accepted as the cooling tube hole size for the current cooling tube. This 3D model was then subjected to further CFD investigation under a uniform temperature boundary condition of 1000°C, which was essentially the internal surface temperature of the parison. This was to produce a simplistic model that assumed the parison internal surface temperature of 1000°C was similar to the external parison surface temperature as previously established [21]. Following this, it was also assumed that the internal surface temperature of the parison was the same as the external plunger surface temperature. Hence the temperature boundary condition (i.e. uniform temperature T= 1000°C) was assumed along the length of the external plunger surface for this CFD investigation.

6.2.2 Results

The boundary conditions (i.e. P_{out}, V_{in}) used in this investigation were maintained the same, as those chosen from the previous laboratory experiment (Experiment 1 of Chapter 3) and used in previous computational work. This investigation was repeated for each of the chosen boundary conditions. Following this investigation, the 3D CFD software computated the outlet

temperature (T_{outlet}) and mass flow rate ($\dot{m}$) of air flowing through the plunger cooling tube system. This data allowed the calculation of the approximate amount of heat extracted by the cooling tube system. The calculation of the heat extracted in this investigation is shown below:

Current cooling tube design (0.6 mm diameter size hole)

Boundary Conditions were: V_{in} = 75.7 m/s; P_{out} = 0 bar; actual P_{in} = 0.69 bar; Assumed constant $C_{p\ air}$ = 1.004 x 10^3 J/kg K; constant density ρ = 1.284 kg/m^3; T_{inlet} = 293 K; T_{outlet} = 802.4 K

$\dot{m}$ = $(\pi r^2)\ V_{in} \times \rho$

= $\pi(3 \times 10^{-3})^2 \times 75.7 \times 1.284$

$\dot{m}$ = 2.7 x 10^{-3} kg/s

Heat absorbed ($\dot{Q}$) = Mass flow rate ($\dot{m}$) x Specific heat of air ($C_{p\ air}$) x Temperature Difference ($\Delta T_{average}$)

= 2.7 x 10^{-3} x 1.004 x 10^3 x (802.4-293)

Heat absorbed ($\dot{Q}$) = 1382.5 W

The tabulated results of this investigation is shown below:

Current cooling tube design (0.6 mm diameter size hole)

Case	V_{in} (m/s)	P_{out} (bar)	P_{in} (bar)	$C_{p\ air}$ (Jkg/K)	ρ (kg/m^3)	T_{inlet} (K)	T_{outlet} (K)	$\dot{m}$ (kg/s)	$\dot{Q}$ (W)
1	75.7	0	0.69	1.004×10^3	1.284	293	802.4	2.7×10^{-3}	1382.5
2	92.73	0.2	1.23	1.004×10^3	1.284	293	798.5	3.31×10^{-3}	1680.6
3	105.97	0.4	1.74	1.004×10^3	1.284	293	794.64	3.78×10^{-3}	1905.9
4	117.33	0.6	2.22	1.004×10^3	1.284	293	790.76	4.19×10^{-3}	2093.9
5	126.79	0.7	2.59	1.004×10^3	1.284	293	798.52	4.53×10^{-3}	2298
6	135.5	1	3.15	1.004×10^3	1.284	293	783	4.84×10^{-3}	2380.4

It was also possible to calculate the amount of power applied/energy expanded in extracting the heat from the cooling tube system. The calculation of the power applied to extract the heat in this investigation is shown below:

Current cooling tube design (0.6 mm diameter size hole)

Boundary Conditions are: V_{in} = 75.7 m/s; P_{out} = 0 bar; actual P_{in} = 0.69 bar;

Assumed constant $C_{p\ air} = 1.004 \times 10^3$ J/kg K; constant density ρ = 1.284 kg/m^3;

T_{inlet} = 293 K; T_{outlet} = 802.4 K

Power (P) $= \Delta p \times Q$

$= \Delta p \times (A \times V_{in})$

$= [(0.69-0) \times 10^5] [\pi(3 \times 10^{-3})^2 \times 75.7]$

Power (P) = 145.3 W

The tabulated result of this investigation is shown below:

Current cooling tube design (0.6 mm diameter size hole)

Case	V_{in} (m/s)	P_{out} (bar)	P_{in} (bar)	P (W)
1	75.7	0	0.69	145.3
2	92.73	0.2	1.23	265.6
3	105.97	0.4	1.74	395
4	117.33	0.6	2.22	528.6
5	126.79	0.7	2.59	666.5
6	135.5	1	3.15	810.2

6.2.3 Discussion

The relationship between the heat absorbed and the inlet airflow velocity for this investigation is shown in Figure 6.2 below. The graph showed that the amount of heat absorbed from the plunger wall increased proportionally with an increase in the airflow velocity of the cooling tube.

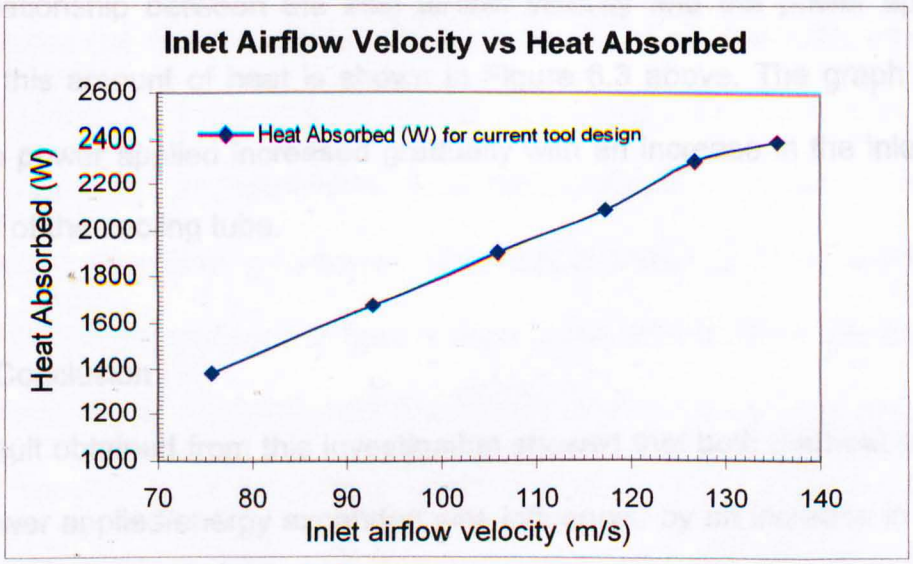

Figure 6.2. Graph of Inlet Airflow Velocity Vs Heat Absorbed for the current tool design

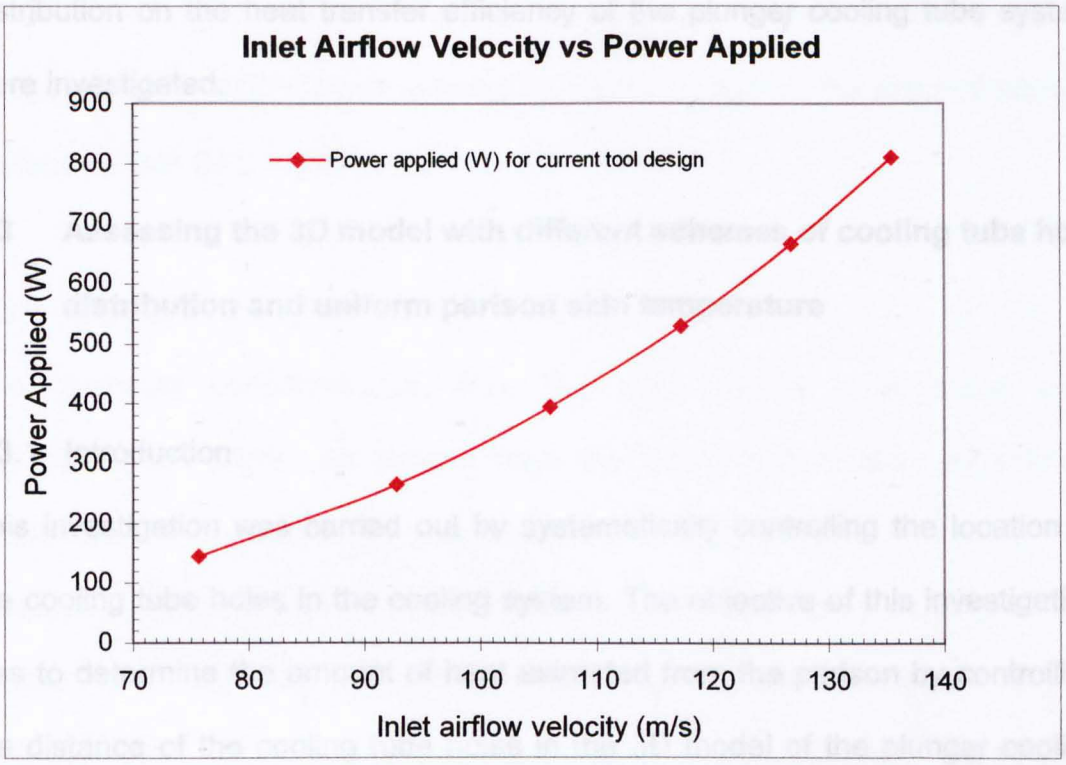

Figure 6.3. Graph of Inlet Airflow Velocity Vs Power Applied for the current tool design

The relationship between the inlet airflow velocity and the power applied to extract this amount of heat is shown in Figure 6.3 above. The graph showed that the power applied increased gradually with an increase in the inlet airflow velocity of the cooling tube.

6.2.4 Conclusion

The result obtained from this investigation showed that both the heat absorbed and power applied/energy expanded was influenced by an increase in the inlet airflow velocity. Following this, the effects of controlling the cooling tube hole

distribution on the heat transfer efficiency of the plunger cooling tube system were investigated.

6.3 Assessing the 3D model with different schemes of cooling tube hole distribution and uniform parison skin temperature

6.3.1 Introduction

This investigation was carried out by systematically controlling the location of the cooling tube holes in the cooling system. The objective of this investigation was to determine the amount of heat extracted from the parison by controlling the distance of the cooling tube holes in the 3D model of the plunger cooling tube system. Five different model configurations consisting of differing cooling tube holes spaces were built. They were the current tool design, equal, 0.75, 0.5 and 0.25 the ratio of the total length from the first to the last hole on the tube. Hence the spacing between the holes on the cooling tube was 0.0133 mm, 0.013 mm, 0.01 mm and 0.0068 mm for the respective equal, 0.75, 0.5 and 0.25 ratio model configurations. The computational 3-D model was then subjected to a uniform temperature boundary condition of 1000°C, which was essentially the internal surface temperature of the parison. This was to produce a simplistic model that assumed the parison internal surface temperature of 1000°C was similar to the external parison surface temperature as previously established [21]. Following this, it was also assumed that the internal surface temperature of the parison was the same as the external plunger surface

temperature. Hence the temperature boundary condition (i.e. uniform temperature T= 1000°C) was assumed along the length of the external plunger surface for this CFD investigation.

6.3.2 Results

The boundary conditions (i.e. P_{out}, V_{in}) used in this investigation were maintained the same, as chosen from the previous laboratory experiment (Experiment 1 of Chapter 3) and used in previous computational work. This investigation was repeated for each of the chosen boundary conditions with different locations of the cooling tube holes. Following this investigation, the 3D CFD software computated the outlet temperature (T_{outlet}) and mass flow rate ($\dot{m}$) of air flowing through the plunger cooling tube system. This data allowed the calculation of the approximate amount of heat extracted by the cooling tube system having different sets of cooling tube hole locations. The calculation of a selected result of this investigation is shown below:

Case 1 (equal ratio spacing)

Boundary Conditions were: V_{in} = 75.7 m/s; P_{out} = 0 bar; actual P_{in} = 0.68 bar;

Assumed constant $C_{p\ air}$ = 1.004 x 10^3 J/kg K; constant density ρ = 1.284 kg/m^3;

T_{inlet} = 293 K; T_{outlet} = 802.4 K

$$\dot{m} = (\pi r^2) V_{in} \times \rho$$

$$= \pi(3 \times 10^{-3})^2 \times 75.7 \times 1.284$$

$\dot{m}$ = 2.7×10^{-3} kg/s

Heat absorbed ($\dot{Q}$) = Mass flow rate ($\dot{m}$) x Specific heat of air ($C_{p\ air}$) x Temperature Difference ($\Delta T_{average}$)

= $2.7 \times 10^{-3} \times 1.004 \times 10^{3} \times (802.4-293)$

Heat absorbed ($\dot{Q}$) = 1382.5 W

The tabulated results of this investigation are shown below:

Equal ratio spacing

Case	V_{in} (m/s)	P_{out} (bar)	P_{in} (bar)	$C_{p\ air}$ (Jkg/K)	ρ (kg/m^3)	T_{inlet} (K)	T_{outlet} (K)	$\dot{m}$ (kg/s)	$\dot{Q}$ (W)
1	75.7	0	0.69	1.004×10^3	1.284	293	802.4	2.7×10^{-3}	1382.5
2	92.73	0.2	1.23	1.004×10^3	1.284	293	798.5	3.31×10^{-3}	1680.6
3	105.97	0.4	1.74	1.004×10^3	1.284	293	794.6	3.78×10^{-3}	1905.7
4	117.33	0.6	2.22	1.004×10^3	1.284	293	790.8	4.19×10^{-3}	2094.1
5	126.79	0.7	2.59	1.004×10^3	1.284	293	798.5	4.53×10^{-3}	2298
6	135.5	1	3.15	1.004×10^3	1.284	293	783	4.84×10^{-3}	2380.4

Current cooling tube design

Case	V_{in} (m/s)	P_{out} (bar)	P_{in} (bar)	$C_{p\ air}$ (Jkg/K)	ρ (kg/m^3)	T_{inlet} (K)	T_{outlet} (K)	$\dot{m}$ (kg/s)	$\dot{Q}$ (W)
1	75.7	0	0.69	1.004×10^3	1.284	293	802.4	2.7×10^{-3}	1382.5
2	92.73	0.2	1.23	1.004×10^3	1.284	293	798.5	3.31×10^{-3}	1680.5
3	105.97	0.4	1.74	1.004×10^3	1.284	293	794.64	3.78×10^{-3}	1905.9

4	117.33	0.6	2.22	1.004×10^3	1.284	293	790.76	4.19×10^{-3}	2093.9
5	126.79	0.7	2.59	1.004×10^3	1.284	293	798.52	4.53×10^{-3}	2298
6	135.5	1	3.15	1.004×10^3	1.284	293	783	4.84×10^{-3}	2380.4

0.75 ratio spacing

Case	V_{in} (m/s)	P_{out} (bar)	P_{in} (bar)	$C_{p\ air}$ (Jkg/K)	ρ (kg/m^3)	T_{inlet} (K)	T_{outlet} (K)	$\dot{m}$ (kg/s)	$\dot{Q}$ (W)
1	75.7	0	0.69	1.004×10^3	1.284	293	802.4	2.7×10^{-3}	1382.5
2	92.73	0.2	1.22	1.004×10^3	1.284	293	798.52	3.31×10^{-3}	1680.7
3	105.97	0.4	1.74	1.004×10^3	1.284	293	794.6	3.78×10^{-3}	1905.74
4	117.33	0.6	2.23	1.004×10^3	1.284	293	790.76	4.19×10^{-3}	2093.88
5	126.79	0.7	2.61	1.004×10^3	1.284	293	798.52	4.53×10^{-3}	2297.98
6	135.5	1	3.17	1.004×10^3	1.284	293	783	4.84×10^{-3}	2380.5

0.5 ratio spacing

Case	V_{in} (m/s)	P_{out} (bar)	P_{in} (bar)	$C_{p\ air}$ (Jkg/K)	ρ (kg/m^3)	T_{inlet} (K)	T_{outlet} (K)	$\dot{m}$ (kg/s)	$\dot{Q}$ (W)
1	75.7	0	0.78	1.004×10^3	1.284	293	802.4	2.7×10^{-3}	1382.5
2	92.73	0.2	1.35	1.004×10^3	1.284	293	798.52	3.31×10^{-3}	1680.7
3	105.97	0.4	1.89	1.004×10^3	1.284	293	794.6	3.78×10^{-3}	1905.74
4	117.33	0.6	2.43	1.004×10^3	1.284	293	790.76	4.19×10^{-3}	2093.88
5	126.79	0.7	2.84	1.004×10^3	1.284	293	798.52	4.53×10^{-3}	2297.98

6	135.5	1	3.43	1.004 x 10^3	1.284	293	783	4.84 x 10^{-3}	2380.5

0.25 ratio spacing

Case	V_{in} (m/s)	P_{out} (bar)	P_{in} (bar)	$C_{p\ air}$ (Jkg/K)	ρ (kg/m^3)	T_{inlet} (K)	T_{outlet} (K)	$\dot{m}$ (kg/s)	$\dot{Q}$ (W)
1	75.7	0	0.96	1.004 x 10^3	1.284	293	802.4	2.7 x 10^{-3}	1382.5
2	92.73	0.2	1.62	1.004 x 10^3	1.284	293	798.5	3.31 x 10^{-3}	1680.6
3	105.97	0.4	2.24	1.004 x 10^3	1.284	293	794.6	3.78 x 10^{-3}	1905.7
4	117.33	0.6	2.85	1.004 x 10^3	1.284	293	790.76	4.19 x 10^{-3}	2094.1
5	126.79	0.7	3.34	1.004 x 10^3	1.284	293	798.52	4.53 x 10^{-3}	2298
6	135.5	1	4.02	1.004 x 10^3	1.284	293	783	4.84 x 10^{-3}	2380.4

It was also possible to calculate the amount of power applied/energy expanded in extracting the heat from the cooling tube system. The calculation of a selected result of this investigation is shown below:

Case 1 (equal ratio spacing)

Boundary Conditions were: V_{in} = 75.7 m/s; P_{out} = 0 bar; actual P_{in} = 0.69 bar;

Assumed constant $C_{p\ air}$ = 1.004 x 10^3 J/kg K; constant density ρ = 1.284 kg/m^3;

T_{inlet} = 293 K; T_{outlet} = 802.4 K

Power (P) $= \Delta p \times Q$

$= \Delta p \times (A \times V_{in})$

$= [(0.69\text{-}0) \times 10^5]\ [\pi(3 \times 10^{-3})^2 \times 75.7]$

Power (P) = 145.3 W

The tabulated results of this investigation is shown below:

Equal ratio spacing

Case	V_{in} (m/s)	P_{out} (bar)	P_{in} (bar)	P (W)
1	75.7	0	0.69	145.3
2	92.73	0.2	1.23	265.6
3	105.97	0.4	1.74	395
4	117.33	0.6	2.22	528.6
5	126.79	0.7	2.59	666.5
6	135.5	1	3.15	810.2

Current cooling tube design

Case	V_{in} (m/s)	P_{out} (bar)	P_{in} (bar)	P (W)
1	75.7	0	0.69	145.3
2	92.73	0.2	1.23	265.6
3	105.97	0.4	1.74	395
4	117.33	0.6	2.22	528.6
5	126.79	0.7	2.59	666.5
6	135.5	1	3.15	810.2

0.75 ratio spacing

Case	V_{in} (m/s)	P_{out} (bar)	P_{in} (bar)	P (W)
1	75.7	0	0.69	145.3
2	92.73	0.2	1.22	263.1
3	105.97	0.4	1.74	395
4	117.33	0.6	2.23	531.9
5	126.79	0.7	2.61	673.5
6	135.5	1	3.17	817.8

0.5 ratio spacing

Case	V_{in} (m/s)	P_{out} (bar)	P_{in} (bar)	P (W)
1	75.7	0	0.78	164.2
2	92.73	0.2	1.35	296.6
3	105.97	0.4	1.89	439.1
4	117.33	0.6	2.43	597.2
5	126.79	0.7	2.84	754.6
6	135.5	1	3.43	915.7

0.25 ratio spacing

Case	V_{in} (m/s)	P_{out} (bar)	P_{in} (bar)	P (W)
1	75.7	0	0.96	202.1
2	92.73	0.2	1.62	366.2
3	105.97	0.4	2.24	542.3
4	117.33	0.6	2.85	734.2

5	126.79	0.7	3.34	931
6	135.5	1	4.02	1138.1

6.3.3 Discussion

The relationship between the heat absorbed and the inlet airflow velocity for this investigation is shown in Figure 6.4 below. The graph showed that the amount of heat absorbed from the plunger wall increased proportionally with an increased in the airflow velocity of the cooling tube. This was true for all the 5 cases investigated. It was also shown that the heat absorption rate was the same for all the different spacing ratios between the cooling tube holes.

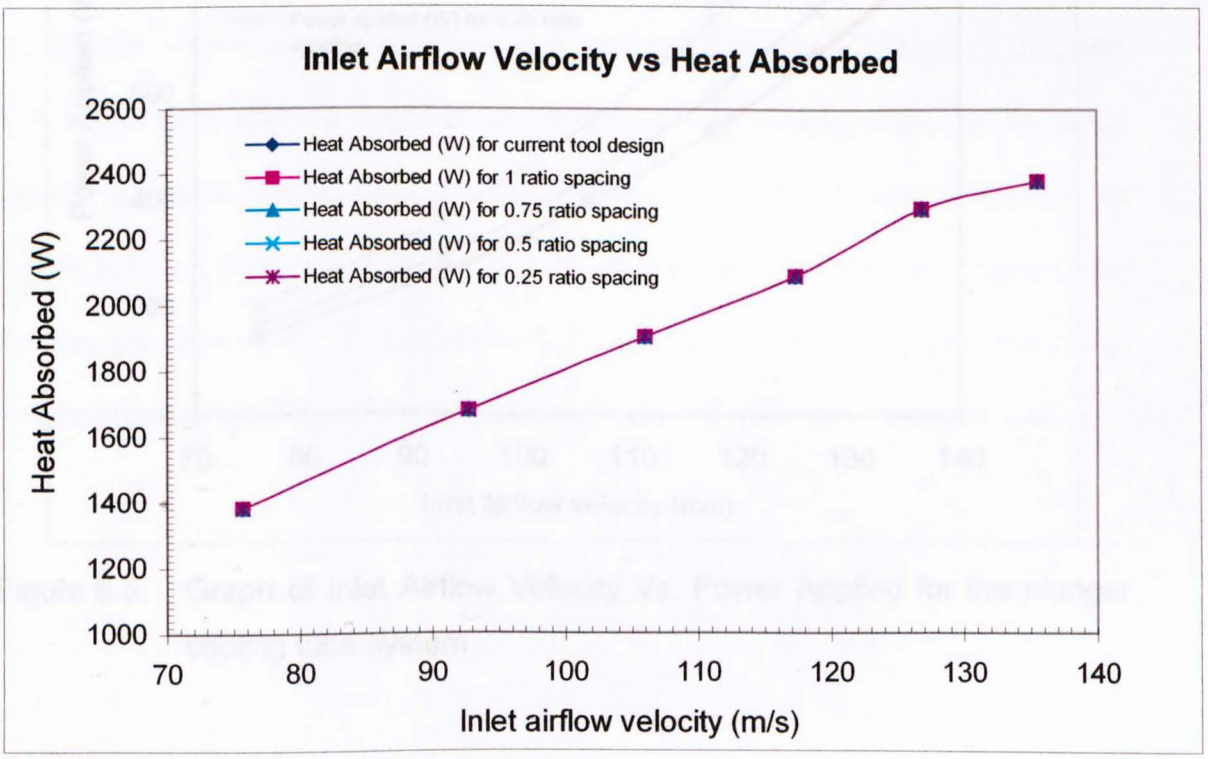

Figure 6.4. Graph of Heat Absorbed Vs. Inlet Airflow Velocity of the plunger cooling tube system.

Following this, the relationship between the inlet airflow velocity and the power applied/energy expanded to extract this amount of heat is shown in Figure 6.5 below. It was shown that the current tool design, 1 (equal) spacing ratio (0.0133 m spacing) and the 0.75 spacing ratio (0.013 m spacing) between the cooling tube holes used the least amount of power/energy in extracting this heat.

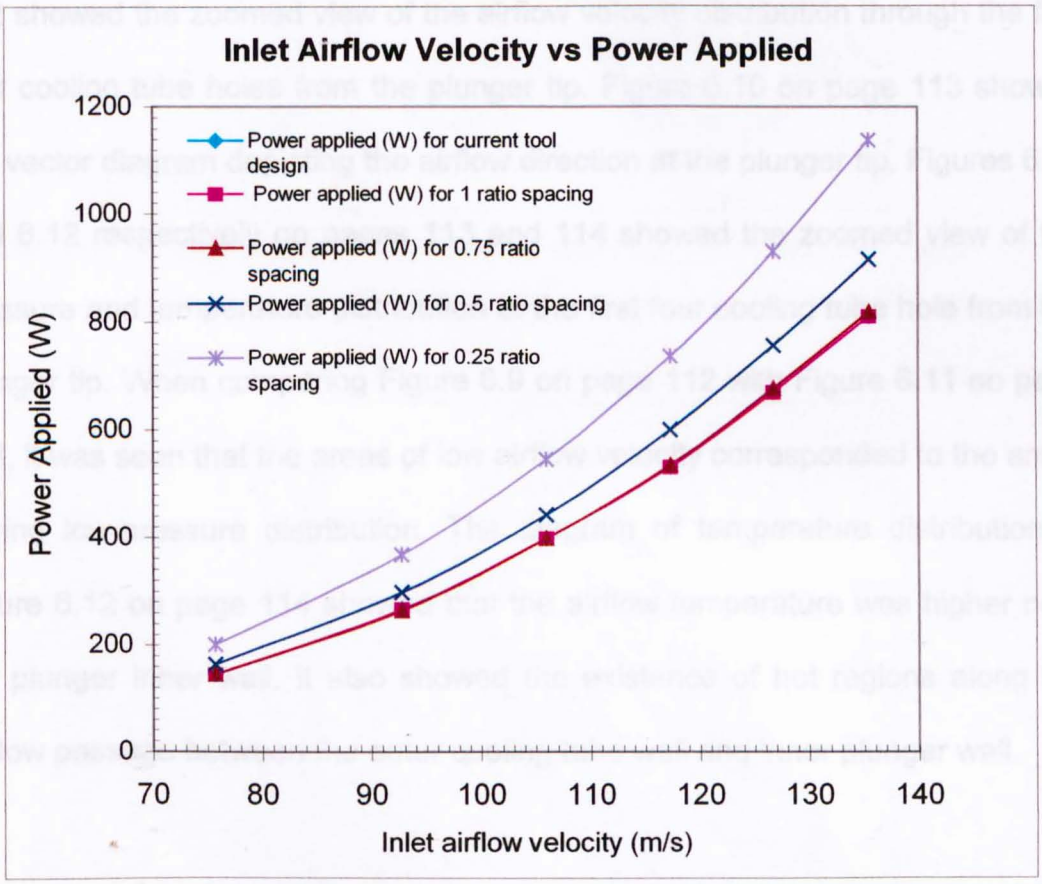

Figure 6.5. Graph of Inlet Airflow Velocity Vs. Power Applied for the plunger cooling tube system.

The CFD results (Figures 6.6 to 6.12 on pages 111 to 114) of the inlet airflow velocity of 105.97 m/s for the current tool design were selected for further discussion. Figure 6.6 on page 111 showed the airflow velocity distribution through the 8 cooling tube holes in the 3D model. The pressure and temperature distribution within the plunger cooling tube system were shown respectively in Figures 6.7 and 6.8 on pages 111 and 112. Figure 6.9 on page 112 showed the zoomed view of the airflow velocity distribution through the first four cooling tube holes from the plunger tip. Figure 6.10 on page 113 showed the vector diagram depicting the airflow direction at the plunger tip. Figures 6.11 and 6.12 respectively on pages 113 and 114 showed the zoomed view of the pressure and temperature distribution at the first four cooling tube hole from the plunger tip. When comparing Figure 6.9 on page 112 with Figure 6.11 on page 113, it was seen that the areas of low airflow velocity corresponded to the areas having low-pressure distribution. The diagram of temperature distribution in Figure 6.12 on page 114 showed that the airflow temperature was higher near the plunger inner wall. It also showed the existence of hot regions along the airflow passage between the outer cooling tube wall and inner plunger wall.

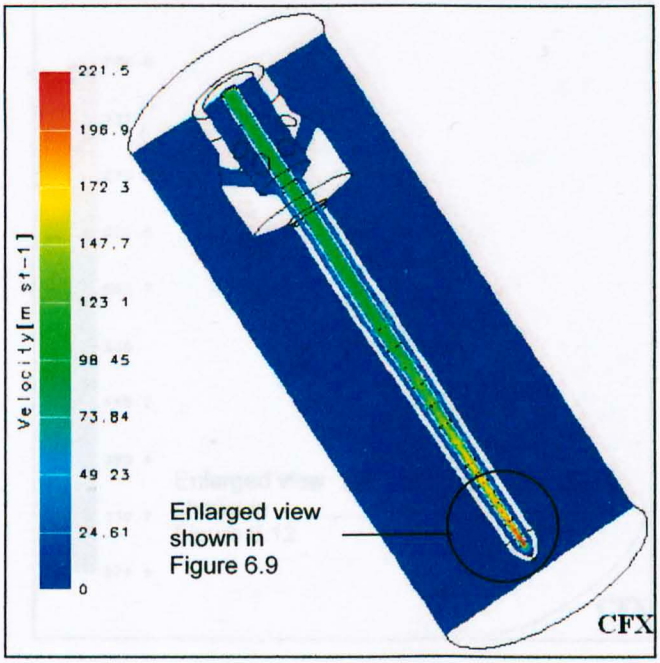

Figure 6.6. Diagram of airflow velocity distribution in the 3-D model of the plunger cooling tube system. Inlet velocity: 105.97 m/s, outlet pressure: 0.4 bar.

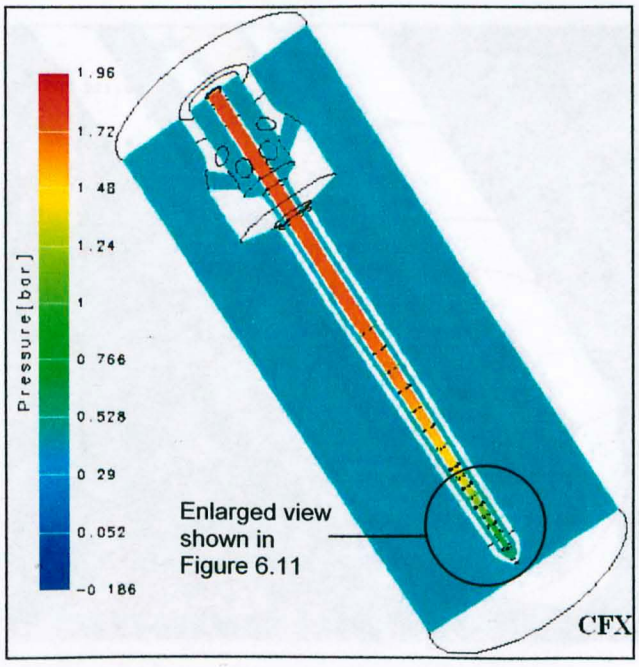

Figure 6.7. Diagram of pressure distribution in the 3-D model of the plunger cooling tube system. Inlet velocity: 105.97 m/s, outlet pressure: 0.4 bar.

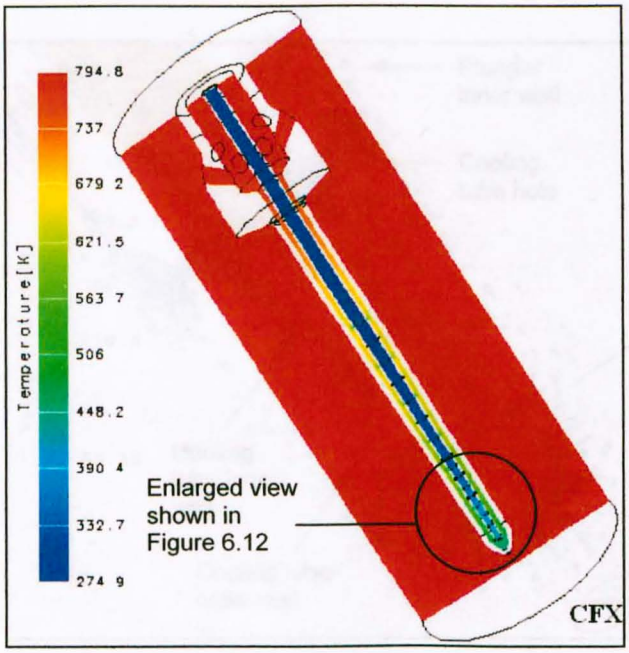

Figure 6.8. Diagram of temperature distribution in the 3-D model of the plunger cooling tube system. Inlet velocity: 105.97 m/s, outlet pressure: 0.4 bar.

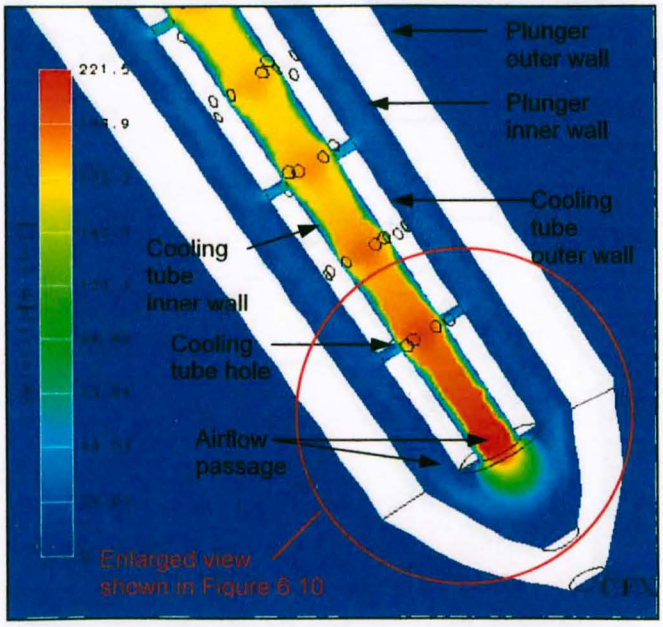

Figure 6.9. Diagram of airflow velocity distribution at the first four holes from the plunger tip of the cooling tube. Inlet velocity: 105.97 m/s, outlet pressure: 0.4 bar.

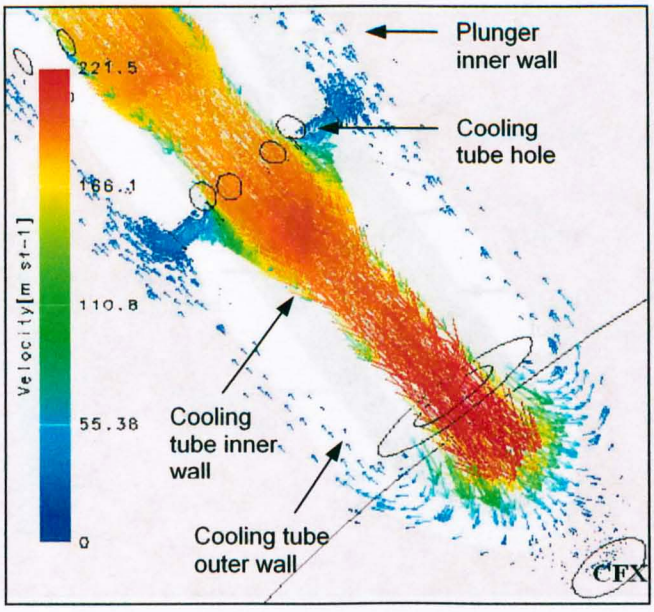

Figure 6.10. Vector diagram of the airflow velocity distribution at the first hole from the cooling tube plunger tip. Inlet velocity: 105.97 m/s, outlet pressure: 0.4 bar.

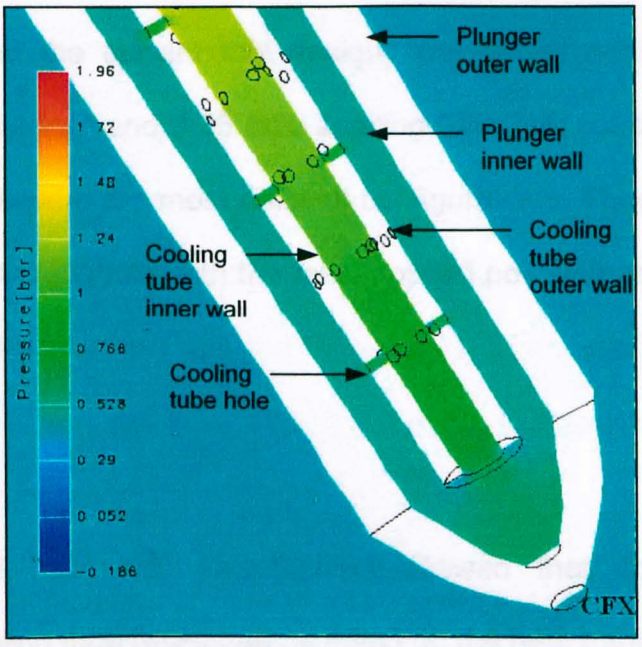

Figure 6.11. Diagram of pressure distribution at the first four holes from the plunger tip of the cooling tube. Inlet velocity: 105.97 m/s, outlet pressure: 0.4 bar.

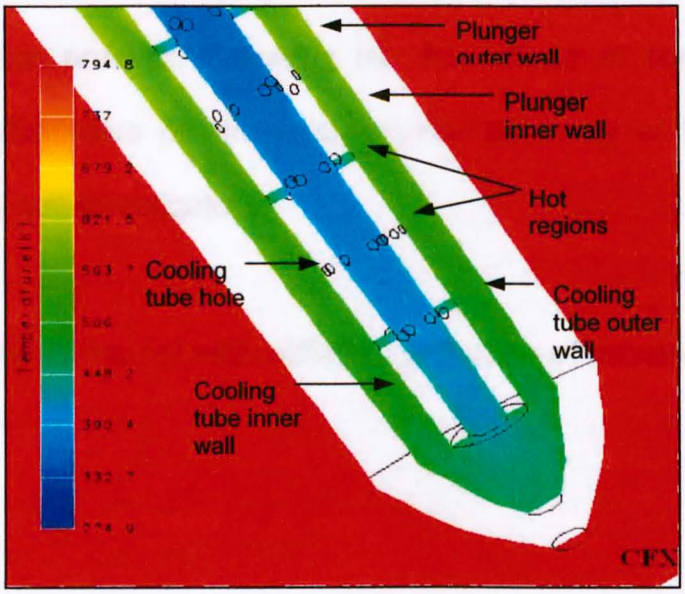

Figure 6.12. Diagram of temperature distribution at the first four holes from the plunger tip of the cooling tube. Inlet velocity: 105.97 m/s, outlet pressure: 0.4 bar.

It was concluded that the current tool design, tool with the 1 (equal) ratio spacing (0.0133 m spacing) and 0.75 ratio spacing (0.013 m spacing) between the cooling tube holes were the most efficient configurations. They provided so far the best heat absorption rate with the least applied power/energy expanded for the heat extraction process.

6.3.4 Conclusion

The result obtained from this investigation showed that controlling the distribution of the cooling tube holes had no effect on the heat transfer efficiency of the plunger cooling tube system. It also showed that the tool with the current design, 1 (equal) ratio spacing (0.0133 m spacing) and 0.75 ratio spacing

(0.013 m spacing) between the cooling tube holes used the least power/energy in the heat extraction process. Following this the effects of controlling the cooling tube hole diameters on the heat transfer efficiency of the plunger cooling tube system was investigated.

6.4 Assessing the 3D model with different schemes of cooling tube hole sizes

6.4.1 Introduction

This investigation was carried out by systematically controlling the diameter of the cooling tube holes in the cooling system. The objective of this investigation was to determine the amount of heat extracted from the parison by controlling the diameter of the cooling tube holes in the 3D model of the plunger cooling tube system. Five different model configurations consisting of differing cooling tube hole diameter sizes were built. The cooling tube hole diameters were 0.5 mm, 0.6 mm (current tool design), 0.7 mm, 0.9 mm and 1.2 mm. The computational 3-D model was subjected to a uniform temperature boundary condition of 1000°C, which was essentially the internal surface temperature of the parison.

6.4.2 Results

As in the previous investigations the temperature boundary condition (i.e. uniform temperature T= 1000°C) [21] was assumed along the length of the

plunger. This was in line with the assumption that the temperature of the parison internal surface, parison external surface and external plunger surface was the same in order to produce a simplistic model. Hence the temperature boundary condition (i.e. uniform temperature T= 1000°C) was assumed along the length of the external plunger surface for this CFD investigation. The boundary conditions (i.e. P_{out}, V_{in}) used in this investigation were maintained the same, as chosen from previous laboratory experimental results (Experiment 1 of Chapter 3) and used in previous computational investigations

Following this investigation, the CFD software (CFX 5.3) computated the outlet temperature (T_{outlet}) and mass flow rate ($\dot{m}$) of air flowing through the plunger cooling tube system. This data enabled the calculation of the approximate amount of heat extracted by the cooling tube system. The calculation of a selected result of the investigation is shown below:

Case 1 (0.5 mm diameter)

Boundary Conditions were: V_{in} = 75.7 m/s; P_{out} = 0 bar; actual P_{in} = 1.21 bar; Assumed constant $C_{p\ air}$ = 1.004 x 10^3 J/kg K; constant density ρ = 1.284 kg/m^3; T_{inlet} = 293 K; T_{outlet} = 802.3 K

$\dot{m}$ = $(\pi r^2)\ V_{in} \times \rho$

= $\pi(3 \times 10^{-3})^2 \times 75.7 \times 1.284$

$\dot{m}$ = 2.7 x 10^{-3} kg/s

Heat absorbed ($\dot{Q}$) = Mass flow rate ($\dot{m}$) x Specific heat of air ($C_{p\ air}$) x Temperature Difference ($\Delta T_{average}$)

$= 2.7 \times 10^{-3} \times 1.004 \times 10^{3} \times (802.3-293)$

Heat absorbed ($\dot{Q}$) = 1382.3 W

The tabulated results of this investigation are shown below:

0.5 mm diameter

Case	V_{in} (m/s)	P_{out} (bar)	P_{in} (bar)	$C_{p\ air}$ (Jkg/K)	ρ (kg/m^3)	T_{inlet} (K)	T_{outlet} (K)	$\dot{m}$ (kg/s)	$\dot{Q}$ (W)
1	75.7	0	1.21	1.004×10^3	1.284	293	802.3	2.7×10^{-3}	1382.3
2	92.73	0.2	2.03	1.004×10^3	1.284	293	798.5	3.31×10^{-3}	1680.6
3	105.97	0.4	2.79	1.004×10^3	1.284	293	794.6	3.78×10^{-3}	1905.7
4	117.33	0.6	3.52	1.004×10^3	1.284	293	790.8	4.19×10^{-3}	2094.1
5	126.79	0.7	4.1	1.004×10^3	1.284	293	798.5	4.53×10^{-3}	2297.9
6	135.5	1	4.88	1.004×10^3	1.284	293	783	4.84×10^{-3}	2380.4

0.6 mm diameter (current tool design)

Case	V_{in} (m/s)	P_{out} (bar)	P_{in} (bar)	$C_{p\ air}$ (Jkg/K)	ρ (kg/m^3)	T_{inlet} (K)	T_{outlet} (K)	$\dot{m}$ (kg/s)	$\dot{Q}$ (W)
1	75.7	0	0.69	1.004×10^3	1.284	293	802.4	2.7×10^{-3}	1382.5

2	92.73	0.2	1.23	1.004 x 10^3	1.284	293	798.5	3.31 x 10^{-3}	1680.6
3	105.97	0.4	1.74	1.004 x 10^3	1.284	293	794.64	3.78 x 10^{-3}	1905.9
4	117.33	0.6	2.22	1.004 x 10^3	1.284	293	790.76	4.19 x 10^{-3}	2093.9
5	126.79	0.7	2.59	1.004 x 10^3	1.284	293	798.52	4.53 x 10^{-3}	2298
6	135.5	1	3.15	1.004 x 10^3	1.284	293	783	4.84 x 10^{-3}	2380.4

0.7 mm diameter

Case	V_{in} (m/s)	P_{out} (bar)	P_{in} (bar)	$C_{p\ air}$ (Jkg/K)	ρ (kg/m^3)	T_{inlet} (K)	T_{outlet} (K)	$\dot{m}$ (kg/s)	$\dot{Q}$ (W)
1	75.7	0	0.4	1.004 x 10^3	1.284	293	801.8	2.7 x 10^{-3}	1381
2	92.73	0.2	0.8	1.004 x 10^3	1.284	293	798.2	3.31 x 10^{-3}	1679.6
3	105.97	0.4	1.18	1.004 x 10^3	1.284	293	794.5	3.78 x 10^{-3}	1905.4
4	117.33	0.6	1.55	1.004 x 10^3	1.284	293	790.7	4.19 x 10^{-3}	2093.6
5	126.79	0.7	1.81	1.004 x 10^3	1.284	293	798.5	4.53 x 10^{-3}	2298
6	135.5	1	2.26	1.004 x 10^3	1.284	293	783	4.84 x 10^{-3}	2380.4

0.9 mm diameter

Case	V_{in} (m/s)	P_{out} (bar)	P_{in} (bar)	$C_{p\ air}$ (Jkg/K)	ρ (kg/m^3)	T_{inlet} (K)	T_{outlet} (K)	$\dot{m}$ (kg/s)	$\dot{Q}$ (W)
1	75.7	0	0.22	1.004 x 10^3	1.284	293	780	2.7 x 10^{-3}	1321.7
2	92.73	0.2	0.53	1.004 x 10^3	1.284	293	796	3.31 x 10^{-3}	1672.3
3	105.97	0.4	0.83	1.004 x 10^3	1.284	293	792.8	3.78 x 10^{-3}	1899

4	117.33	0.6	1.12	1.004 x 10^3	1.284	293	789.5	4.19 x 10^{-3}	2088.6
5	126.79	0.7	1.3	1.004 x 10^3	1.284	293	797	4.53 x 10^{-3}	2291.1
6	135.5	1	1.69	1.004 x 10^3	1.284	293	782	4.84 x 10^{-3}	2375.6

1.2 mm diameter

Case	V_{in} (m/s)	P_{out} (bar)	P_{in} (bar)	$C_{p\ air}$ (Jkg/K)	ρ (kg/m^3)	T_{inlet} (K)	T_{outlet} (K)	$\dot{m}$ (kg/s)	$\dot{Q}$ (W)
1	75.7	0	0.14	1.004 x 10^3	1.284	293	798.4	2.7 x 10^{-3}	1371.7
2	92.73	0.2	0.4	1.004 x 10^3	1.284	293	795	3.31 x 10^{-3}	1669
3	105.97	0.4	0.66	1.004 x 10^3	1.284	293	792	3.78 x 10^{-3}	1896
4	117.33	0.6	0.92	1.004 x 10^3	1.284	293	789	4.19 x 10^{-3}	2086.5
5	126.79	0.7	1.07	1.004 x 10^3	1.284	293	796.4	4.53 x 10^{-3}	2288.3
6	135.5	1	1.42	1.004 x 10^3	1.284	293	782	4.84 x 10^{-3}	2375.6

It was also possible to calculate the amount of power applied/energy expanded in the heat extraction from the cooling tube system. The calculation of a selected result of this investigation is shown below:

Case 1 *(0.5 mm diameter)*

Boundary Conditions were: V_{in} = 75.7 m/s; P_{out} = 0 bar; actual P_{in} = 1.21 bar;

Assumed constant $C_{p\ air}$ = 1.004 x 10^3 J/kg K; constant density ρ = 1.284 kg/m^3;

T_{inlet} = 293 K; T_{outlet} = 802.3 K

Power (P) $= \Delta p \times Q$

$= \Delta p \times (A \times V_{in})$

$= [(1.21-0) \times 10^5] [\pi(3 \times 10^{-3})^2 \times 75.7]$

Power (P) $= 260.5$ W

The tabulated results of this investigation are shown below:

0.5 mm diameter

Case	V_{in} (m/s)	P_{out} (bar)	P_{in} (bar)	P (W)
1	75.7	0	1.21	260.5
2	92.73	0.2	2.03	472
3	105.97	0.4	2.79	704.4
4	117.33	0.6	3.52	952.8
5	126.79	0.7	4.1	1199
6	135.5	1	4.88	1462.2

0.6 mm diameter (current tool design)

Case	V_{in} (m/s)	P_{out} (bar)	P_{in} (bar)	P (W)
1	75.7	0	0.69	145.3
2	92.73	0.2	1.23	265.6
3	105.97	0.4	1.74	395
4	117.33	0.6	2.22	528.6
5	126.79	0.7	2.59	666.5
6	135.5	1	3.15	810.2

0.7 mm diameter

Case	V_{in} (m/s)	P_{out} (bar)	P_{in} (bar)	P (W)
1	75.7	0	0.4	82.2
2	92.73	0.2	0.8	103.2
3	105.97	0.4	1.18	229.9
4	117.33	0.6	1.55	310
5	126.79	0.7	1.81	391.4
6	135.5	1	2.26	474.8

0.9 mm diameter

Case	V_{in} (m/s)	P_{out} (bar)	P_{in} (bar)	P (W)
1	75.7	0	0.22	46.3
2	92.73	0.2	0.53	85.1
3	105.97	0.4	0.83	126.7
4	117.33	0.6	1.12	169.7
5	126.79	0.7	1.3	211.6
6	135.5	1	1.69	260

1.2 mm diameter

Case	V_{in} (m/s)	P_{out} (bar)	P_{in} (bar)	P (W)
1	75.7	0	0.14	29.5
2	92.73	0.2	0.4	51.6
3	105.97	0.4	0.66	76.6
4	117.33	0.6	0.92	104.4

5	126.79	0.7	1.07	130.3
6	135.5	1	1.42	158.3

6.4.3 Discussion

The relationship between the heat absorbed and the inlet airflow velocity for this investigation is shown in Figure 6.13 on page 123. The graph showed that the amount of heat absorbed from the plunger wall increased proportionally with an increase in the airflow velocity of the cooling tube. This was true for all the 5 cases investigated. It also showed that the difference between the heat extracted for all the 5 cases was negligible.

Following this, the relationship between the inlet airflow velocity and the power applied/energy expanded to extract this amount of heat was shown in Figure 6.14 on page 123. The model with the 1.2 mm diameter cooling tube hole used the least amount of power/energy in extracting the heat from the parison. The most power applied/energy expanded in extracting the heat from the parison was with the model having the 0.5 mm diameter cooling tube hole.

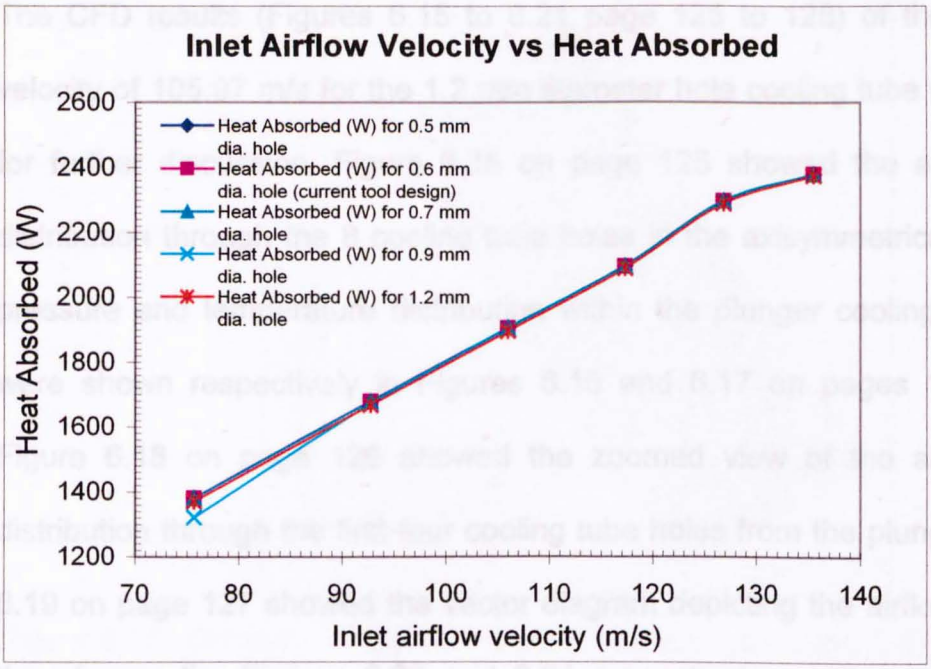

Figure 6.13. Graph of Heat Absorbed Vs. Inlet Airflow Velocity of the plunger cooling tube system.

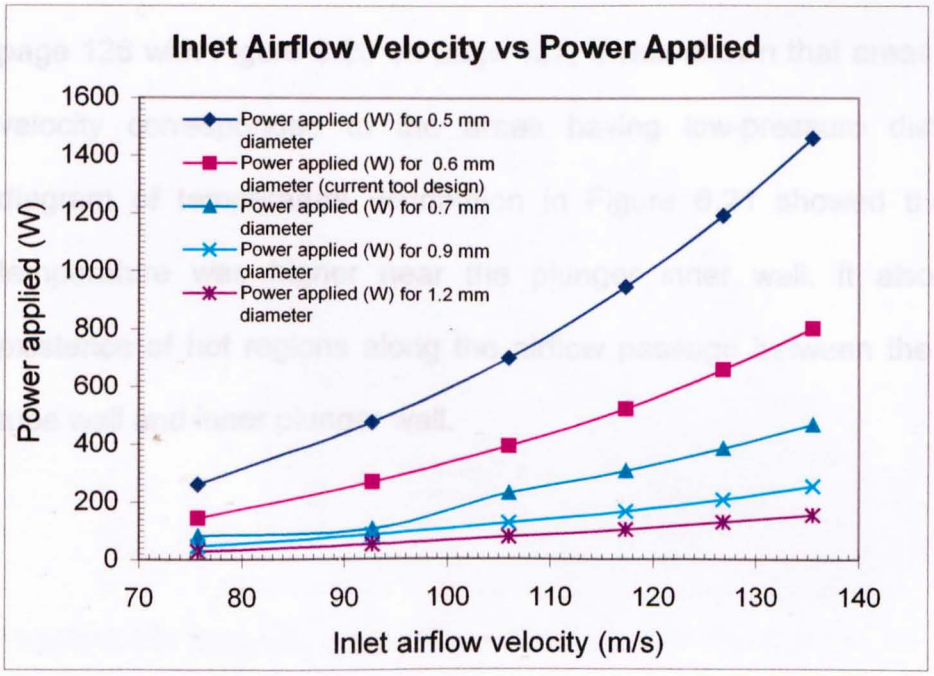

Figure 6.14. Graph of Inlet Airflow Velocity Vs. Power Applied for the plunger cooling tube system.

The CFD results (Figures 6.15 to 6.21 page 125 to 128) of the inlet airflow velocity of 105.97 m/s for the 1.2 mm diameter hole cooling tube were selected for further discussion. Figure 6.15 on page 125 showed the airflow velocity distribution through the 8 cooling tube holes in the axisymmetrical model. The pressure and temperature distribution within the plunger cooling tube system were shown respectively in Figures 6.16 and 6.17 on pages 125 and 126. Figure 6.18 on page 126 showed the zoomed view of the airflow velocity distribution through the first four cooling tube holes from the plunger tip. Figure 6.19 on page 127 showed the vector diagram depicting the airflow direction at the plunger tip. Figures 6.20 and 6.21 respectively on pages 127 and 128 showed the zoomed view of the pressure and temperature distribution at the first four cooling tube hole from the plunger tip. When comparing Figure 6.18 on page 126 with Figure 6.20 on page 127, it was shown that areas of low airflow velocity corresponded to the areas having low-pressure distribution. The diagram of temperature distribution in Figure 6.21 showed that the airflow temperature was higher near the plunger inner wall. It also showed the existence of hot regions along the airflow passage between the outer cooling tube wall and inner plunger wall.

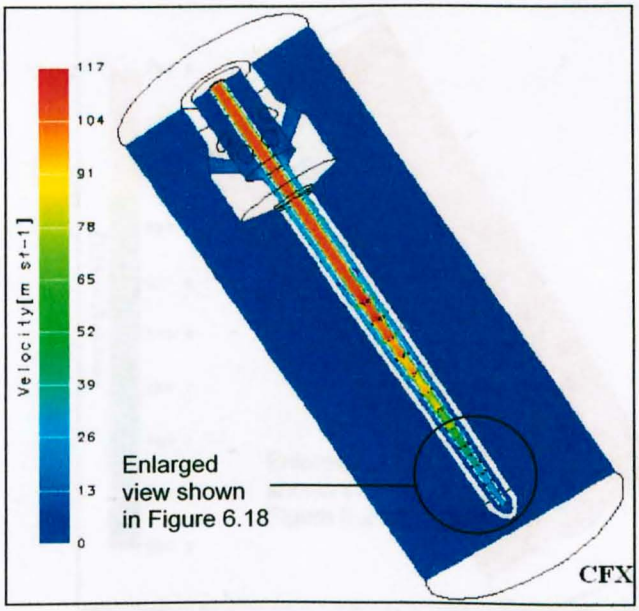

Figure 6.15. Diagram of airflow velocity distribution in the 3-D model of the plunger cooling tube system. Inlet velocity: 105.97 m/s, outlet pressure: 0.4 bar.

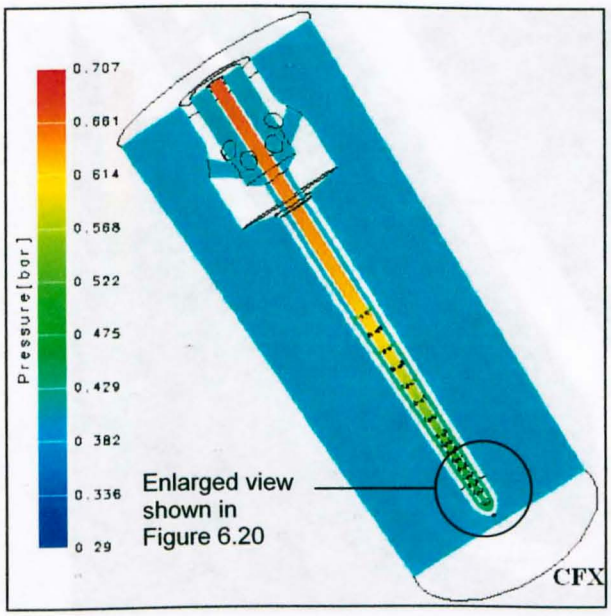

Figure 6.16. Diagram of pressure distribution in the 3-D model of the plunger cooling tube system. Inlet velocity: 105.97 m/s, outlet pressure: 0.4 bar.

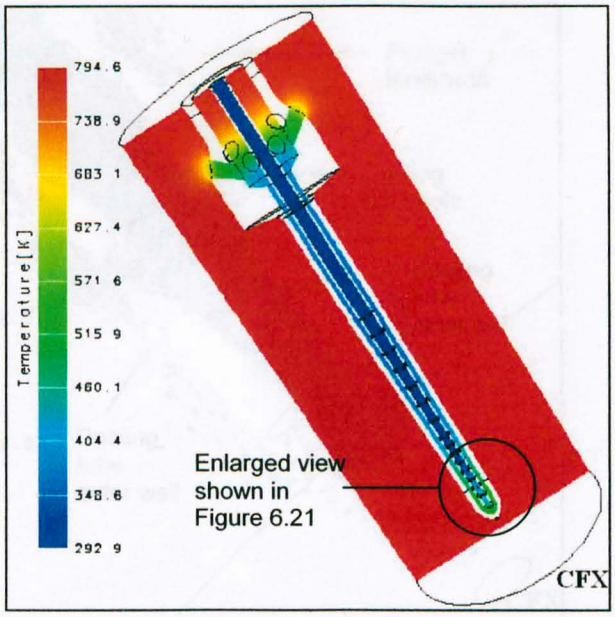

Figure 6.17. Diagram of temperature distribution in the 3-D model of the plunger cooling tube system. Inlet velocity: 105.97 m/s, outlet pressure: 0.4 bar.

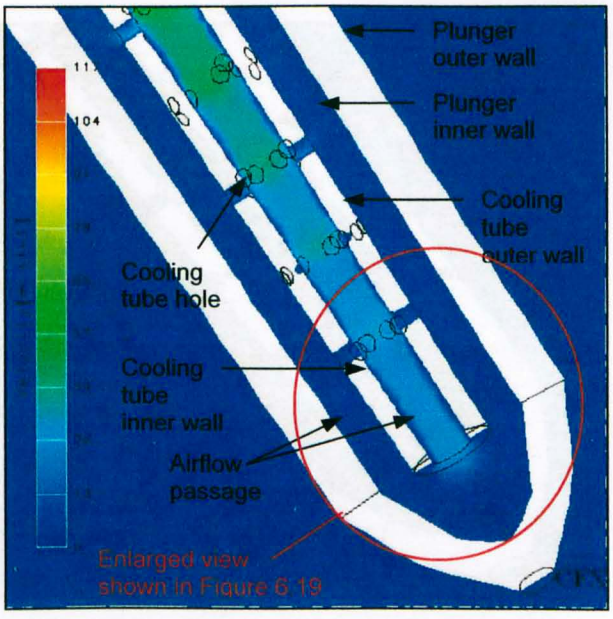

Figure 6.18. Diagram of airflow velocity distribution at the first four holes from the plunger tip of the cooling tube. Inlet velocity: 105.97 m/s, outlet pressure: 0.4 bar.

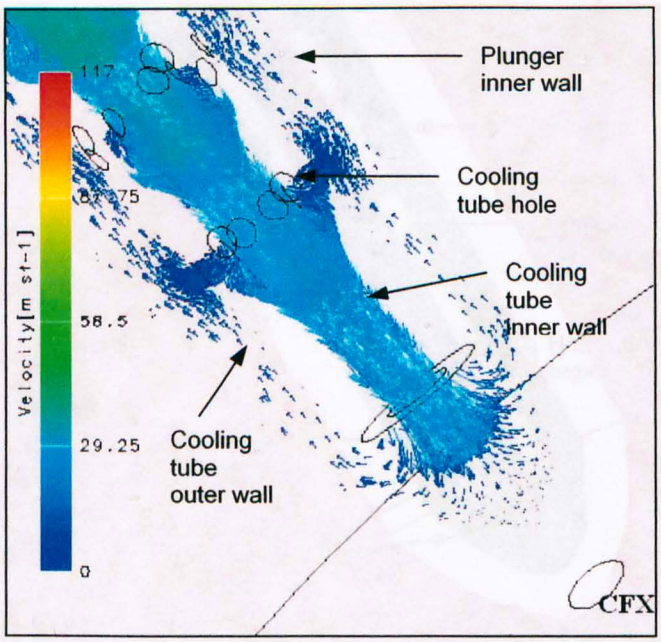

Figure 6.19. Vector diagram of the airflow velocity distribution at the first hole from the cooling tube plunger tip. Inlet velocity: 105.97 m/s, outlet pressure: 0.4 bar.

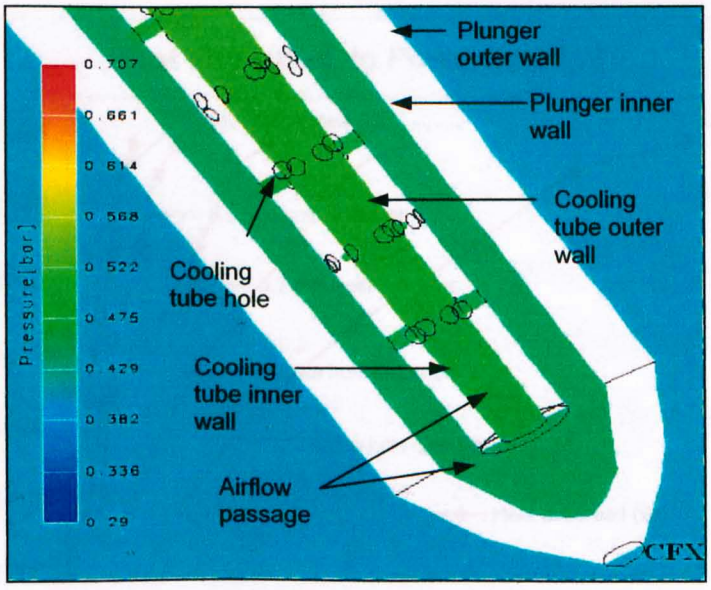

Figure 6.20. Diagram of pressure distribution at the first four holes from the plunger tip of the cooling tube. Inlet velocity: 105.97 m/s, outlet pressure: 0.4 bar.

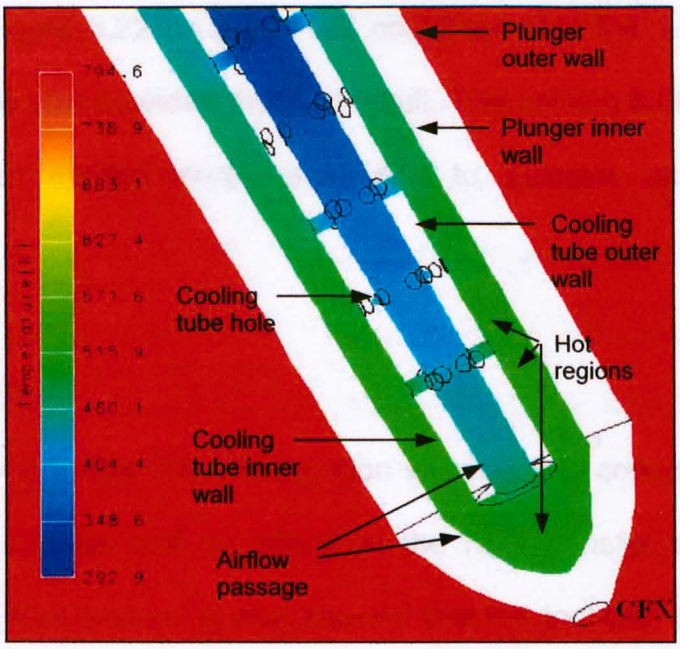

Figure 6.21. Diagram of temperature distribution at the first four holes from the plunger tip of the cooling tube. Inlet velocity: 105.97 m/s, outlet pressure: 0.4 bar.

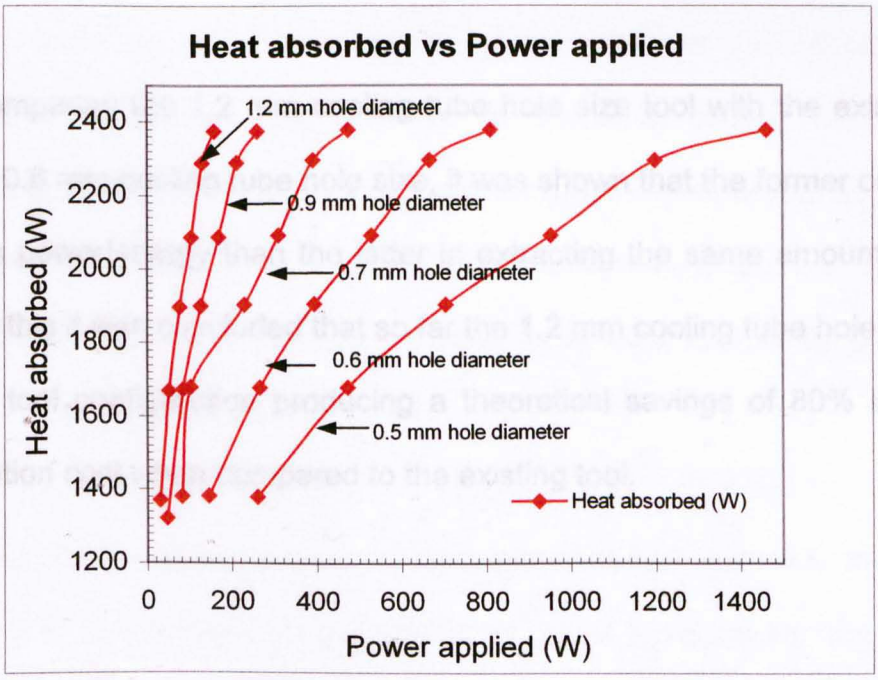

Figure 6.22. Graph of Inlet Airflow Velocity Vs. Power Applied for the plunger cooling tube system.

The graph in Figure 6.22 on page 128 confirmed that the 1.2 mm diameter cooling tube hole size provided the best result. This cooling tube hole size used minimum power applied/energy expanded to achieve an efficient heat absorption rate.

6.4.4 Conclusion

The result obtained from this investigation showed that controlling the size of the cooling tube holes had an effect on the heat transfer efficiency of the plunger cooling tube system. It also showed that the tool with the 1.2 mm hole diameter used the least power/energy during the heat extraction process. This tool produced the best heat extraction and power applied/energy expanded configuration.

When comparing the 1.2 mm cooling tube hole size tool with the existing tool having a 0.6 mm cooling tube hole size, it was shown that the former consumed 80% less power/energy than the latter in extracting the same amount of heat. Owing to this it was concluded that so far the 1.2 mm cooling tube hole size was the best tool configuration producing a theoretical savings of 80% in energy consumption cost when compared to the existing tool.

Chapter 7 DISCUSSION OF RESULTS

The glass container industry relies heavily on the narrow neck press and blow (NNPB) process to stay competitive in the packaging industry. This method gives the glass container industry a competitive edge in the packaging industry by reducing container weight by 15%-30% [10]. Hence needing less energy. Glass also has a higher recyclable value as compared to plastic containers. It is vital that this process achieves advances in the NNPB manufacturing process in conjunction with the final product quality.

It was clear when the idea of this project was conceived that there was limited scientific information relating to the plunger cooling system. There is a great need for more scientific approach to glass container manufacture. This information can then be used to assist in improving current manufacturing processes and thus producing advances in the glass container forming industry. There was limited published data on operational boundary conditions associated with the NNPB process. So these have to be established prior to any CFD modelling work being undertaken.

The NNPB plunger when assessed for performance has to include the process variables (i.e. IS machine set-up parameters, glass temperatures and tooling). This would ensure the production of better quality glass containers (i.e. defect free, lighter in weight, better in strength) at a higher manufacturing rate. Ideally

extensive advancement can be attained in the industrial process if the NNPB plunger met the following requirements:

- No material should be removed from the plunger surface during operation.
- Original thermal characteristics of the plunger must be maintained during its full working life.
- There must be no chemical reaction between the plunger and molten glass (i.e. sticking).

This research programme has assessed the cooling tube system design for the NNPB process. This included investigating the following:

- Plunger and parison temperature assessments.
- Design and development of the plunger and cooling tube test rig to establish boundary conditions from the laboratory experimental study.
- Assessing the airflow distribution in a 2D and axisymmetric model using the CFD analysis.
- Incorporating the plunger material properties (i.e. thermal conductivity and wall thickness) into the axisymmetric CFD model analysis to assess the airflow distribution.
- Developing the 3D model with different schemes of cooling tube hole distribution and sizes to assess the airflow distribution.

Although there is a lack of relevant scientific information associated with boundary conditions (i.e. inlet airflow velocity, outlet pressure, plunger and

parison temperature), initial work carried out by the author [68,69] confirms previous data [21,48]. The effects of high temperature bands (>750°C) along the length of the plunger surface and final container quality have been discussed. The inefficient operation of the cooling tube reduces the efficiency and heat transfer capability of the plunger leading to a poor plunger performance and shorter plunger operational life [21,39]. As the circulation of coolant air becomes inefficient (i.e. recirculation and stagnation of air), surface temperature increases causing the plunger surface to overheat and hence lose plunger material. This shortens its operational life causing an increase in machine downtime and defective products.

A complete assessment of the glass container forming process (i.e. IS machine, machine operation, control and associated tooling) is required to fully utilise the NNPB plunger potential. It is accepted that the usage of the plunger to reduce container weight has its difficulties. The plunger produces micro surface damage on the internal surface of the container necessitating longer reheat times to reduce the stresses formed during the pressing stage. A better fundamental understanding of these situations is required to assist in the assessment of the plunger design. There is a need for the NNPB plunger to operate at uniform temperature with no plunger material adhering to the inside surface of the glass container. At present the plunger cooling tube design is inefficient, which results in the plungers operating at uneven temperatures causing hot bands.

This research programme assessed the temperature distribution along both the plunger and parison during the glass container forming process. The thermal imaging analysis technique was carried out on the plunger and parison to establish the temperature boundary condition. The temperatures of both the plunger (642.2°C) and parison (986.44°C) obtained from this thermal analysis confirmed previous data [21,38]. In order to produce a simplistic CFD model, the temperatures of the parison internal surface, parison external surface and plunger external surface were assumed to be the same (i.e. 1000°C). Hence the temperature boundary condition (i.e. uniform temperature T = 1000°C) was assumed along the length of the external plunger surface in the CFD modelling analysis.

The design and development of the plunger and cooling tube test rig was an essential part of the research programme. This test rig was devised to simulate the IS machine conditions for the plunger cooling tube system, which was conducted in a laboratory environment. The purpose of this experimental study was to establish the inlet airflow velocity (V_{in}) and outlet pressure (P_{out}) boundary conditions. These boundary conditions were used in the CFD analysis to ensure that the CFD models i.e. (2D, axisymmetric and 3D) replicated the actual plunger cooling tube working system. This study was carried out between a pressure difference range of 0.5 bar to 3 bar, which was the actual compressed air pressure range that was used on the shop floor. It was observed from this experimental study that the airflow increased proportionally

with an increase in the pressure difference. It was also noticed that the compressor experienced difficulties in delivering the required compressed air at inlet pressures higher than 4 bar.

This research programme also assessed the airflow within the cooling tube system design using the CFD analysis. Initially the CFD analysis was carried out using the 2D and axisymmetric computer generated mathematical models of plunger cooling tube system. The CFD analysis showed that the 2D model predicted a more accurate result than the axisymmetric model. However, this should not be the case as the axisymmetrical model was actually a closer geometrical replication of the practical NNPB plunger cooling tube system. After further reassessment and implementation of the distributed resistance constant values (k) of the cooling tube holes to control the porosity of the cooling tube holes, the axisymmetrical model was able to replicate the actual plunger cooling tube system. This was only possible after the exercise of empirically determining the respective distributed resistance constant values (k), through an iterative method of solution based on the laboratory test rig results. Following this the axisymmetrical model was used to assess the distribution of the cooling tube holes and it showed that the 0.5 spacing ratio (0.01 m spacing) between the cooling tube holes provided the best heat absorption rate. The same model was also used to assess the influence of the plunger material properties (i.e. thermal conductivity, wall thickness) on the heat transfer efficiency of the plunger cooling tube system. It showed that the plunger material properties do

affect the heat absorption rate. This further confirms previous data [38]. However further work needs to be carried out in this area using different materials and their associated properties.

The 3D CFD investigation for the 330 ml beer bottle has shown that the plunger cooling tube system with the current design, 1 (equal) ratio spacing (0.0133 m spacing) and 0.75 ratio spacing (0.013 m spacing) between the cooling tube holes consumed the least power/energy during the heat extraction process. It also showed that the plunger cooling tube system with the cooling tube hole diameter size of 1.2 mm produced a tool, which has theoretically reduced the energy consumption by 80% during the heat extraction process as compared to the existing tool design. This considerable reduction in energy consumption is a major savings in cost to the glass container manufacturer.

As a result this information would enable advances to be attained in the design of the cooling tube system. The improvements made in the extraction of heat energy would increase the heat transfer efficiency of the NNPB plunger. Hence leading to an improvement in the final product quality, process control as well as cost savings associated with energy reductions. The result of this investigation was obtained using boundary conditions (i.e. inlet airflow velocity and outlet pressure) from the laboratory experiment that was conducted under ideal conditions. However the actual inlet airflow velocities in the IS machine owing to the mechanics, dynamics and quality of air maybe different. This requires

further confirmation. Using boundary conditions (i.e. inlet airflow velocity, outlet pressure and parison temperature) established from the shop floor observations in the CFD modelling exercise and furthermore a knowledge of the IS machine operating parameters together with the gob characteristics would present advances in producing a better quality glass container with reduced machine downtime. Hence leading to an overall savings in glass container production.

The sensitivity of the assumed temperature boundary condition (i.e. uniform parison temperature T= 1000°C) used in this investigation was also assessed by comparing the resultant heat absorbed assuming the uniform parison temperature T= 1000°C boundary condition with the resultant heat absorbed using two different uniform parison temperature boundary conditions T= 950°C and 1050°C. It was shown that the heat absorbed when using the boundary conditions (P_{out} = 0.4 bar and V_{in}= 105.97 m/s) and temperature boundary conditions of T= 950°C, 1000°C and 1050°C were 1809 W, 1905.9 W and 1998.7 W respectively. There is an approximate +/- 4 to 5% difference in the amount of heat absorbed with a +/- 5% difference in the assumed temperature boundary condition of 1000°C. The sensitivity of a particular inlet pressure (i.e. Inlet pressure P_{in} =1 bar) used in this investigation was also assessed by comparing the resultant heat absorbed when using this inlet pressure with the inlet pressures of 0.9 bar and 1.1 bar. The amount of heat absorbed when inserting the inlet pressure of 0.9 bar, 1 bar and 1.1 bar were 1610.3 W, 1680.6 W and 1767.2W respectively. Again there is an approximate +/- 4 to 5%

difference in the amount of heat absorbed with a +/- 10% difference in the inlet pressure of 1 bar. This showed that a +/- 5% difference in the quantified parison temperature and a +/- 10% difference in the inlet pressure does not significantly influence the amount of the heat absorbed by the plunger cooling system.

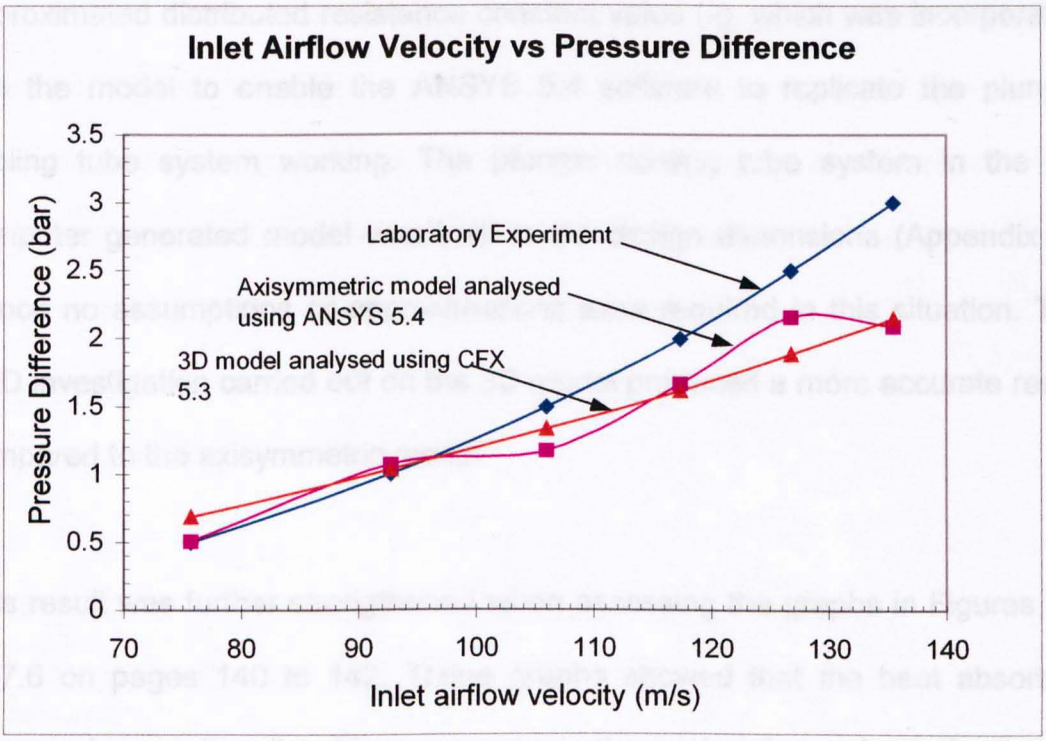

Figure 7.1. Graph of Inlet airflow velocity Vs Pressure Difference of the current cooling tube system design

The research programme also compared the axisymmetric and 3D models of the plunger cooling tube system, which were analysed respectively with the CFD software packages, ANSYS 5.4 and CFX 5.3. Figure 7.1 above showed the influence of the inlet airflow velocity on the pressure difference for the two models (axisymmetric and 3D) and their comparison with the experimental

work. The characteristics of the 3D model curve showed that the increase in the inlet airflow velocity was proportional to an increase in the pressure difference. The behaviour of the 3D model better mirrors the laboratory experimental result compared to the axisymmetric model, which was analysed with the ANSYS 5.4 software. The behaviour of the axisymmetric model was affected by the approximated distributed resistance constant value (*k*), which was incorporated into the model to enable the ANSYS 5.4 software to replicate the plunger cooling tube system working. The plunger cooling tube system in the 3D computer generated model was built to the design dimensions (Appendix 1). Hence no assumptions or approximations were required in this situation. The CFD investigation carried out on the 3D model produced a more accurate result compared to the axisymmetric model.

This result was further strengthened when assessing the graphs in Figures 7.2 to 7.6 on pages 140 to 142. These graphs showed that the heat absorbed increased proportionally with an increase in the inlet airflow velocity for the 3D model for each case when assessing the different schemes of cooling tube hole distribution. Whereas with the axisymmetric model it was shown that the heat absorbed did not consistently increase with an increase in the inlet airflow velocity. The behaviour of the axisymmetric model curve in each case was also different. The current design, equal ratio spacing and 0.75 ratio spacing between the cooling tube holes of the axisymmetric model produced heat absorbed results which were underestimated when compared with the 3D

model. Whilst the axisymmetric models of the 0.5 and 0.25 ratio spacing between the cooling tube holes produced heat absorbed results, which were over estimated.

Owing to the inconsistent behaviour of the axisymmetric model it was impossible to introduce a common correction factor in each case to reduce the difference between the axisymmetric and 3D model. This clearly showed that the axisymmetric model was unreliable in comparison to the 3D model. This again confirmed that the 3D model was more accurate in replicating the actual plunger working system than the axisymmetric model.

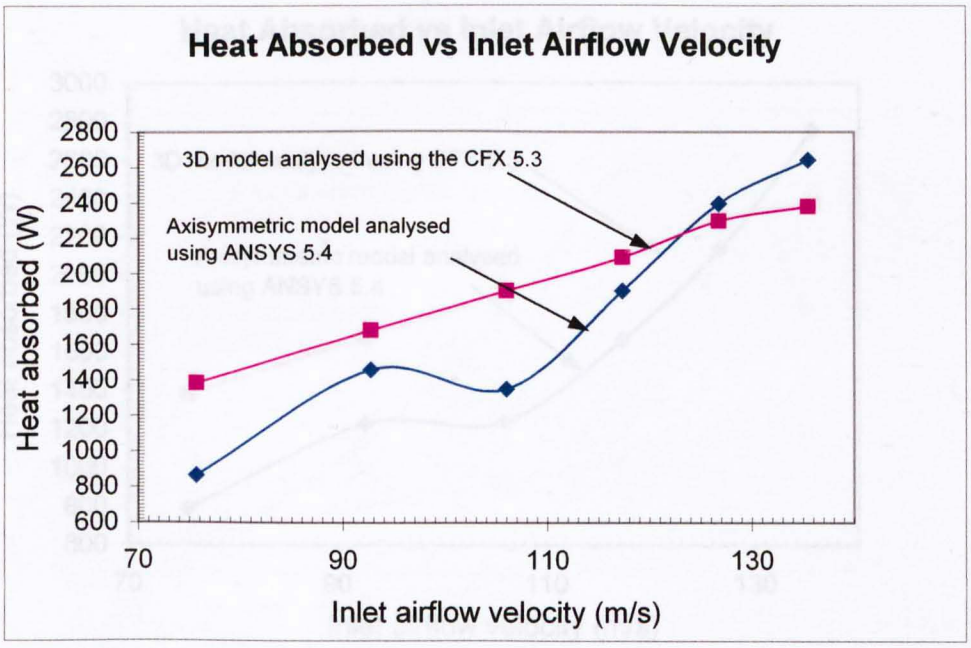

Figure 7.2. Graph of Heat absorbed Vs Inlet airflow velocity for the current tool design

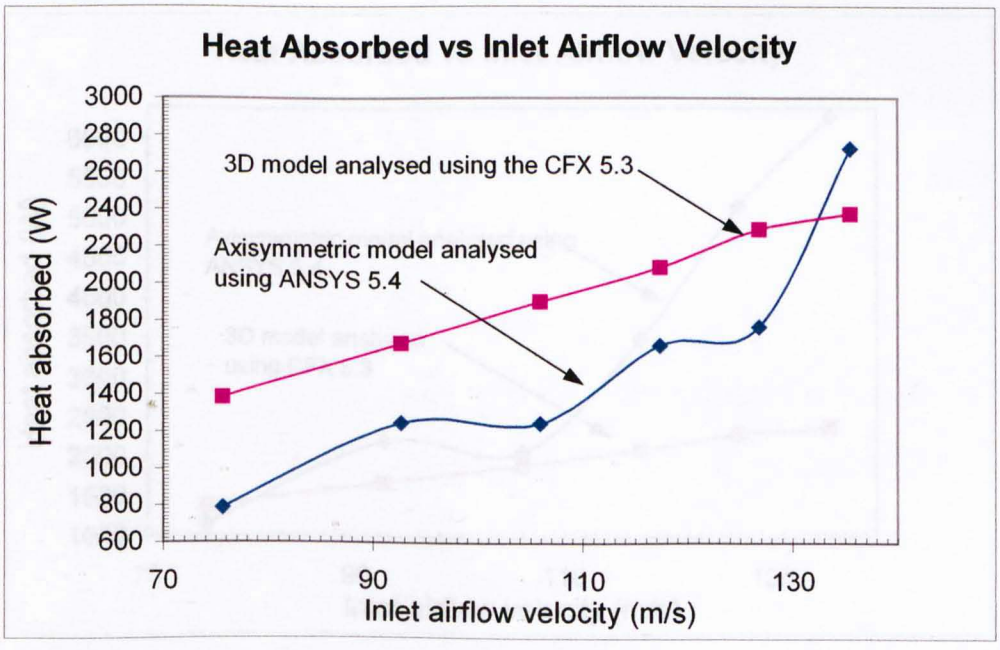

Figure 7.3. Graph of Heat absorbed Vs Inlet airflow velocity for the equal ratio (0.0133 m) spacing distance between the cooling tube holes

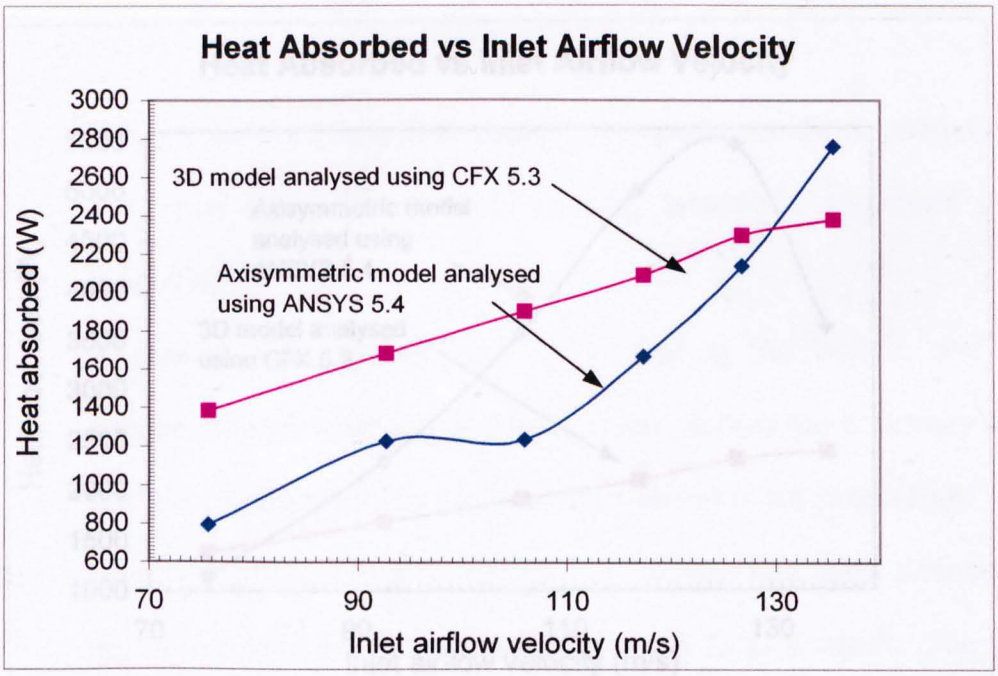

Figure 7.4. Graph of Heat absorbed Vs Inlet airflow velocity for the 0.75 ratio (0.013 m) spacing distance between the cooling tube holes

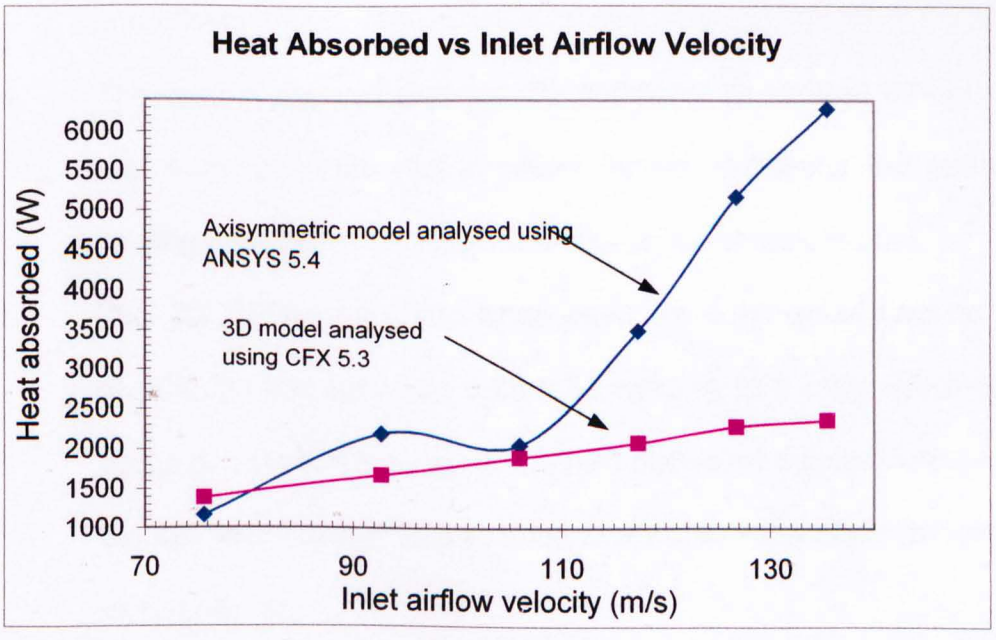

Figure 7.5. Graph of Heat absorbed Vs Inlet airflow velocity for the 0.5 ratio (0.01 m) spacing distance between the cooling tube holes

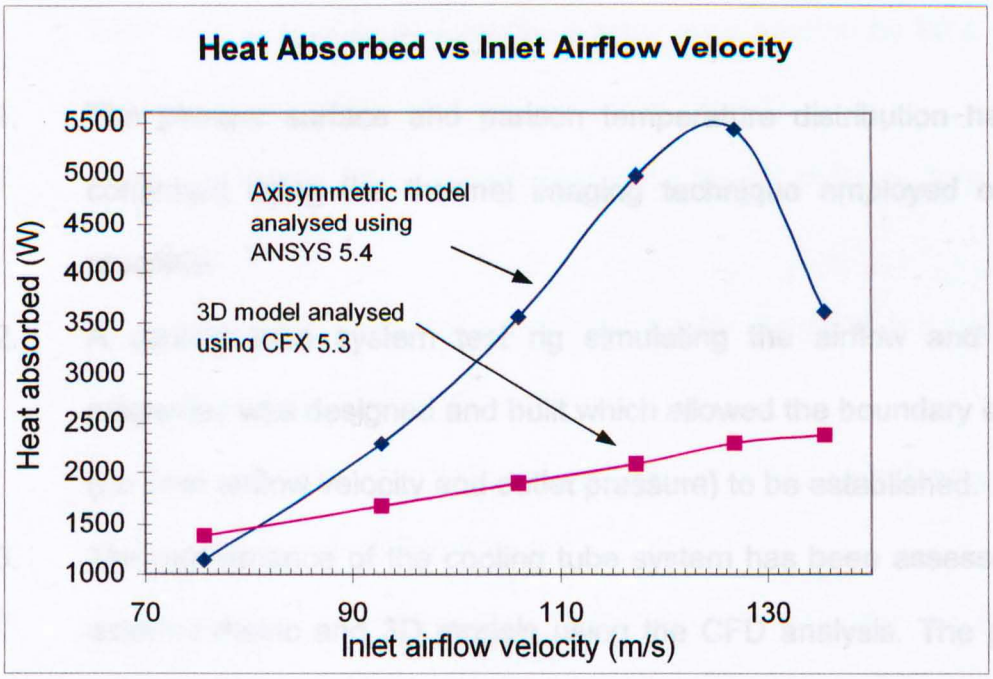

Figure 7.6. Graph of Heat absorbed Vs Inlet airflow velocity for the 0.25 ratio (0.0068 m) spacing distance between the cooling tube holes

Chapter 8 CONCLUSIONS

1. The plunger surface and parison temperature distribution have been confirmed using the thermal imaging technique employed on the IS machine.
2. A cooling tube system test rig simulating the airflow and pressure properties was designed and built which allowed the boundary conditions (i.e. inlet airflow velocity and outlet pressure) to be established.
3. The performance of the cooling tube system has been assessed in 2D, axisymmmetric and 3D models using the CFD analysis. The poor heat transfer performance and airflow pattern has been identified. These are related to the hot bands exhibited on the plunger surface observed on the shop floor.
4. The results showed that the 3D computer generated model is a better and more accurate mathematical model replicating the actual plunger cooling tube working system than the axisymmetric model.
5. The 3D CFD model has been used for a range of cooling tube hole distribution (i.e. between 0.25 ratio spacing to 1 ratio spacing) and hole size (i.e. between 0.5 mm to 1.2 mm diameter) successfully by improving the efficiency of the heat extraction process for a particular product (330 ml beer bottle).

6. This improvement in the plunger cooling tube system design (i.e. cooling tube hole size) has reduced the energy consumption by 80%. This is a major cost savings to the glass container industry.

7. The CFD modelling will assist in design modification by contributing to the following:

   - Improving the heat extraction rate by changing the cooling tube hole sizes and distribution.
   - Using alternative plunger materials to assist in achieving a better heat transfer performance.

8. The above knowledge is paramount to the extension of the NNPB plunger working life. It is also vital to the achievement of lower cost higher quality glass container wares.

Chapter 9 PROPOSED FUTURE WORK

- Further refine the computer generated mathematical model mesh to improve the results of the CFD modelling exercise.
- Improve the mathematical model by using the boundary conditions (i.e. inlet airflow velocity and outlet pressure) measured directly from the IS machine on the shop floor. With the above parameters a better estimation could be made of the thermal distribution along the plunger at the design stage.
- It will be advantageous to further assess the size and distribution of cooling tube holes to assist in the optimisation of the plunger cooling tube system design.
- It would be beneficial to assess both the cooling tube wall and plunger wall thickness together with the size of gap between the cooling tube and plunger wall. The thickness of the material as well as the size of the gap would influence the heat extraction rate.
- Another area that requires further investigation is the use of alternative plunger and cooling tube materials. These materials should have a high conductivity rate to maintain a low surface temperature and sufficient hardness to withstand abrasive damage.
- It would also be useful to investigate the inner plunger wall surface finish as the surface roughness affects the flow of the coolant air through the cooling tube system

REFERENCES

[1] *Leendertse, AC; Van Veen, JPW*; " Dutch Notes on BAT for the Glass and Mineral Wool Industry", Final report, December 1998

[2] *Sarwar, M; Armitage, AW*; "Improving Glass Container Quality in the NNPB Process with the Aid of Technology Transfer"; Proceeding of the XV A.T.I.V. Conference, Parma, 15-17 September 1999, pp 169-173.

[3] *Mann, PA*; "Machine and process technology through the 1990's", Glass Technology, 31, 6, 1990, pp 221-25.

[4] *Weeden, C*; "The glass container industry 1916-1976", Glass Technology, 17, 5, 1976, pp 165-181

[5] *Grüninger, W*; "IS-Section Performance: A strong base for innovation", International Glass Review, Spring/Summer 1997, pp 87/89.

[6] *Corves, B*; "IS-Machine Technology: Engineered to meet today's and future demands", Podebrady: 10th Czech Conference on Glass, 1997, S. 4/10.

[7] *Grüninger, W*; "Successful Gob Delivery.....Everytime", Glass International, 17 (1994), No. 6, pp 87/89.

[8] *Corves, B*; "IS-Machine technology engineered for precision demands required for NNPB light weighting containers", EPSRC Industrial Seminar, Barnsley, 3rd June 1998, Process Development for Narrow Neck Light weighting Containers.

[9] *Wray, G*; "Glass Conditioning Technology", EPSCR Industrial Seminar, Barnsley, 3rd June 1998, Process Development for Narrow Neck Light weighting Containers.

[10] *Edgington, JH*; "Developments in forming equipment today and for the future", Glass Technology, Vol 25, No. 6,Dec. 1984, pp 265-269

[11] *Sidler, W*; "IS-Machine developments", Glass Technology, 29,1, 1988, pp 11-16

[12] *Schupback, DE*; "Heat transfer and the physical requirements of container forming", Glass Technology, 11, 4, 1970, pp 100-108.

[13] *Doyle, PJ*; Glass Making Today, Portcullis Press 1979

[14] *Green, I*; "Innovation in glass container production machinery", Glass International, December 1985, pp 41

[15] *Price, RW*; "Container forming technology: Past trends and future outlook", Glass, February 1991, pp 53-54.

[16] *Seidel, H.G; Williams, H.P; Heather, R.P*; "Contributions to glass container strength", Glass, March 1984, pp 85-86

[17] *Ensor, T.F*; "Review of literature on mould materials used in the glass industry", Glass Technology, 11, 2, 1970, pp 42-47

[18] *Sidler, W*; "IS-machine development", Glass Technology, 29, 1, 1988, pp 11-16

[19] *Angus, H.T*; Cast iron: Physical and Engineering Properties, Butterworths, pp 445

[20] *Ensor, TF*; "Mould materials", Glass Technology, Vol. 19/5, 1978, pp 113 - 119.

[21] *Penlington, R; Sarwar, M; Marshall, GW; Lewis, DB; Cockerham, G*; "Wear Mechanism in Narrow Neck Press and Blow Plunger", Proceedings of the 2nd European Society of Glass Science and Technology Conference, Venice, Italy, June 1993, pp 279-284

[22] *Benson, B*; "Plunger manufacture", EPSRC Industrial Seminar, Barnsley, 3rd June 1998, Process Development for Narrow Neck Light weighting Containers

[23] *Ètelis, L.S; Chernyshora, N.V; Gurtovaya, S.F*; "Resistance to scaling of cast iron"; Soviet Casting Technology, 9, 1987, pp 28-29

[24] *Hughes, I.C.H*; " Growth and scaling of scaling of cast iron", BCIRA Journal, 8, January, 1960, pp 7-28

[25] *Ètelis, L.S; Chernyshora, N.V; Zolotareva, R.S; Borul'ko, I.V*; "Increasing the scale-resistance of cast iron molds", Steklò I Keramika 11, 6, November, 1986

[26] *Schumacher, E*; "Improved Technologies for mould components", Glass Production Technology International, 1990, pp 123-126

[27] *Ensor, T.F*; "Mould Materials", Glass Technology, Vol.31, No.3, 1990, pp 85-88

[28] *Augustsson, B.O*; " Changes in the structure of glass from sliding contact", Glasteknisk Tidskrift, Vol. 36, No.2-3, 1981, pp 23-29

[29] *Augustsson, B.O*; " Changes in the glass surface structure from plunger contact", Glasteknisk Tidskrift, Vol. 51, No.3, 1996, pp 90-96

[30] *Penlington, R; Sarwar, M; Lewis, DB*; "Applications of advanced coatings to narrow neck press and blow plungers in the glass container industry", Surface and Coatings Technology, Vol. 76-77, 1995, pp 81-85

[31] Manns, P; Döll, W; Kleer, G; "Glass in contact with mould materials for container production", Glastechnische Berichte Glass Science Technology, Vol. 68, No. 12, 1995, pp 389-399

[32] *Turner, S; Sarwar, M; Penlington, R; Lewis, DB*; "Wear modes associated with thermal cycling in NNPB plungers in the glass container industry", Proceedings of the International Conference On Advances in Materials and Processing Technologies, Dublin City University (AMPT'95) 8-12 August 1995, pp 540-546.

[33] *Knotek, O; Steine, H.T*; " Diffusions-und grenzflächenvoğange in und an Ni-Cr-B-Si-legierungen", 1972, Vol.3/4, Radex-Rundschau, pp 266-269

[34] *Sarwar, M;* Development and modelling of plunger operating parameters for lightweighting glass container manufacture; EPSCR Final Report, GR/K 97233, 1998

[35] *Penlington, R;* "Parison pressing and plunger contact during lightweight glass container forming", International Glass Journal, No.98, 1998, pp 50-52

[36] *Augusstson, BO;* "Experimental studies of NNPB glass and plunger surfaces", Glass, Nov. 1998, pp 376-678

[37] *Penlington, R;* "Advancing NNPB plunger technology", Glass, September 1997, pp 337-339

[38] *Penlington, R; Sarwar, M; Marshall, GW; Cockerham, G; Lewis, DB;* "Material Requirements for Narrow Neck Press and Blow Plungers

within the Glass Container Industry", Key Engineering Materials, 86-87,1993, pp 55-60.

[39] *Penlington, R; Lewis, DB; Marshall, GW; Sarwar, M*; "The wear of coatings used on glass manufacturing equipment", Proceedings of EAST Kongreβ, Schwäbisch Gmünd, Germany, Nov. 1993, pp 86-90.

[40] *Anon*; "Shaping can costs plunge?", Glass Newsletter 4, December 1997.

[41] *Geotti-Bianchini, Franco*; "Parameters affecting the workability of container glass", Glastechnische Berichte, Vol 65, December 1992, pp 329-337

[42] *Penlington, R*; *Sarwar, M;* "Thermal operating environment of the Narrow Neck Press and Blow Plunger", 4th International Conference-Advance in Fusion and Processing of Glass, Wurzburg, Germany, 22-24 May 1995, pp 164-171

[43] *Penlington, R*; "Investigation the performance of the plunger cooling system", Glass, Nov. 1998, pp 382-383

[44] *Donelly, A; Grayhurst, P; Roberts, M*; "Process development in lightweighting of glas containers", International Glass Journal, No.98, 1998, pp 29-32

[45] *Chinella, R*; "How O-I approaches light weighting", Glass Industry, April 1990, pp 14-16

[46] *Rawson, H*; Glasses and their applications, The Institute of Metals, London 1991

[47] *Winther, S; Schaeffer, HA*; "Effects of aggressive gases on the behaviour of glass surface in contact with mould materials", Glastechnische Berichte, Vol. 61, Nr 7, 1988, pp 184-190

[48] *Penlington, R; Sarwar, M ;Armitage, AW*; "The cooling of Narrow Neck Press and Blow Plungers for container production", Proceedings of the International Conference on Advances in Materials and Processing Technologies, Dublin City University (AMPT'95) 8-12 August 1995, Vol. 3, pp 1053-1063

[49] *Seidel, H*; "The bottle manufacturing process and improvements regarding monitoring and control", Glass Technology, Vol. 33, No.1, February 1992, pp 13-18

[50] *Tiainen, T; Reuhkala, P; Ristola, J*; "A new tool material for use in glass manufacture", Glasteknisk Tidskrift, Vol 50, 1995, pp 62-67

[51] *Cerbone, G; Alvigi, N*; "Plungers for the NNPB Process", Glass Machinery Plants and Accessories, 4/95, pp 103-106

[52] *Schumacher, E*; "Improved technologies for mould components", Glass, May 1989, pp 171

[53] *Vickers, T*; "The changing face of mould technology", Glass International, March 1987, pp 45-47

[54] *Khramkov, V.P*; "Chromium electroplating of glass press mouolds", Glass Ceramics, Vol. 445-6, 1987, pp 189-191

[55] *Trier, W*; "Contact between hot glass and wet porous material (Part 1. Theoretical considerations and experimental results)", Glastechnische Berichte, Vol. 67, No.10, 1994, pp 280-292

[56] *Trier, W*; "Contact between hot glass and wet porous material (Part 2. Trials on a continuously operating container forming machine)", Glastechnische Berichte, Vol. 67, No.11, 1994, pp 312-317

[57] *Seidel, H*; "Glass container manufacturing machinery-present situation and trends", Glass Technology, Vol. 33, No.5, October 1992, pp 161-164

[58] *Roger, K*; "Mould Temperature and Heat Flux Measurements and the Control of Heat Transfer during the Production of Glass Containers", IEEE Transactions on Industry Application, Vol 1A-112, No.4, July/August 1976, pp 432-439

[59] *Edgington, JH*; "Investigating five crucial areas of the NNPB process", Glass, November 1998, pp 385-386.

[60] *Wasylyk; JS*; "AGRAPSIP Target Container - Performance - Limiting Factors", Glass Industry, April 1991, pp 10, 13 - 15.

[61] *Lubitz,G*;" How can the glass container industry achieve quality glass?", Glass International, March 1989, pp 47-49

[62] *Cesar de Sa, J.M.A*; " Numerical modelling of glass forming processes", Engineering Computations, Vol.3, December 1986, pp 266-275

[63] *Stork, K; Loyd, D*;" Heat transfer modelling of the parison forming in glass manufacturing", Glass Technology, Vol.39, No.6, December 1998, pp 210-216

[64] *Babcock, CL; McGraw, DA*; "Application of Glass Properties Data to Forming Operations -1. Temperature Distribution in Glass and Mold During Forming", Proceedings of the 4th International Congress on Glass, Paris, 2-7 July 1956, pp 164-176

[65] Land TI 35 sm Thermal Imager Operation Instructions, 1994

[66] *Philippi, et al*, Measurement of thermal diffusivities through processing infrared images, Rev.Sci.Instrum. 66 (1), pp. 182-192, Jan. 1995

[67] ANSYS Theory Manual, Fluid Flow Fundamentals, Chapter 7, p7-1 to 7-8

[68] *Perera, N;* UNN Confidential Interim Report No.10 (April-June 2000) to PLM Redfearn plc, Barnsley, U.K

[69] *Sarwar, M; Leung, P.S; Perera, N; Armitage, A.W*; " Mathematical Modelling of the Fluid Flow in the NNPB Plunger Cooling System", International Glass Journal, No.107, May-June 2000, pp 26-29

APPENDIX 1

Contents

Engineering drawings of the plunger cooling tube system i

TOLERANCES EXCEPT WHERE STATED ARE 0.0≤0.2 0.00≤0.05 0<≤0<30			PEMHeatBath	
M/c all over except where stated ▽ Cast	N8 ▽ Fine M/c	N6 ▽ Polish	DRG No S70 SPECIAL	
Third Angle Projection			Drn GE	Date 1999 FEB 25 Chkd GE
Mat	Mod	Revision	Intl	Date

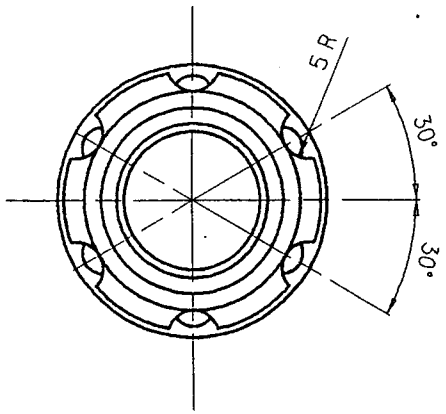

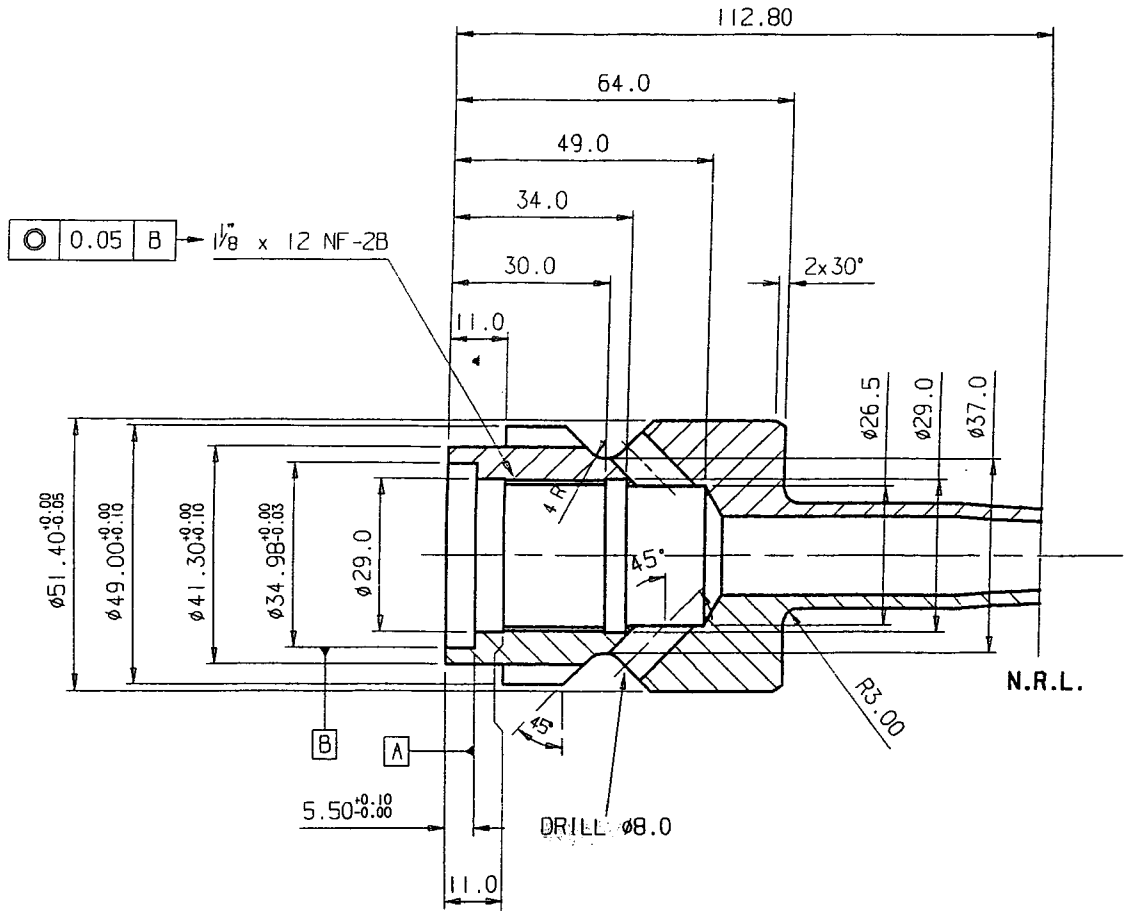

BS 5750
BSI REGISTERED FIRM
Certificate No. Q5796

Scale	1:1
DRG No	S70S

Cooling Tube For 330ml NON-REFILLLABLE BEER.

Use Adaptor as Drg No S83A

DO NOT SCALE IF IN DOUBT ASK
REMOVE ROUGH EDGES EXCEPT ON CAVITY
TOLERANCES EXCEPT WHERE STATED ARE
0.0≡0.2 0.00≡0.05 0∝≡0∝30
M/c all over except where stated ▽ Cast N8/▽ Fine M/c N6/▽ Polish
Third Angle Projection
Mat SAE 30310

PLM Redfearn

DRG No 80-0398-63500

Drn MH Date 1998 SEP 14 Chkd MH

Mod	Revision	Intl	Date
00	REDESIGNED TO WORK WITH 70-0398-63500 5.5mm PLN NOSE RAD ,WITH EMHART WT.CONT.	MH	98 Sep 14
01	BTM ROW OF COOLING HOLES BLOCKED OFF SEE JCS 2134 JOB No 0728/63501	MH	00 Mar 06

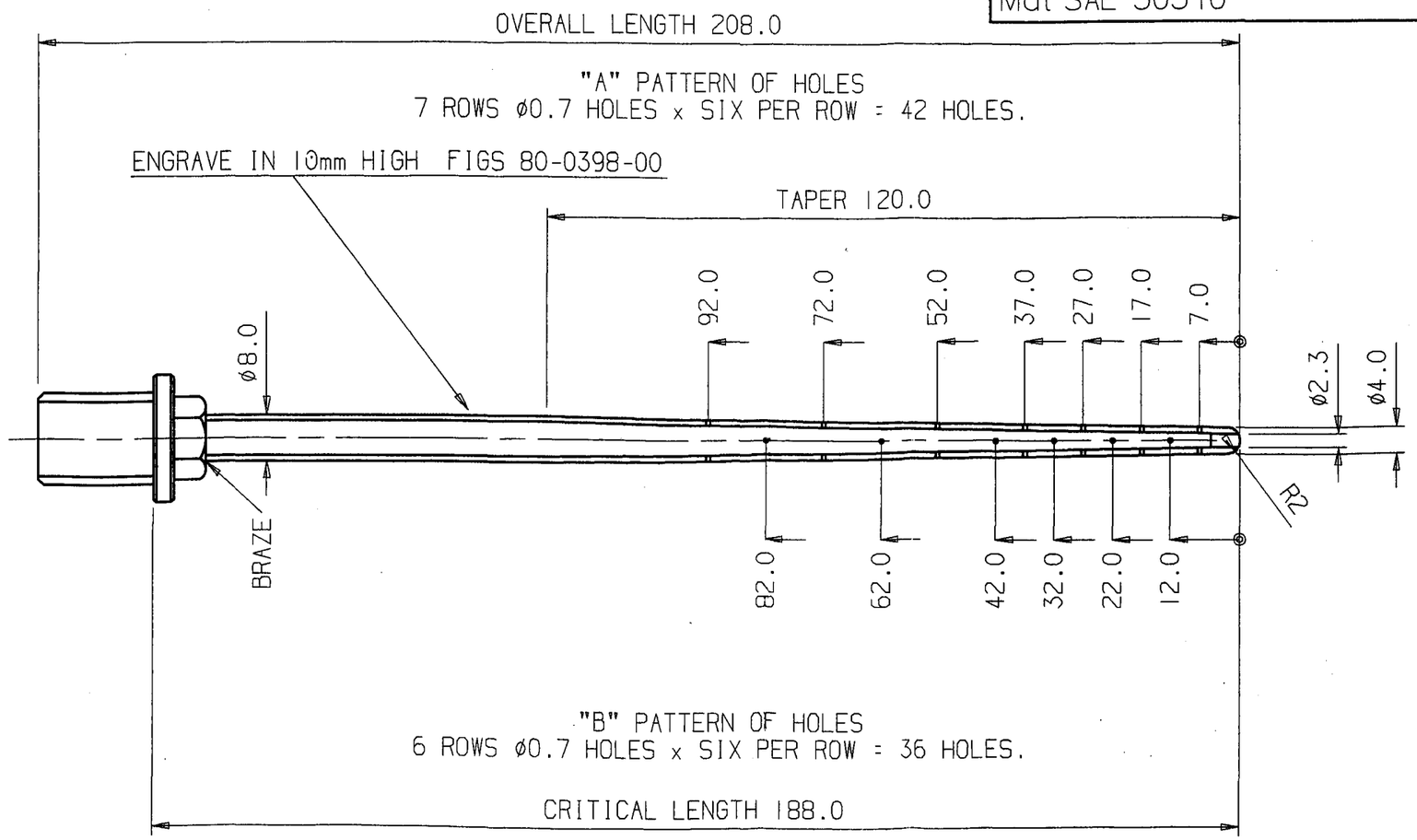

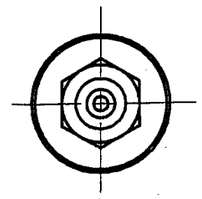

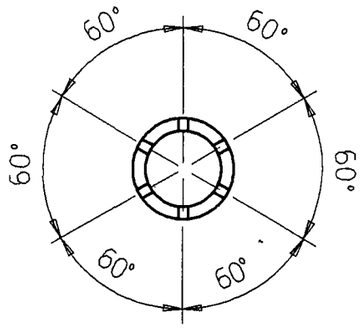

"A" PATTERN
TWICE FULL SIZE

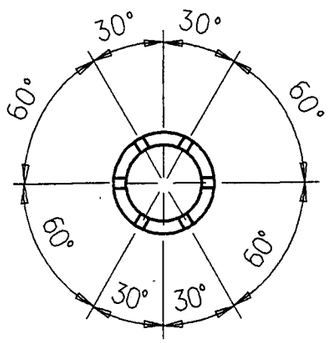

"B" PATTERN
TWICE FULL SIZE

PLEASE NOTE "A" PATTERN IS SAME AS "B" PATTERN APART FROM 30° STAGGER ON HOLES.

BS EN ISO 9001
BSI REGISTERED FIRM
Certificate No. Q5796

Scale 1:1

DRG No 80-0398-63500

Plunger For 330ml NON-REFILLLABLE BEER.

Use adaptor as DRG. No. S70

DO NOT SCALE IF IN DOUBT ASK

REMOVE ROUGH EDGES EXCEPT ON CAVITY

TOLERANCES EXCEPT WHERE STATED ARE
0.0±0.2 0.00±0.05 0°±0°30

M/c all over except where stated ✓ Cast ▽N8 Fine M/c ▽N6 Polish

Third Angle Projection

Mat N.C.C.I

PLM Redfearn

DRG No 70-0398-63500

Drn MH Date 1998 Sep 11 Chkd MH

Mod	Revision	Intl	Date
00	REDESIGNED WITH 5.5mm PLN NOSE RAD AND TO WORK EMHART WT.CONTROLLER.	MH	98 Sep 14

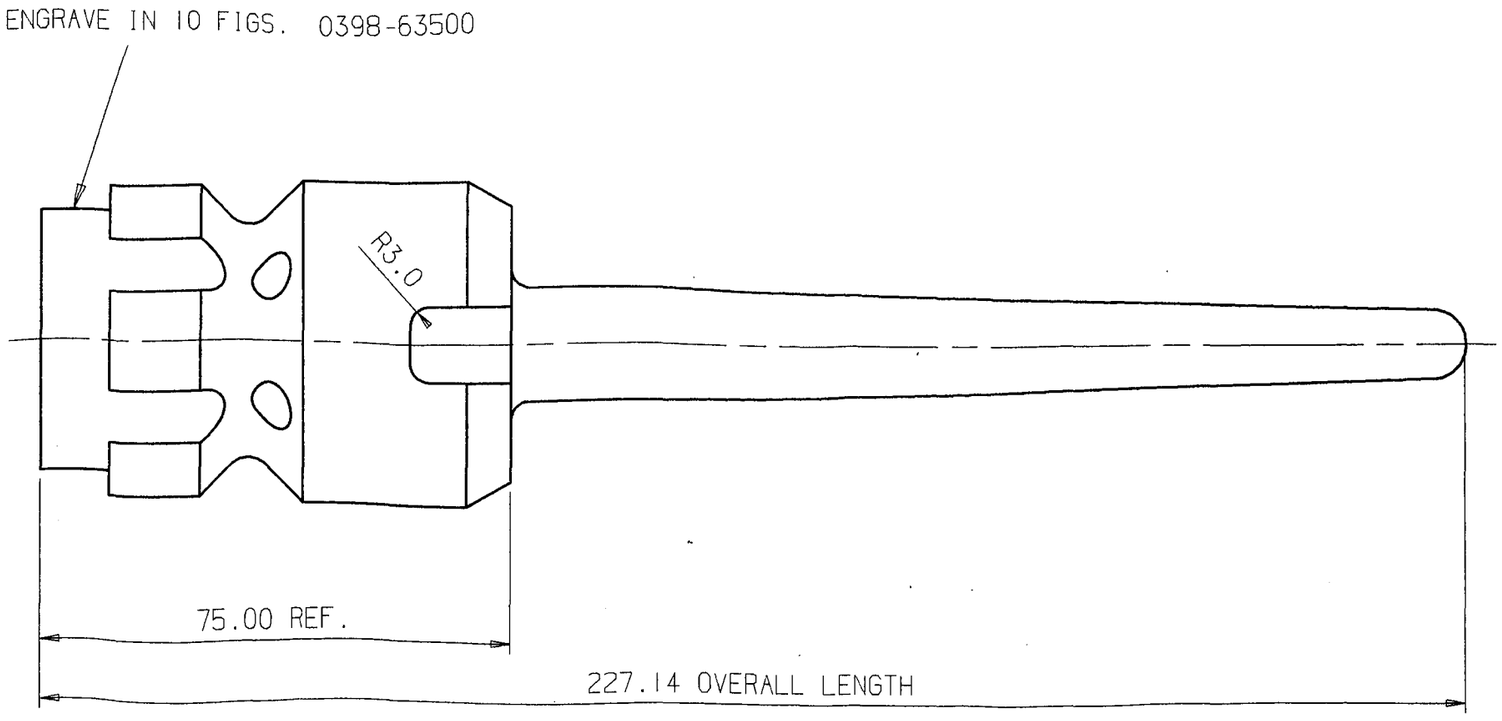

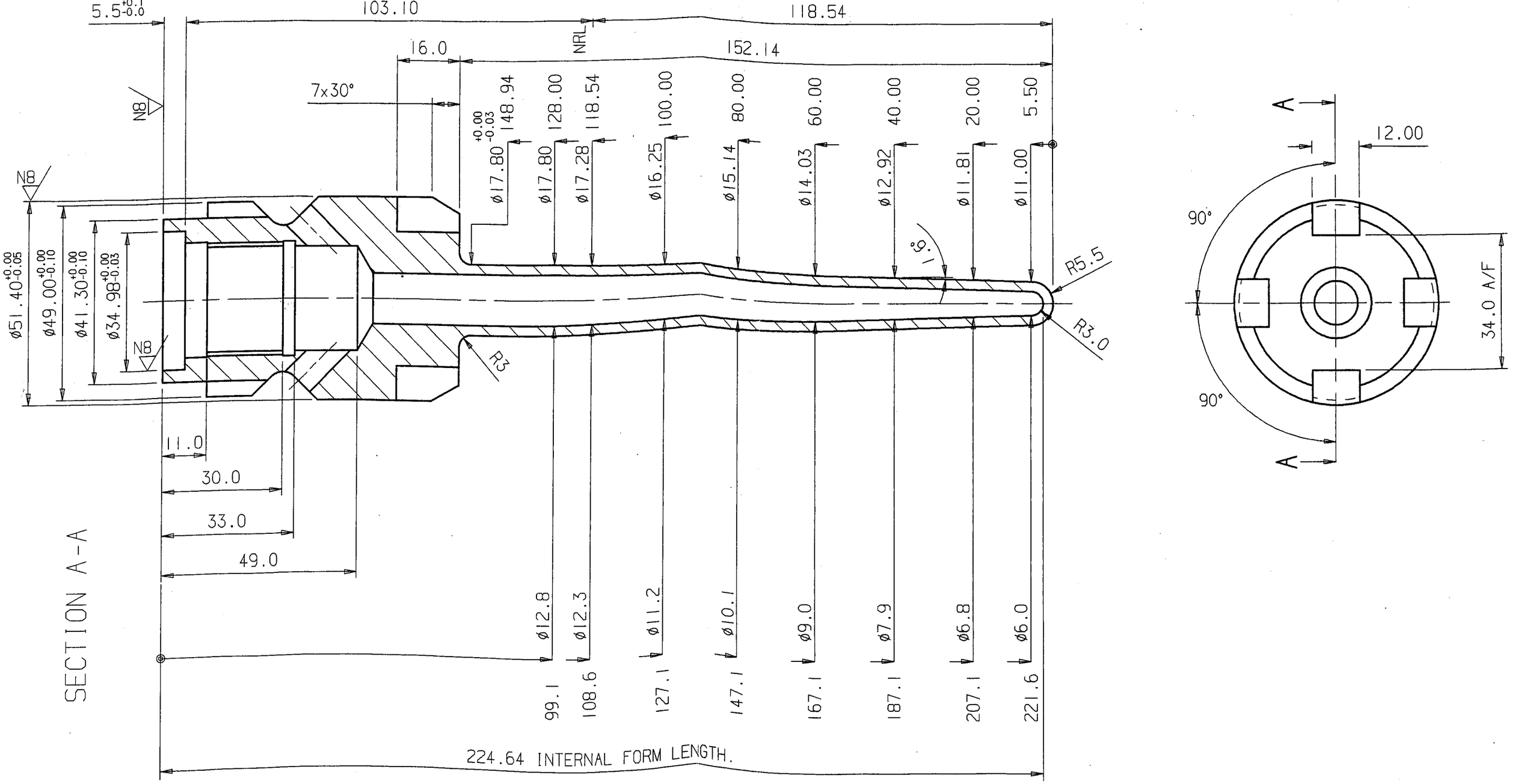

ALAN BRADLEY	PROFILE "SUB ROUTINE" FOR AUDIT FORM FROM TIP END			
G03 R5.50	N5000 G02 G91	X11	Z-5.35 I 0	K5.5 *
	N5010 G01	X6.8	Z-122.65 *	
	N5020	X0.04	Z-21.14 *	

ALAN BRADLEY	PROFILE "SUB ROUTINE" FOR AUDIT FORM FROM RING END			
	N5000 G01 G91		Z-46.15 *	
	N5010	X-6.8	Z-122.62 *	
G03 R3.00	N5020 G02	X-6	Z-2.92 I 3	K0.08 *

S EN ISO 9001

APPENDIX 2

Contents

The observations of the airflow simulation within the 2D model of the plunger cooling tube system i

The observations of the airflow simulation within the axisymmetric model of the plunger cooling tube system iii

The CFD simulation of the airflow within the 2 dimensional model of the cooling tube

Observations

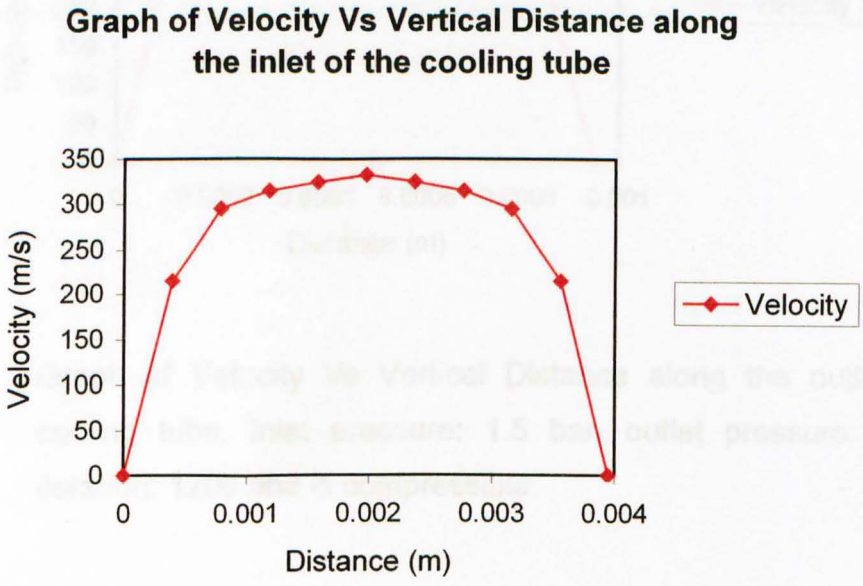

Figure 1. Graph of Velocity Vs Vertical Distance along the inlet of the cooling tube. Inlet pressure: 1.5 bar, outlet pressure: 0.4 bar, iteration: 1200 and is compressible.

- The graph shows that the highest value of the airflow velocity is 333.207 m/s.
- The highest airflow velocity is at the vertical mid-point along the inlet.
- The average airflow velocity along the inlet is 166.66 m/s.
- The airflow velocity range is 0 m/s-333.207 m/s.

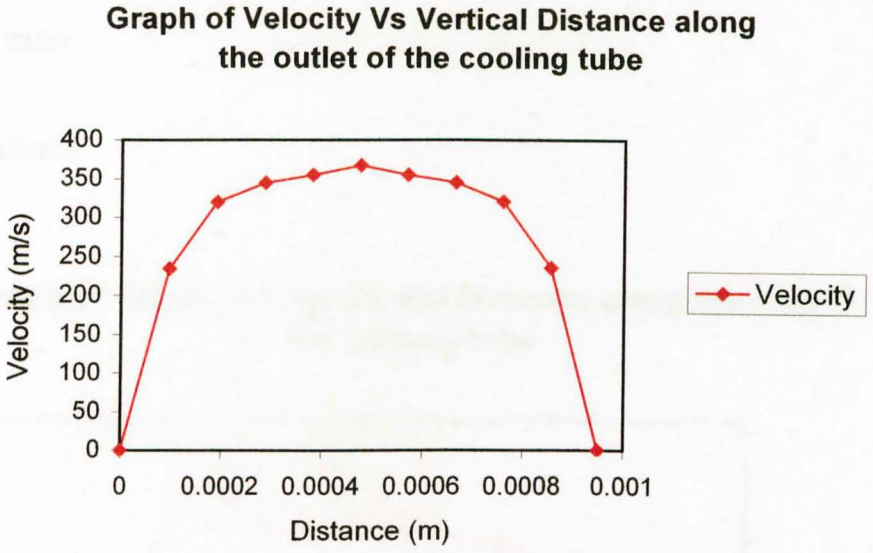

Figure 2. Graph of Velocity Vs Vertical Distance along the outlet of the cooling tube. Inlet pressure: 1.5 bar, outlet pressure: 0.4 bar, iteration: 1200 and is compressible.

- The graph shows that the highest value of the airflow velocity is 367.769 m/s.
- The highest airflow velocity is at the vertical mid-point along the outlet.
- The average airflow velocity along the outlet is 183.88 m/s.
- The airflow velocity range is 0 m/s-367.769 m/s.

The CFD simulation of the airflow within the axisymmetric model of the cooling tube

Observations

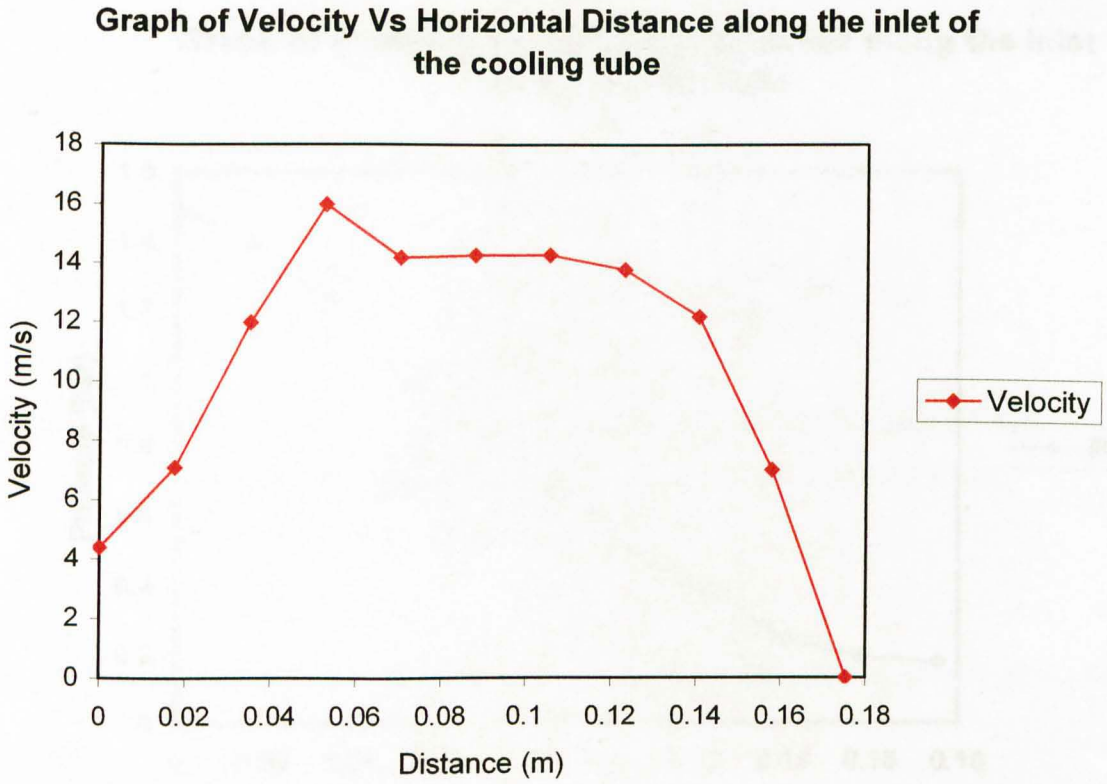

Figure 1. Graph of Velocity Vs Horizontal distance along the inlet of the cooling tube. Inlet pressure: 1.5 bar, outlet pressure: 0.4 bar, iteration: 1200 and is compressible

- There is a gradual increase in the airflow velocity from 4.4 m/s at the inlet as it flows along the tube. It reaches a peak of 16 m/s at the first hole along the cooling tube.

- The airflow velocity then gradually decreases to a value of 0 m/s as it flows through the tube to the tip of the plunger.
- The velocity range is between 0-16 m/s.

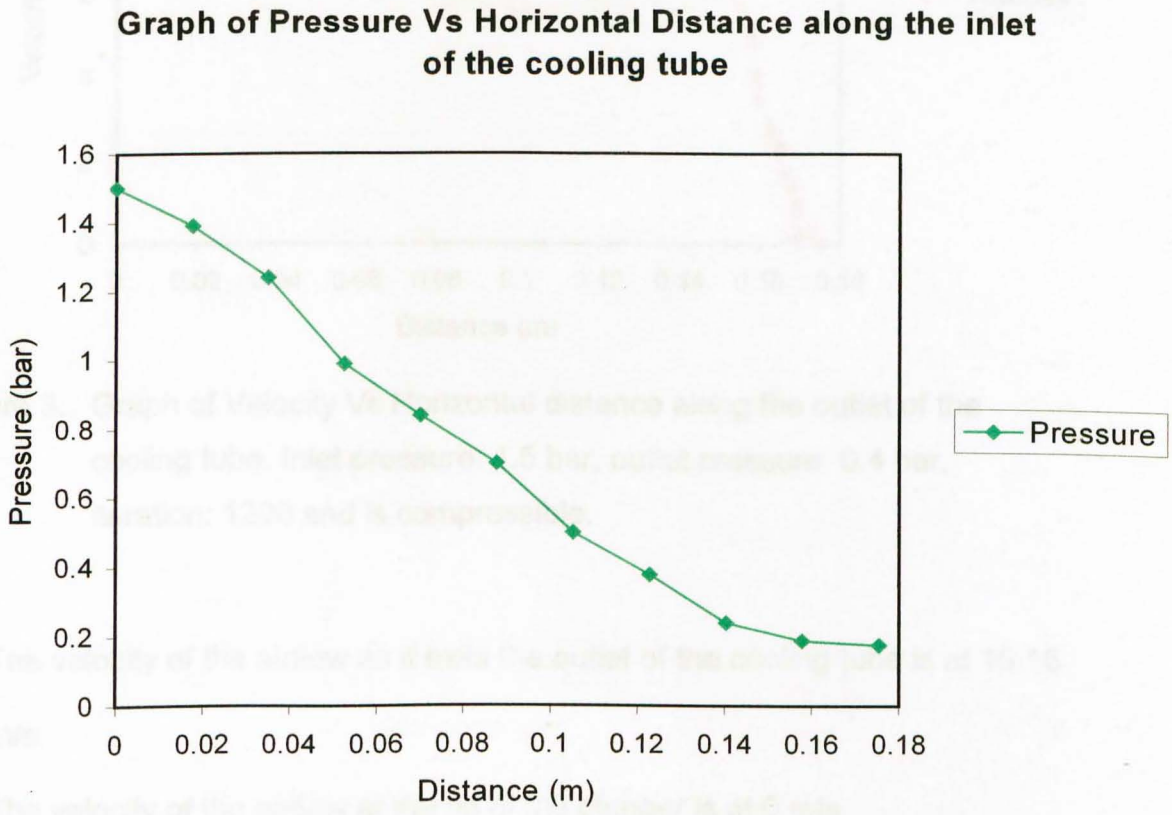

Figure 2. Graph of Pressure Vs Horizontal distance along the inlet of the cooling tube. Inlet pressure: 1.5 bar, outlet pressure: 0.4 bar, iteration: 1200 and is compressible.

- The pressure at the inlet, in the center of the tube is at a value of 1.5 bar. It decreases gradually to a minimum value of 0.176 bar at the tip of the plunger.

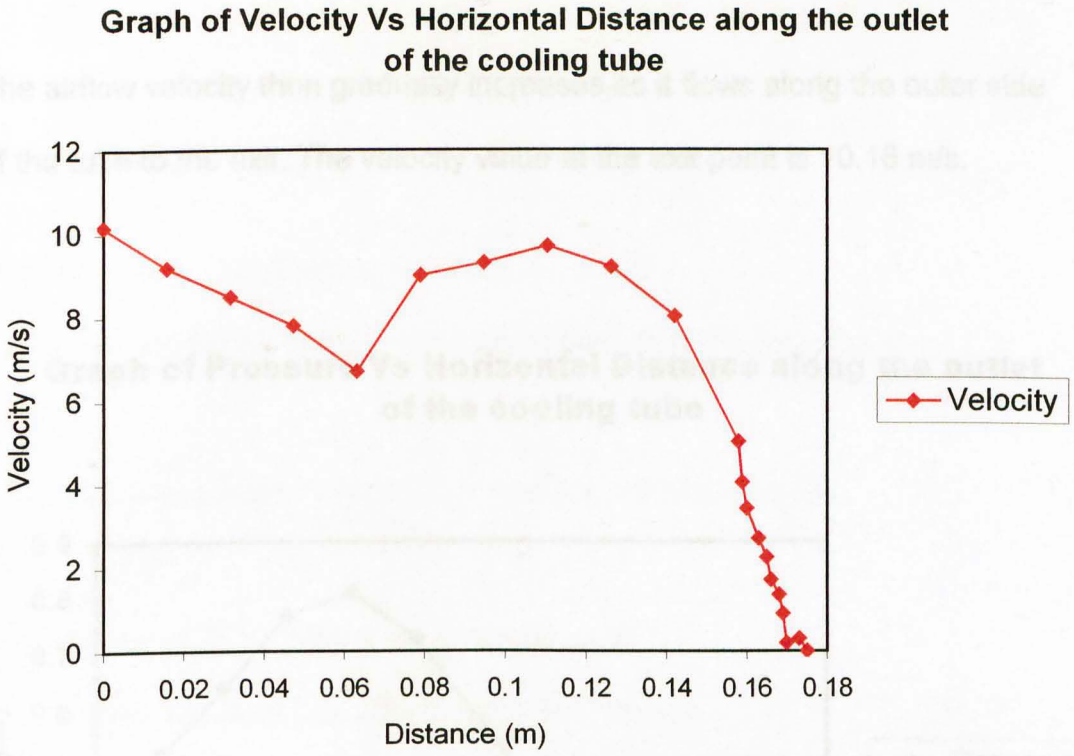

Figure 3. Graph of Velocity Vs Horizontal distance along the outlet of the cooling tube. Inlet pressure: 1.5 bar, outlet pressure: 0.4 bar, iteration: 1200 and is compressible.

- The velocity of the airflow as it exits the outlet of the cooling tube is at 10.16 m/s.
- The velocity of the airflow at the tip of the plunger is at 0 m/s.
- The velocity of the airflow gradually increases as it moves further away from the tip of the plunger till it reaches a peak of 9.7 m/s. This is at a distance of 0.12 m from the exit point of the tube.
- The airflow velocity then decreases to a value of 6.7 m/s at the first hole along the cooling tube. This is at a distance of 0.06 m from the exit point of the tube.

- The airflow velocity then gradually increases as it flows along the outer side of the tube to the exit. The velocity value at the exit point is 10.16 m/s.

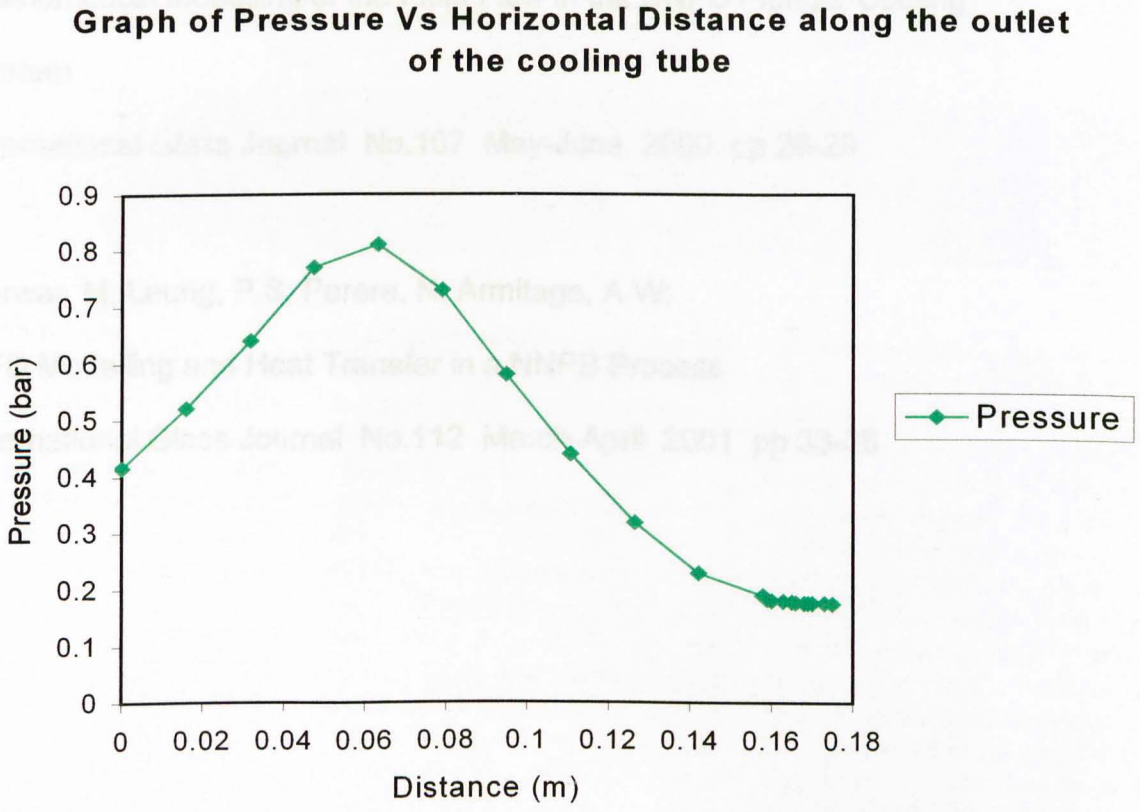

Figure 4. Graph of Pressure Vs Horizontal distance along the outlet of the cooling tube. Inlet pressure: 1.5 bar, outlet pressure: 0.4 bar, iteration: 1200 and is compressible.

- The pressure at the tip of the plunger is at the lowest value of 0.176 bar.
- The pressure increases gradually as it moves away from the tip of the plunger.
- The pressure increases till it reaches a maximum value of 0.81 bar. This at a distance of 0.06 m from the exit point of the tube.

APPENDIX 3

Published material

Sarwar, M; Leung, P.S; Perera, N; Armitage, A.W;

Mathematical Modelling of the Fluid Flow in the NNPB Plunger Cooling System

International Glass Journal No.107 May-June 2000 pp 26-29

Sarwar, M; Leung, P.S; Perera, N; Armitage, A.W;

CFD Modelling and Heat Transfer in a NNPB Process

International Glass Journal No.112 March-April 2001 pp 33-38

MATHEMATICAL MODELLING OF THE FLUID FLOW IN THE NNPB PLUNGER COOLING SYSTEM

M.SARWAR[1], P.S LEUNG[1], N.PERERA[1], A.W ARMITAGE[2]
[1]University of Northumbria at Newcastle, U.K, [2]PLM Redfearn plc, Barnsley, U.K

This paper reviews the mathematical modelling associated with the plunger cooling tube system in the NNPB process and highlights the results achieved and some of the problems encountered. Preliminary results obtained using a computational fluid dynamics (CFD) software package show that there are areas within the airflow passage along the cooling tube system that experience recirculation and choking. Further work is being undertaken by the authors using the ANSYS CFD software package to establish the appropriate parameters for optimum plunger cooling to overcome plunger failure.

1 - INTRODUCTION

The narrow neck press and blow (NNPB) process was developed in the late 60's to produce lightweight containers that have thin walls and closer dimensional tolerances contributing to a reduction in container weight by 15%-30% [2].
Up to that period, containers could only be produced by the blow and blow process with its inherent disadvantages like weight reduction limit, inconsistent mould cooling and poor container quality [2].

The NNPB process was a huge boost to the glass container industry that was facing economic pressures due to alternative packaging forms, changing consumer trends and growing environmental awareness.

Whilst a considerable amount of research work has been done in predicting the glass forming process [3,4] and the associated temperatures [5-9] very little modelling work has been carried out associated with the fluid flow within the plunger cooling system.

Since the plunger is required to remove a quantity of heat from the parison in the parison forming stage, the airflow through the cooling tube plunger system has to be sufficient to adequately remove the excessive heat from the plunger walls.
Current investigation on the shop floor [1,10] show that some plungers under normal operating conditions on the IS machines are working under temperatures which are detrimental to plunger life and can cause material loss from the plunger [10]. This contributes to

Fig. 1 - Velocity vectors for the longitudinal flow field at the plunger tip. (Arrow size indicates velocity magnitude).

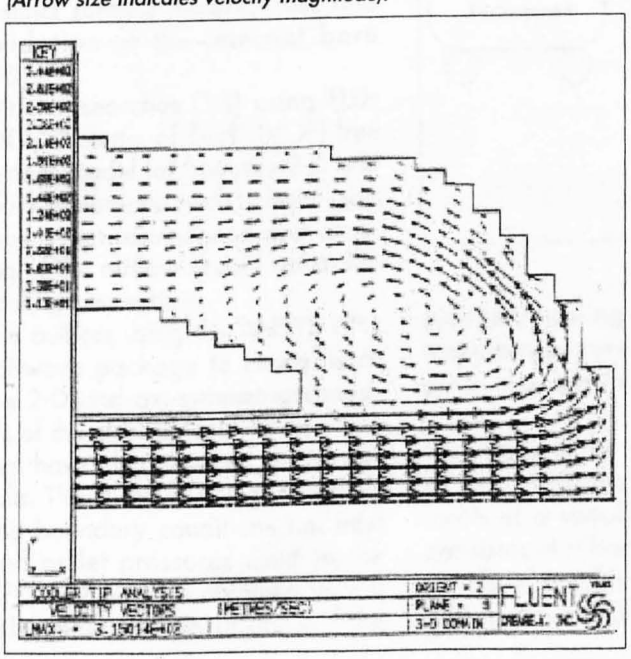

Fig. 2 - The location of the temperature points and hot spots along the visible length of the plunger.

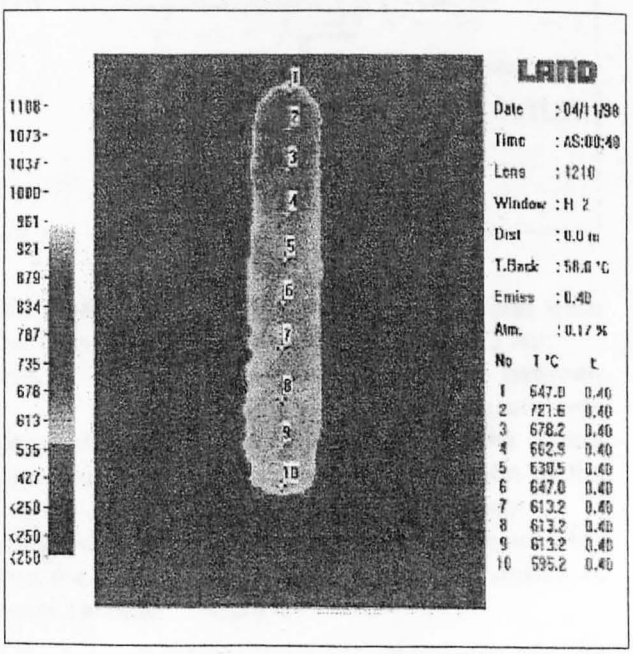

glass container contamination [10] and a reduction in the hardness of the plunger coating material [11].
In order to avoid container defects caused by plunger material loss it is absolutely vital that the plunger operates at a uniform temperature within a required range, which is between 500°C-920°C [12]. The plunger should remove sufficient heat so that the parison can be inverted without distortion and not effect the plunger surface substrate material.

2 - COMPUTATIONAL ANALYSIS ASSOCIATED WITH PLUNGER COOLING

Penlington, Sarwar and Armitage [1] have carried out computational fluid dynamics (CFD) modelling using the FLUENT software package to model the plunger/cooling tube system in 2-D and axi-symmetric and investigated the airflow through the cooling tube system (Fig. 1).
They found that the regions of excessive temperature and rapid tool wear were associated with the areas of ineffective cooling [1]. Furthermore, they link the areas of insufficient cooling within the cooling tube system to the areas exhibiting hot bands on the plunger surface (Fig. 2).
These areas of hot bands have a distinct surface material loss and oxidation of the internal bore [10].
Other researches [13] using FLUENT's "Volume of fluid" (VOF) free surface model for both the 2-D and axi-symmetrical models have also shown that recirculation and choking of the airflow occurs within the cooling tube system.
The authors using the ANSYS CFD software package to model both the 2-D and axi-symmetrical models of the plunger/cooling tube system have also obtained similar results. This is shown in Fig. 3 and 4.
The boundary conditions i.e. inlet and outlet pressures used in the CFD analysis were obtained from a laboratory experiment of the plunger/cooling tube system at room temperature. The laboratory set-up is as shown in Fig. 5

.

The results of the experimental set-up were recorded from 7 experiments at a specified range of exit pressures of 0 bar to 3 bar with intervals of 0.5 bar. Also the specified pressure difference between the inlet and outlet pressures were for a range of 0.5 bar to 3 bar.
The pressure difference between the inlet and outlet pressure was obtained by controlling the control valve at the outlet section of the plunger/cooling tube system.
A selected table of results for the experiment is as shown in Table 1.

Fig. 3 - Predicted airflow through the 2-D model of the plunger/cooling tube system using the ANSYS CFD software package.

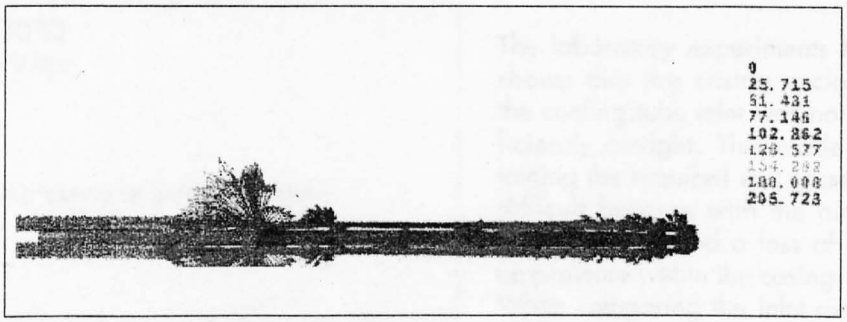

Fig. 4 - An enlarged view showing the recirculation and choking of airflow along the cooling passage in a 2-D model of plunger/cooling tube system.

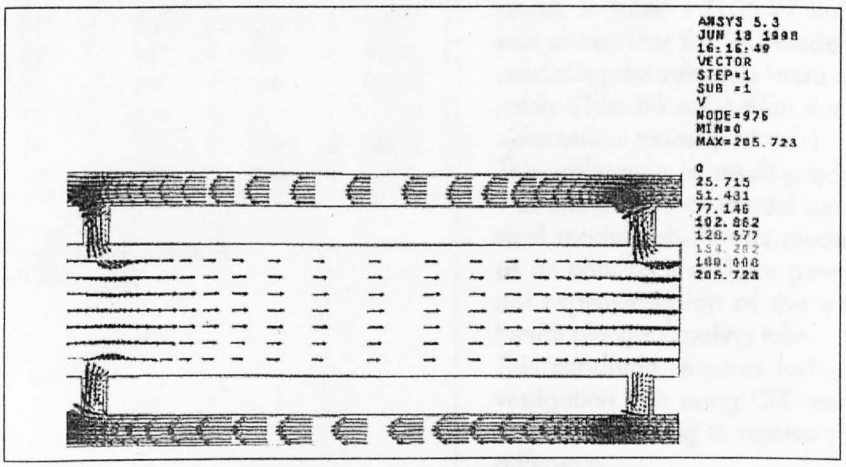

Fig. 5 - Plunger/cooling tube system experimental set-up.

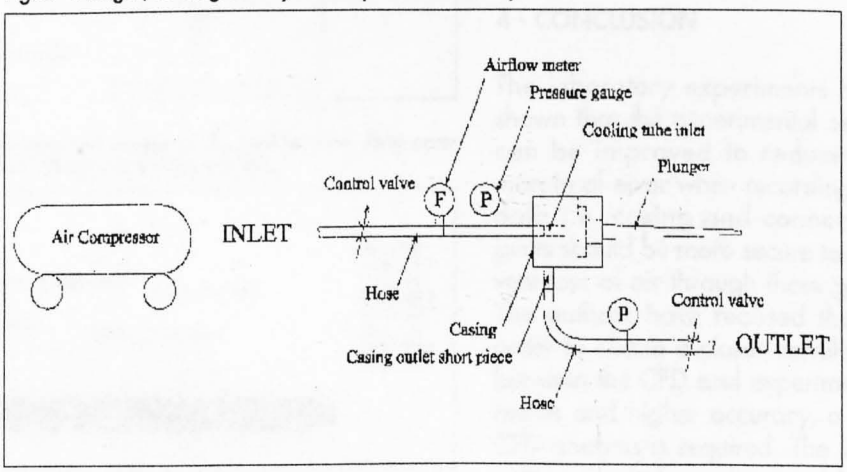

Tab. 1 - Selected table of experimental results.

Temperature = Room temperature (20°C)
For a given exit pressure, i.e. P_{out} = 0 bar

DP = P_{in} - P_{out} where

DP = Difference between the inlet pressure and outlet pressure
P_{in} = Inlet pressure (bar)
P_{out} = Outlet pressure (bar)

Experiment 1	Exit pressure P_{out} (bar)	P_{in} (bar)	Actual P_{out}	ΔP (bar) (bar)	Volumetric airflow ($10^{-3}m^3/s$)	Airflow velocity (m/s)
	0	0.5	0.0	0.5	2.0	75.7
	0	1.0	0.2	1.0	2.45	92.73
	0	1.5	0.4	1.5	2.8	105.97
	0	2.0	0.6	2.0	3.1	117.33
	0	2.5	0.7	2.5	3.35	126.79
	0	3.0	1.0	3.0	3.58	135.5

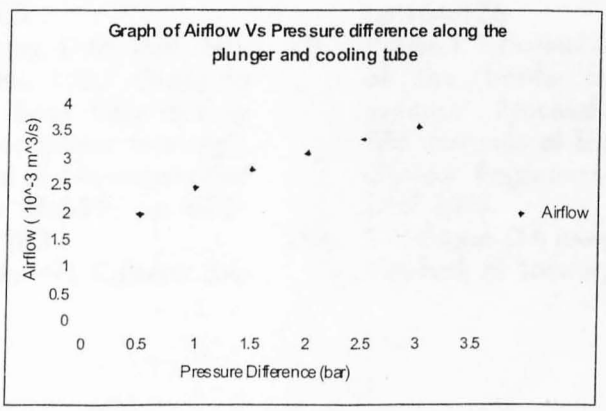

Fig. 6 - Diagram of airflow through the 2 dimensional model of the cooling tube. Inlet pressure: 1.5 bar, outlet pressure: 0.4 bar, iteration: 1200 and is compressible.

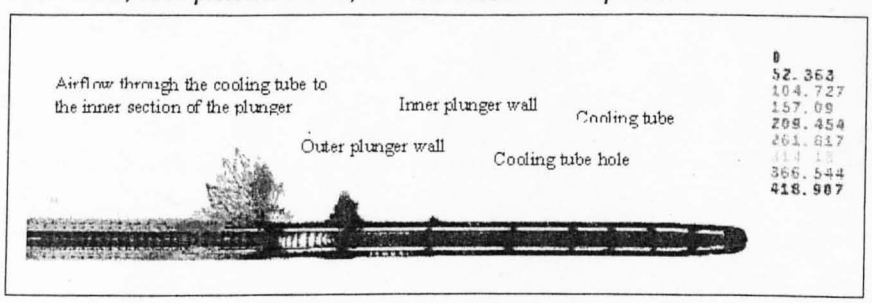

Fig. 7 - Diagram of the airflow through the axi-symmetric model of the cooling tube. Inlet pressure: 1.5 bar, outlet pressure: 0.4 bar, iteration: 1200 and is compressible.

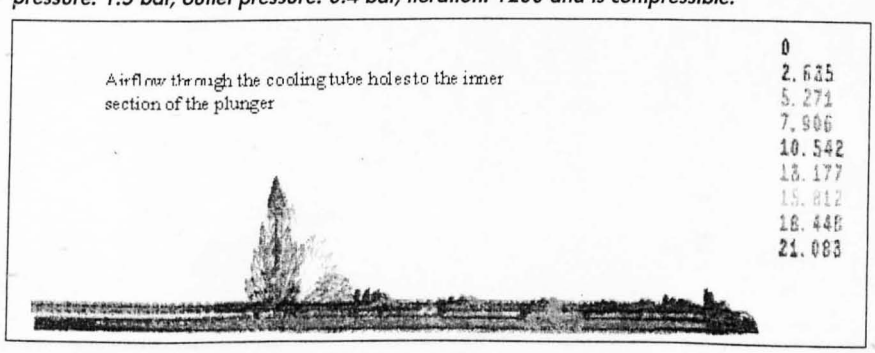

3 - DISCUSSION OF RESULT

The laboratory experiments have shown that the casing enclosing the cooling tube inlet was not sufficiently airtight. This made obtaining the required exit pressures difficult because with the air escaping this caused a loss of built up pressure within the casing.
When comparing the inlet airflow velocities obtained from the 2-D (Fig. 6) and axi-symmetrical models (Fig. 7) with the experimental results in Table 1 (105.97 m/s), it was shown that the 2-D model was predicting the velocities more accurately (166.66 m/s) than the axi-symmetrical model (4.4 m/s).
This difference in result produced was unexpected as the axi-symmetrical model, which was modelled, as an annulus is a closer geometrical representation of the actual NNPB plunger/cooling tube.
This condition requires further investigation into using CFD computational modelling to resolve above difference.

4 - CONCLUSION

The laboratory experiments have shown that the experimental set-up can be improved to reduce the margin of error when recording the data i.e. casing and connection joints should be more secure to prevent loss of air through these gaps.
The authors have realised that in order to obtain a closer correlation between the CFD and experimental results and higher accuracy, a 3-D CFD analysis is required. The latter software package is capable of producing a realistic and more accurate geometrical representation of the tool in its working environment and should produce an acceptable solution to this problem.

REFERENCES

[1] R Penlington, M Sarwar, A W Armitage," The cooling of Narrow Neck Press and

Blow Plungers for the container production", Advances in Materials and Processing Technologies 1995, pp 1055-1063

[2] J H Edgington, " Developments in forming equipment today and for the future", pp 266, Glass Technology, Vol. 25, Dec. 1994.

[3] Dr.Henry J Anderson, Dr Melanie E Armstrong, "Process Development for Narrow Neck Lightweight Containers, The Engineered NNPB container", Industrial Seminar, 3rd June 1998

[4] Dr.Ing.Heinrich Uhe, "Process Control- A system for monitoring the press and blow process", pp 16, Glastekniknisk Tidskrift, Vol 46, 1991

[5] Shetterley, D.M, Huff, N.T, Hisbitts, L.C," Glass to metal heat flow during glass container forming", Journal of Non-crystalline Solids 38&39, pp 873-878, 1980

[6] Holscher, H.H, Coleman, J.C, Cooke, C.C, "Study of glass and mould temperatures in commercial glass container forming operations", The Glass Industry, pp 74-81, 113, February 1960

[7] Howse, T.K.G, Kent,R, Rawson, H, " The determination of glass-mould heat fluxes from mould temperature measurements", pp 84-93, Glass Technology 12 1971 no. 4

[8] Babcock, C.L,Mc Graw, D.A, "Application of glass properties data to forming operations, 1.Temperature distribution in glass and mould during forming", Proceedings of the 4th international Congress on Glass. Paris 2-7 July 1956 pp 164-176

[9] Wilson,J, " Thermal Analysis of the bottle forming process", Proceedings of SPIE International Society of Optical Engineering Vol 1467 1991

[10] R Penlington D B Lewis, G W Marshall, M Sarwar; " The Wear of Coatings Used on Glass Manufacturing Equipment", EAST-REPORT 1993, European Academy of Surface Technology, Schw‰bisch Gm,nd, Germany

[11] R Penlington, M Sarwar, GW Marshall, G Cockerham, DB Lewis, "Material Requirements for Narrow Neck Press and Blow Plungers within the Glass Container Industry", Key Engineering Materials, 86-87, 1993, pp 55-60

[12] R Penlington, M Sarwar, " Thermal operating Environment of the Narrow Neck Press and Blow Plunger", 4th International Conference-Advances in Fusion & Processing of Glass, Wurzburg, Germany, 22-24 May1995, pp 164-171

[13] Private Report-CFD Calculations Carried Out for UNN on PLM Glass Forming Process, in Conjunction with the Newcastle Upon Tyne RCID, Newcastle University, Final Report (1998)

CFD MODELLING AND HEAT TRANSFER IN A NNPB PROCESS

M. SARWAR[1], P.S LEUNG[1], N. PERERA[1], A.W ARMITAGE[2]
[1]University of Northumbria at Newcastle, U.K, [2]Rexam Glass plc, Barnsley, U.K

The metal plunger in an Narrow Neck Press and Blow (NNPB) process serves a dual function of forming the parison and extracting sufficient heat to stabilise the parison when going into the blow stage of producing a glass container. Previous work (1,2,3,4,5) in this area has indicated that there is a need to understand and quantify the heat transferred from the parison to the plunger and subsequently extract sufficient heat without causing "chill" defects in the final product. Preliminary work using computational fluid dynamics (CFD) modelling that has been carried out by others (6,7,8,9) shows that recirculation and choking of the airflow pattern within the bore of the plunger cooling tube system corresponds to the areas of poor cooling. Thus producing areas of ineffective heat extraction from the parison by the air flowing through the plunger cooling tube system.
The current work addresses the above problem by examining the cooling tube design using CFD modelling and analyses the heat transfer from the parison to the plunger. These results should prove to be of immense value to designers and manufacturers associated with the glass production industry.

1 - INTRODUCTION

The narrow neck press and blow (NNPB) process has evolved over the years due to attempts to reduce container weight. The NNPB process has successfully produced lightweight containers with a reduction in weight of 15%-30% [2]. This development is paramount to the economic progress of glass as a packaging material thereby deserving further investigation. The plunger is the most important component of the tooling in the NNPB process. It is responsible for the forming of the parison and distribution of glass within the container. Plunger surface temperatures and the inefficiency of the cooling system directly cause the NNPB plunger deficiencies and critical container defects [2,3].

M. Sarwar

The NNPB process of manufacturing lightweight containers is a two-stage process as shown in Figure 1.

The gob is delivered under gravity into the blank mould and the plunger forms the parison. The plunger presses and distributes the hot glass within the blank mould cavity in the first stage. The contact between the hot glass and metal mould tooling cools the parison but retains sufficient viscosity in order to maintain its geometrical form during the invert stage. The parison is inverted and held by its finish in the second stage. In the blow mould the parison hangs and stretches under its own weight. The blow head then covers the blow mould and blows the parison to its final shape.
The NNPB plunger extracts the thermal energy from the inner wall of the parison. This thermal energy

Nomenclature

V_{in}	Inlet velocity (m/s)
V_x	Velocity vector along the x axis
$\|V\|$	Velocity magnitude along the x axis (m/s)
P_{in}	Inlet pressure (bar)
P_{out}	Outlet pressure (bar)
T_{inlet}	Inlet temperature (K)
T_{outlet}	Outlet temperature (K)
κ	Distributed resistance constant
ρ	Density (kg/m^3)
C_p	Specific heat of air at constant pressure (J/kgK)
m®	Mass flow rate (kg/s)
Q®~®®®$_2$	Heat absorbed (W)

Fig. 1 - Narrow Neck Press and Blow Process.

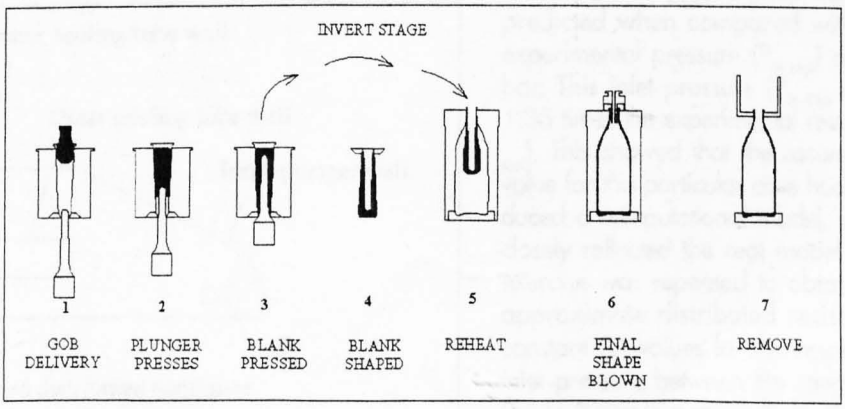

Fig. 2 - Cross section of a typical NNPB plunger.

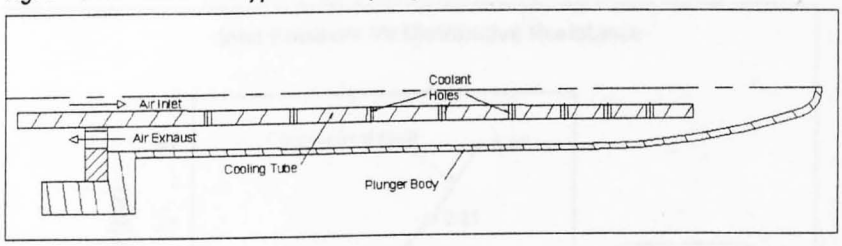

is removed from the plunger by the air circulating within the plunger bore (Figure 2). The cooling tube, which distributes the air within the plunger bore, is a tapered steel tube with an arrangement of radial holes. Preliminary results [6, 7] show that there is recirculation and choking of air within the airflow passage of the cooling tube system (Figure 3) leading to inefficient cooling. These areas correspond to the areas of poor cooling and regions of excessive temperature (>750°C) and tool wear.

2 – DETERMINING THE POROSITY OF THE COOLING TUBE HOLES

The plunger cooling tube system is modelled as an axisymmetric model portraying a simplistic representative of the real model. Following this the cooling tube holes, which are porous, are essentially slots since it is modelled as an annulus. Controlling the porosity of these cooling tube holes by adjusting their distributive resistance constant values further enables the computational model to mirror the practical model. The distributed resistance is a convenient way to approximate the effects of porous media (i.e. filter) or other such flow domain features without actually modelling the geometry of those features. It is an artificially imposed, unrecoverable loss associated with a geometry not explicitly modelled (see Figure 4).

The total pressure gradient is as shown below for the X direction.

$$\frac{fp}{fx}_{\text{resistance}} = \{k\rho V_x |V|\}$$

The respective distributed resistance constant (κ) values for the corresponding boundary conditions (i.e. inlet airflow velocity and outlet pressure) were obtained empirically through an iterative method of solution based on experimental results. Using the boundary conditions (i.e. exit pressure P_{out} = 0.4 bar and inlet velocity V_{in} = 105.97 m/s) chosen from a laboratory experiment [10], the distributed resistance constant (κ) value was obtained through an iterative process by comparing the inlet pressures (P_{in}) of the previous experimental and computational results (Figure 5).

As an example, when a constant value of 1.5 x 104 for the distributed resistance constant (κ) was used, an inlet pressure ($P_{in\ CFD'}$) of 1.58 bar was predicted when compared with the experimental pressure ($P_{in\ exp}$) of 1.5 bar. This inlet pressure ($P_{in\ CFD'}$) was 1.05 times the experimental result ($P_{in\ exp}$). This showed that the assumed κ value for this particular case had produced a computational model, which closely reflected the real model. This exercise was repeated to obtain the approximate distributed resistance constant (κ) values for the respective inlet pressure between the ranges of 0.5 to 3 bar (Figure 6). From this ex-

Fig. 3 - An enlarged view showing the recirculation and choking of airflow along the cooling passage in a 2-D model of plunger/cooling tube system.

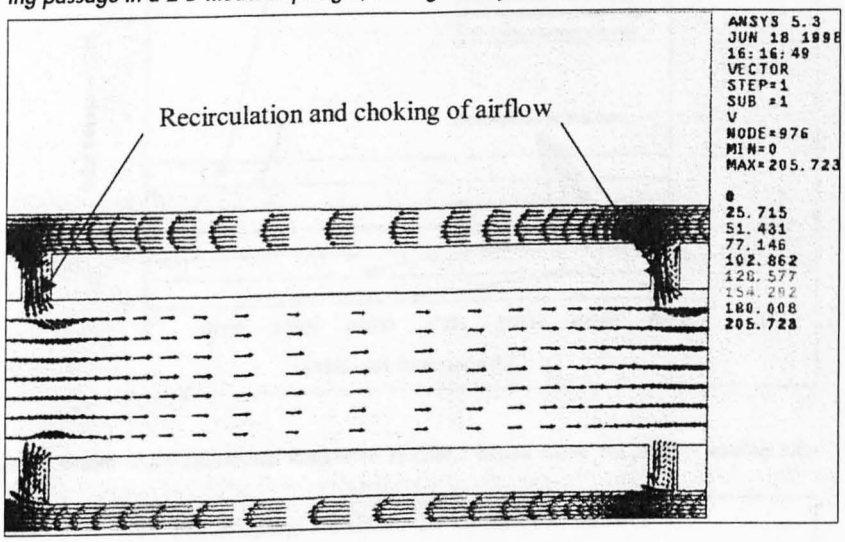

Fig. 4 - Diagram showing the plunger tip and cooling tube with the area of the applied distribute resistance.

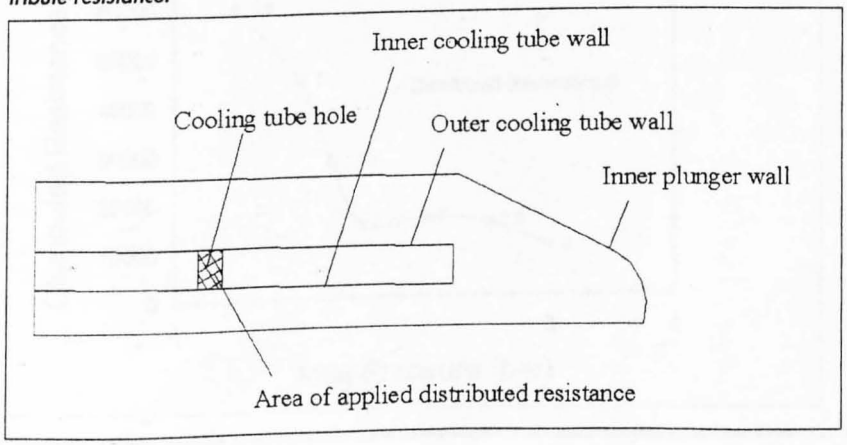

Fig. 5 - Graph of Inlet Pressure Vs Distributive resistance for an inlet pressure of 1.5 bar. (Boundary conditions used are exit pressure P_{out} = 0.4 bar and inlet velocity V_{in} = 105.97 m/s.

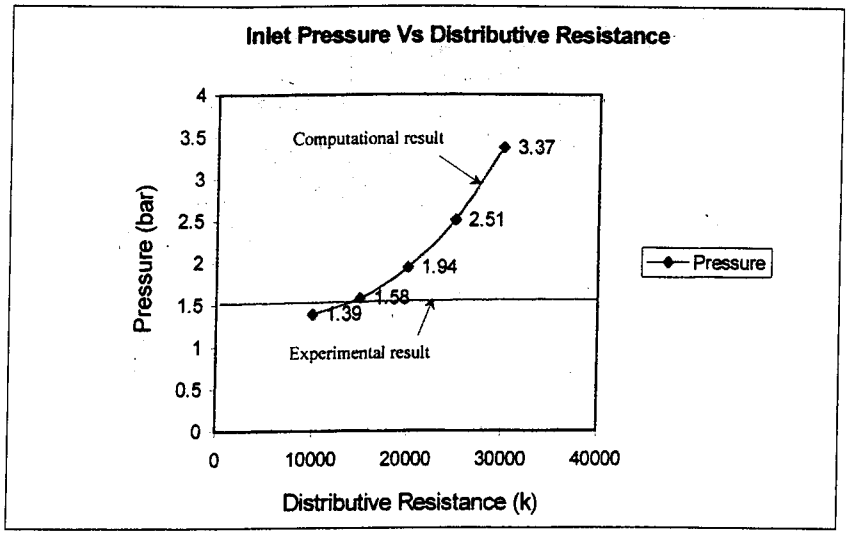

Fig. 6 - Graph of Inlet Pressure (0.5 bar to 3 bar) vs Distributed Resistance of the plunger cooling tube system.

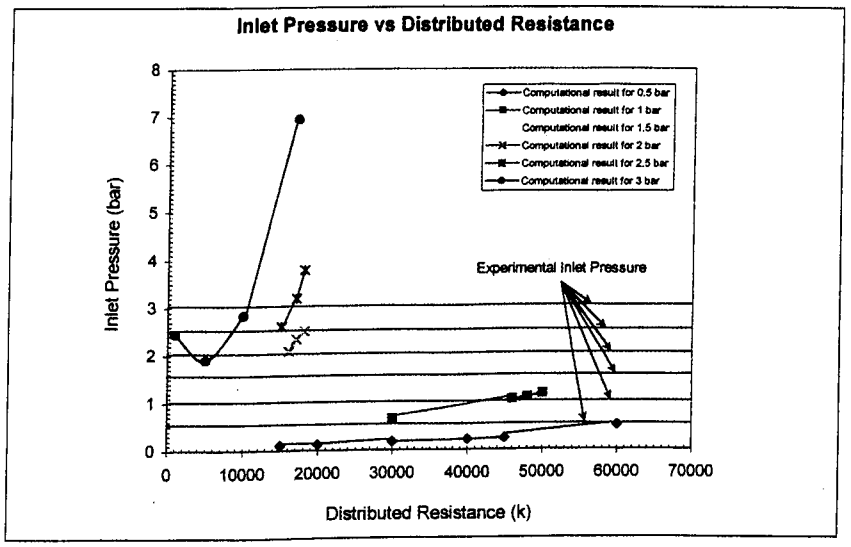

Fig. 7 - Graph of the Distributed Resistance Vs Inlet Pressure along the plunger cooling tube system.

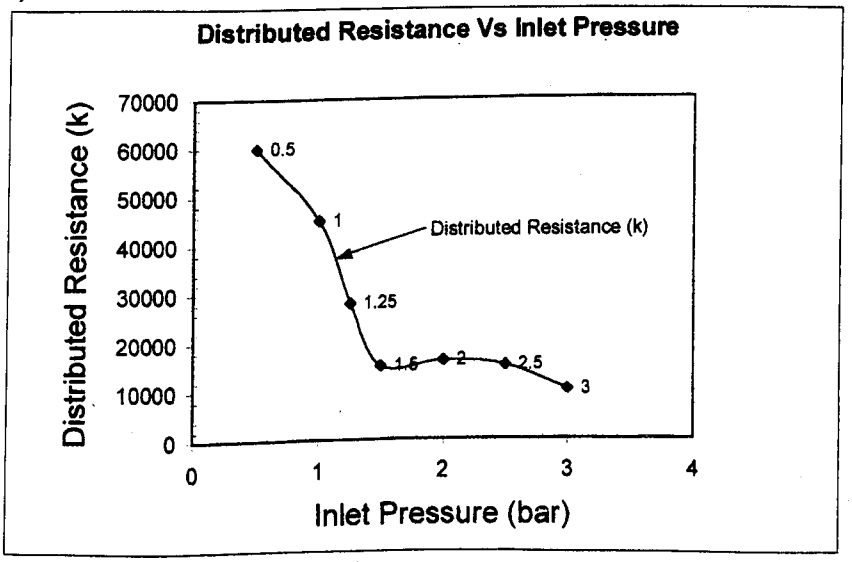

ercise the relationship between the inlet pressure (0.5 bar to 3 bar) and the distributed resistance constant (κ) value for the axisymmetrical model of the plunger cooling tube system was determined (Figure 7). This graph shows that there is a gradual decrease in the distributed resistance constant (κ) value as the inlet pressure increases. The curve starts to taper off and stabilises when the inlet pressure reaches 1.5 bar.

A possible explanation for the decrease in the distributed resistance constant (κ) value could be because of the recirculation and choking of the airflow at the tip of the plunger when the inlet pressure increases. When the air is blocked at the tip of the plunger, it is forced by the inlet pressure to flow through the cooling tube holes. Following this, the cooling tube holes must have a low distributed resistance constant value to allow sufficient air to flow through the plunger cooling tube system. The relationships between the boundary conditions (i.e. outlet pressure and inlet velocity) and the distributed resistance constant were also established shown in Figure 8 and 9 respectively.

3 - COMPUTATIONAL INVESTIGATION AND HEAT EXTRACTION FROM THE PLUNGER COOLING TUBE SYSTEM

Following the determination of distributed resistance constant (κ) values for the cooling tube holes, the temperature boundary condition was added to the CFD analysis. From the thermal imaging experiment of the parison (Figure 10), it was shown that the average temperature along the external surface of the parison was approximately 986.44°C [11]. This confirms the work carried out by Penlington, Sarwar, Marshall, Lewis and Cockerham [1] indicating that the external parison surface temperature was approximately 1000°C. Following this it was assumed that the temperature of the parison internal surface is the same as the parison external surface in order to pro-

Fig. 8 - Graph of the Distributed Resistance Vs Outlet Pressure along the plunger cooling tube system.

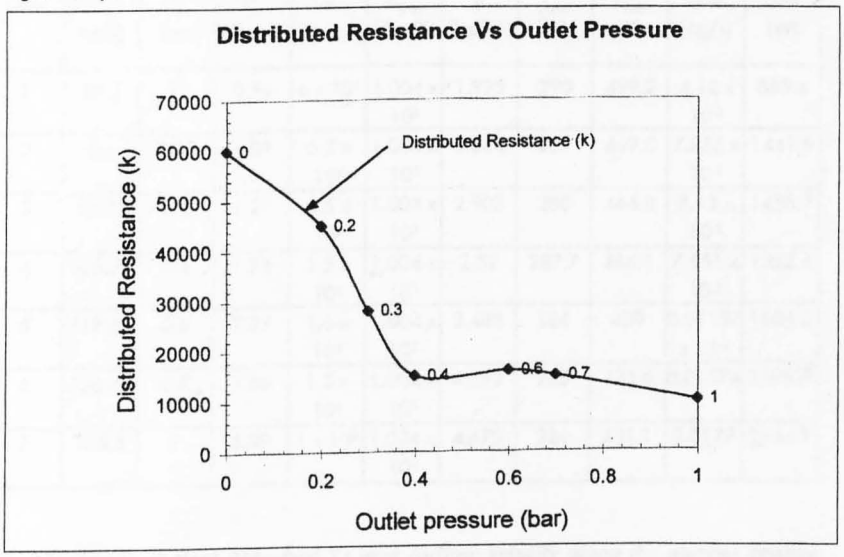

Fig. 9 - Graph of Distributed Resistance Vs Inlet Pressure along the plunger cooling tube system.

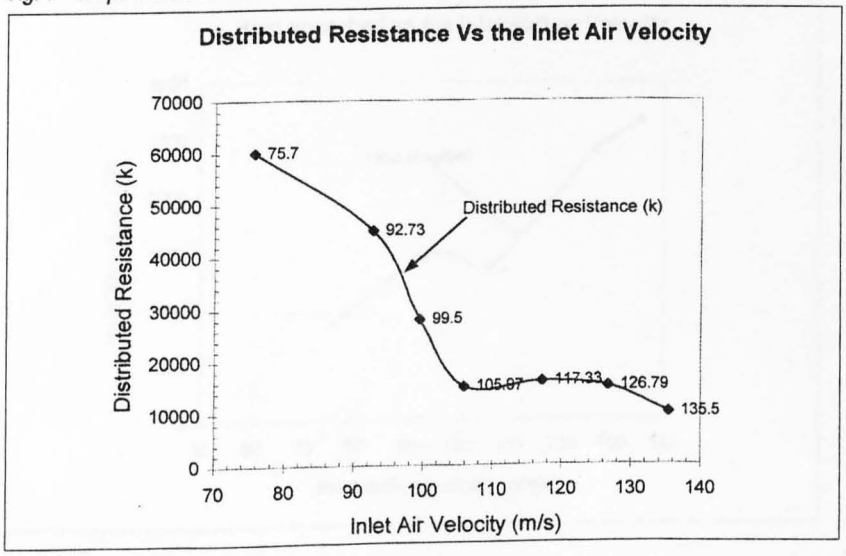

Fig. 10 - The temperature points along the lenght of the parison.

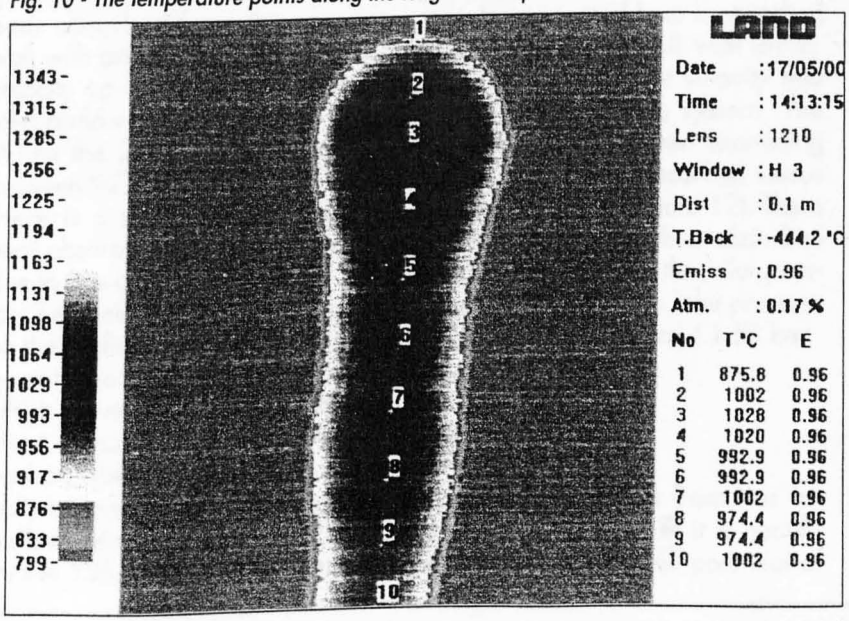

duce a simplistic model. Hence the temperature boundary condition (i.e. uniform temperature T= 1000°C) was assumed along the length of the plunger in the analysis. The boundary conditions (i.e. P_{out}, V_{in}) used in this exercise were maintained the same, as chosen from the previous laboratory experiment and used in previous computational work. This exercise was repeated for each of the chosen boundary conditions.

Following this exercise the CFD software computated the inlet temperature (T_{inlet}), outlet temperature (T_{outlet}) and density (ρ) values of air flowing through the plunger cooling tube system. Using this data, the mass flow rate ($\mu\rightarrow$) of air flowing into the cooling tube system and the approximate amount of heat that was extracted by the air was calculated. A selected table of results is as shown below:

Case 1

The boundary conditions used are:
V_{in} = 75.7 m/s;
P_{out} = 0 bar;
actual P_{in} = 0.51 bar;
κ = 6 x 104;

The assumed CFD software generated data are:

$C_{p\ air}$ = 1.004x10^3 J/kg K;
ρ = 1.925 kg/m^3;
T_{inlet} = 290 K;
T_{outlet} = 499.2 K

m® = (πr^2) V_{in} x ρ
m® = 4.12 x 10^{-3} kg/s

Heat absorbed = Mass flow rate (Q®~®®) ($\mu\rightarrow$) x Specific heat of air ($C_{p\ air}$) x Temperature Difference ($\Delta T_{average}$)
= 865.4W

4 - DISCUSSION OF RESULTS

The relationship between the heat absorbed and the inlet airflow velocity is shown in Figure 11. From the graph it is shown that there is a

Tab. 1 - The tabulated results of this exercise are as shown below.

Case	V_{in} (m/s)	P_{out} (bar)	P_{in} (bar)	κ	$C_{p\ air}$ (Jkg/K)	ρ (kg/m³)	T_{inlet} (K)	T_{outlet} (K)	μ→ (kg/s)	Q→ (W)
1	75.7	0	0.51	6×10^4	1.004×10^3	1.925	290	499.2	4.12×10^{-3}	865.4
2	86	0.12	1.09	5.2×10^4	1.004×10^3	3.034	289	469.5	7.955×10^{-3}	1441.5
3	92.73	0.2	1.27	4.5×10^4	1.004×10^3	2.903	288	466.8	8.13×10^{-3}	1458.7
4	105.97	0.4	1.58	1.5×10^4	1.004×10^3	2.52	287.7	466.1	7.551×10^{-3}	1352.4
5	117.33	0.6	2.27	1.6×10^4	1.004×10^3	3.488	286	450	0.01157×10^{-3}	1905.3
6	126.79	0.7	2.86	1.5×10^4	1.004×10^3	4.392	285	436.6	0.01574	2395.7
7	135.5	1	3.09	1×10^4	1.004×10^3	4.673	284	431.1	0.0179	2644.1

Fig. 11 - Graph of Heat Absorbed Vs Inlet Airflow Velocity along the plunger cooling tube system.

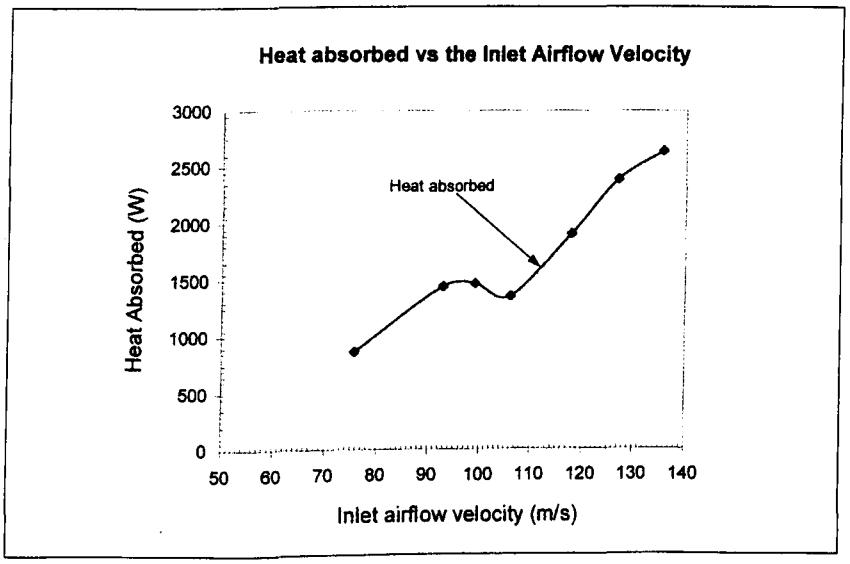

gradual increase in the amount of heat absorbed from the plunger wall with an increase in the airflow velocity up to the point where the inlet airflow velocity is 92.73 m/s. When the inlet airflow velocity is between 92.73 m/s to 105.97 m/s there is a slight decrease in the heat absorption rate. This could be due to one or a combination of factors i.e. recirculation of air, choking of the airflow pattern, insufficient quantity of cooling tube holes, which prevents the smooth and efficient extraction of heat from the parison. The heat absorption gradually increases again when the inlet airflow velocity is between 105.97 m/s to 135.5 m/s.

The graph shows that generally a greater amount of heat is absorbed from the plunger wall with an increase in the airflow velocity into the plunger cooling system. The same is also true when examining the graph of heat absorbed versus the inlet pressure (Figure 12). There is an increase in the heat absorbed with an increase in the inlet pressure except when the inlet pressure is between 1.27 bar and 1.58 bar.

5 - CONCLUSIONS

The result obtained from this investigation shows that it is beneficial to explore the full potential of the plunger cooling tube system in efficiently extracting and dispersing the thermal energy from the parison wall. By assessing the cooling tube design (i.e. quantity and distribution of the cooling tube holes) the heat transfer efficiency of the plunger cooling tube system can be improved. This improvement should eliminate/reduce the recirculation and choking of the airflow pattern within the cooling tube. Hence allowing for an even temperature distribution on the plunger surface and a smooth extraction of heat from the parison.

REFERENCES

[1] Penlington, R; Sarwar, M; Marshall, GW; Lewis, DB; Cockerham, G; "Wear Mechanism in Narrow Neck Press and Blow Plunger", Proceedings of the 2nd European Society of Glass Science and Technology Conference, Venice, Italy, June 1993, pp 279 - 284.

[2] Penlington, R; Lewis, DB; Marshall, GW; Sarwar, M; "The wear of coatings used on glass manufacturing equipment", Proceedings of EAST Kongreb, Schwäbisch Gmünd, Germany, Nov. 1993, pp 86 - 90.

[3] Ensor, T.F; "Mould materials", Glass Technology, Vol.19, No.5, 1978, pp 113-119

[4] Rawson, H; Glasses and their Applications, The Institute of Metals, London, 1991.

[5] Winther, S; Schaeffer, H.A; "Effects of aggressive gases on the behaviour of glass surface in contact with mould materials", Glastechnische Berichte, Vol 61, Nr 7, 1988, pp 184 – 190

[6] Penlington, R; Sarwar, M; Armitage, AW; "The cooling of narrow neck press and blow plungers for container production", Proceedings of the International Conference on Advances in Materials and Processing Technologies, August 1995, Vol. 3, pp 1053 – 1063

[7] Sarwar, M; Leung, PS; Perera, N; Armitage, AW; "Mathematical modelling of the fluid flow in the

Fig. 12 - Graph of Heat Absorbed Vs Inlet Pressure along the plunger cooling tube system.

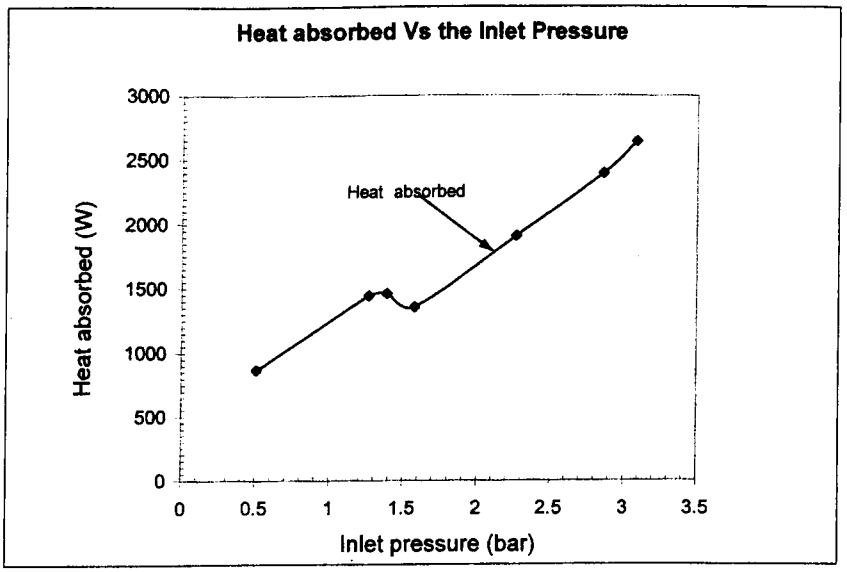

NNPB plunger cooling system", International Glass Journal, May/June 2000, Issue 107
[8] Anon; "Shaping can costs plunge", Glass Newsletter 4, Dec. 1997
[9] Penlington, R; Sarwar, M; "Thermal operating environment of the Narrow Neck Press and Blow Plunger", 4th International Conference-Advance in Fusion and Processing of Glass, Wurzburg, Germany, 22-24 May 1995, pp 164-171
[10] Sarwar, M; Leung, PS; Perera, N; Armitage, A W; Confidential Interim Report No.4 (February 1999)
[11] Sarwar, M; Leung, PS; Perera, N; Armitage, A W; Confidential Interim Report No.10 (April-June 2000)